Otic Regeneration and Development: Advancement of Stem Cell-Based Methodology for *In Vitro* Modeling of Mammalian Inner Ear Sensory Epithelia

by

Stacy A. Schaefer

A dissertation submitted in partial fulfillment
of the requirements for the degree of
Doctor of Philosophy
(Neuroscience)
in the University of Michigan
2018

Doctoral Committee:

Associate Professor Robert K. Duncan, Chair
Professor Gregory R. Dressler
Associate Professor David C. Kohrman
Professor Yehoash Raphael
Professor Linda C. Samuelson
Professor Michael D. Uhler

Stacy A. Schaefer

sschaef@umich.edu

ORCID iD: 0000-0002-6190-7031

Dedication

For their constant support, this dissertation is dedicated to

Gary Schaefer, father

Hollie Schaefer, mother

Scott Schaefer, brother

And, with extraordinary gratitude, to

Kyle Pentecost, husband

As well as to our family and friends.

Acknowledgments

The work described in this thesis was possible due to the support of my mentor, Dr. R. Keith Duncan. He simultaneously encouraged my creativity and focused my ambitions to fit the scope of a graduate thesis. I am extremely grateful for the opportunities to learn, to grow, and to pursue my lofty goals in his lab.

I am also grateful to my committee. When I was lost in a tangle of details, they helped me disengage so that I could see the bigger picture. Their perspicacity was much appreciated. Ultimately, their questions and comments challenged me to achieve my best work.

Special thanks go to lab manager Liqian Liu for her tireless efforts facilitating my experiments and those of everyone in the lab. Her ability to maintain a long and varied list of commitments with patience and generosity is extraordinary.

Special thanks also go to Neuroscience Graduate Program director Dr. Edward Stuenkel for his invaluable guidance. I would also like to acknowledge the Neuroscience Graduate Program and Kresge Hearing Research Institute for supporting my progress in so many ways.

Additionally, I am grateful for the following sources of funding for my training and research: NIH T32-NS076401 (Early Stage Training in the Neurosciences), NIH T32-DC00011 (Hearing, Balance, and Chemical Senses Predoctoral Training Grant), and DoD USAMRMC W81XWH-12-1-0492.

Table of Contents

Lists of Tables

Lists of Figures

Glossary of Common Terms/Abbreviations

ABR	Auditory brainstem response
AVE	Anterior visceral endoderm
BFL	BMP4, FGF2, LDN193189
BMP	Bone morphogenetic protein
BSFL	BMP4, SB431542, FGF2, LDN193189 (ectodermal differentiation cues)
CHIR99021	Wnt agonist (GSK3β inhibitor)
CNS	Central nervous system
ECAD	E-cadherin
EGFP	Enhanced green fluorescent protein
F-actin	Filamentous actin
FGF	Fibroblast growth factor
GO	Gene ontology
hESC	Human embryonic stem cell
Isl1/2	Islet-1/2
KSR	KnockOut serum replacement
LDN193189	BMP inhibitor
mESC	Mouse embryonic stem cell
Myo7a	Myosin 7a
NDS	Normal donkey serum
OV	Otic vesicle
PBS	Phosphate-buffered saline
PCA	Principal component analysis
pERK	Phosphorylated ERK
PFA	Paraformaldehyde
PPE	Preplacodal ectoderm
RA	Retinoic acid
RNASeq	RNA sequencing
SFEBq	Serum-free floating culture of embryoid body-like aggregates with quick reaggregation
SHH	Sonic hedgehog
tERK	Total ERK
TGFβ	Transforming growth factor beta

Abstract

Hearing loss treatments have improved significantly with the advent of cochlear implants and advancement of hearing aids. Still, they fall short of full restoration of function and do not benefit severe cases. An ideal approach to hearing restoration would be replacement of hair cells as loss or dysfunction of these cells is a major cause of sensorineural deafness. Therefore, recent efforts have focused on differentiation of pluripotent embryonic stem cells toward hair cell fate. A relatively novel 3-dimensional organoid method of differentiation has produced results remarkably similar to native hair cells in form and function. However, several challenges remain: Organoid hair cells are immature, vestibular instead of auditory, and low in yield, limiting practical use in the clinic or in the lab.

Our goal was to advance the current state of hair cell regeneration efforts through effective adaptation of developmental signaling cues. In these studies, we investigated parallels between early embryonic inner ear development and derivation of inner ear organoids using cell and molecular biology techniques. Specific experimental questions include the following:

1. Do inner ear organoids recapitulate mechanisms downstream of fibroblast growth factors (FGFs) involved in embryonic otic induction, establishing progenitors with inner ear fate?

2. Are outcomes dependent upon transforming growth factor beta (TGFβ) inhibition used to recapitulate embryonic germ layer patterning?
3. How closely do derived otic vesicles mimic native embryonic vesicles at the transcriptome level?

A fluorescent reporter cell line was used to track differentiation through Pax2 upregulation at the crucial otic induction stage. The results established the utility of this reporter cell line and revealed key parallels with embryogenesis and opportunities for advancing the organoid technology. In a follow-up study, the first differentiation step directing stem cells toward an inner ear lineage—inhibition of TGFβ signaling—was modified. The results demonstrated that this step was dispensable for formation of otic progenitors but necessary for later maturation into organoid epithelia. We performed comparative transcriptome analysis of stem cell-derived otic vesicles treated differentially at this stage and embryonic otic vesicles. From our analysis, targets for further optimization efforts emerged, including retinoic acid signaling and several key otic genes.

Elucidating parallels between organoid differentiation and embryonic development will contribute knowledge necessary to scale organoid production for practical use. In the future, this work may provide suitable models of inner ear development, physiology, and disease for laboratory study and provide replacement cells for clinical treatment.

CHAPTER 1: Introduction

Hearing and balance are major components of how we perceive and interact with the world. Though unique, both sensory modalities arise in the inner ear through a common mechanism: A mechanical event is transduced by highly specialized sensory cells into a neural representation interpreted by the brain. The sensorineural elements of the inner ear—sensory hair cells and their associated neurons—are intricate and fragile. Genetic aberrations are responsible for up to 80% of congenital deafness [1]. In addition, myriad insults including physical trauma, disease, drug toxicity, and aging can impact hearing and balance. As a result, deficits are widespread. Nearly 360 million people worldwide are living with hearing loss [2]. In the United States alone, 15% of adults age 18 and older report difficulty hearing, and 35% age 40 and older exhibit vestibular dysfunction [3,4]. The impacts include learning ability, social engagement, safety, and economic stability. Because hair cells and neurons are limited in their potential for spontaneous regeneration, the effects of their loss or severe damage are permanent. Therefore, the need to regenerate these cells by adapting knowledge of embryonic development toward new stem cell replacement strategies is a major goal of auditory and vestibular research and the focus of this dissertation.

STRUCTURE AND FUNCTION OF THE INNER EAR

The ear is responsible for the early stages of auditory and vestibular processing. Hearing begins when high-frequency pressure oscillations move through all three major divisions of the ear (Figure 1A, [5]). In brief, sound waves enter the outer ear and agitate the ossicles of the middle ear, which causes vibration of membranes in the inner ear. Vestibular input—angular or linear acceleration of the head—stimulates one of five balance organs of the inner ear, the two otolith organs (saccule and utricle) and the three semicircular canals. In the auditory and in vestibular organs, mechanical forces stimulate sensory hair cells to send information via primary afferent neurons of the 8th cranial nerve (Figure 1B-C, [5]).

Therefore, hair cells are the sensory receptors of the inner ear responsible for hearing and balance. Through the deflection of bundled hair-like projections called stereocilia on their apical

Figure 1: Anatomy of the ear

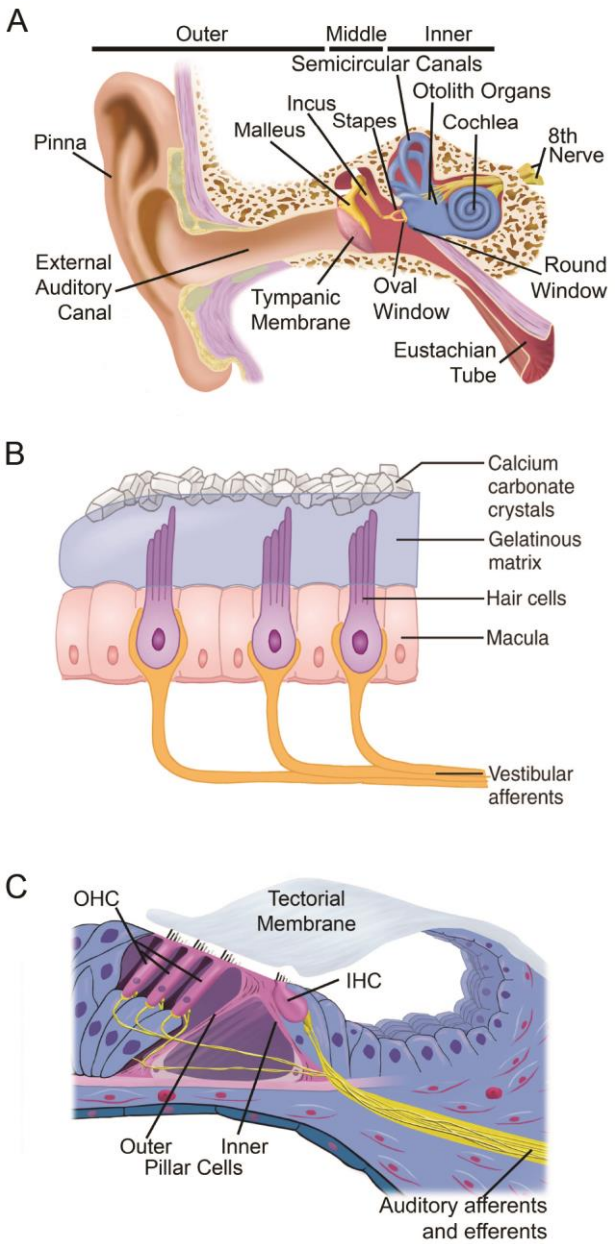

Figure from a book chapter in preparation [5]. A: Schematic of the outer, middle, and inner ear (left to right). B: General structure of the vestibular sensory epithelia. C: Arrangement of hair cells and neurons within the organ of Corti.

ends, hair cells transduce mechanical stimuli into electrical signals interpreted by the brain. This process begins with depolarization and repolarization of hair cells through the opening of ion channels, which triggers release of synaptic vesicles from their basal ends onto auditory and vestibular neurons. Consequently, hair cells themselves can be considered highly specialized neurons. In addition to sharing basic mechanistic features, hair cells and inner ear primary afferent neurons share an ectodermal germ layer origin and arise from the same primordial tissue, the otic placode.

The cochlea is the auditory portion of the inner ear. It houses the organ of Corti (Figure 1C), which is the sensory epithelium comprising hair cells and supporting cells. These anatomical structures have a unique spiral shape following the coiled bony labyrinth of the cochlea. Frequency sensitivity is distributed along the longitudinal axis of the cochlea in a frequency-place, or tonotopic, code, with low-frequency sounds processed towards the apex of the spiral and high-frequency sounds towards the base. In addition to this longitudinal organization, the organ of Corti is arranged laterally into rows of hair cells and supporting cells. Towards the outside of the spiral are three rows of outer hair cells, and towards the interior is a single row of inner hair cells. The precise organization of cells is established in development: Hair cells differentiate directionally from the mid-base of the cochlea and from inner to outer rows [6,7]. The center axis of the cochlear spiral is called the modiolus, and it serves as a conduit for neuronal processes that innervate the hair cells. Inner hair cells are primarily responsible for sending signals to the brain as they receive 90-95% of afferent innervation [8,9]. Outer hair cells primarily receive efferent inputs, yet they account for up to 40-50 dB SPL of sound amplification [8,10].

The vestibular portion of the inner ear is dorsal to the cochlea. At its most dorsal aspect are 3 fluid-filled semicircular canals with associated chambers (ampullae) containing sensory epithelia (cristae). Between the canals and the cochlea are 2 additional vestibular chambers called the utricle and saccule, which contain their own sensory epithelia (maculae) (Figure 1B). The vestibular hair cells respond to differences in movement between the endolymph and a gelatinous matrix surrounding the apical hair-like bundles; thus, they are sensitive to acceleration [11]. Vestibular hair cells are of two types. Type I hair cells are characteristically flask-shaped, each with a single afferent calyx nerve terminal [12]. Efferent projections terminate on the calyx rather than directly on the hair cell [13]. Type II hair cells are cylindrical, and each receives multiple nerve terminals, both afferent and efferent [12,13].

Several features of hair cell epithelia can be considered characteristic markers. For instance, the apical stereocilia bundles for which hair cells are named are key to their mechanosensitivity. The stereocilia are composed of actin and are thus more similar to microvilli than to true, tubulin-based cilia [14]. Nascent hair cells express an unconventional myosin, Myosin 7a (Myo7a), found almost exclusively in epithelial cells with microvilli or cilia. Its expression begins in the otic vesicle at embryonic day 9 (E9) in mice and persists through adulthood in both cochlear and vestibular portions of the inner ear [15,16]. A genetic defect in *Myo7a* results in deafness and impaired balance in *shaker-1* mice [17]. In humans, defective *MYO7A* is the underlying cause of Usher syndrome type IB [18]. At the base of the stereocilia in vestibular maculae is a network of thick filamentous actin (F-actin) bands formed by neighboring supporting cells. This network of F-actin thickens over time, perhaps underlying the reduction in regenerative

potential of vestibular sensory epithelia observed in mice after birth [19,20]. Finally, the presynaptic ribbon synapse is specialized for tethering large numbers of synaptic vesicles; this allows sound and acceleration stimuli to be rapidly and reliably transduced [21–23].

With specialized form and unique function, hair cells are a precious resource in life and in the lab. A single human cochlea contains only 3500 inner and 12000 outer hair cells [24]. A mouse cochlea, by comparison, has only 750 inner and 2500 outer hair cells [25]. These cells are well-protected by the temporal bone; however, insults to inner ear physiology including noise exposure, disease, toxins, aging, and genetic aberrations can all cause permanent impairment of hearing and balance. The scarcity and inaccessibility of hair cells presents a major challenge for inner ear research and medicine. The following section presents the case for a stem cell-based approach to hair cell regeneration with a focus on restoration of hearing.

STEM CELL REGENERATION OF INNER EAR HAIR CELLS

Current strategies for the treatment of deafness are palliative rather than restorative. Hearing aids work by amplifying sound, so they primarily benefit patients who retain inner hair cell-auditory nerve assemblies with only mild hearing loss. Patients who do wear hearing aids may be able to detect sound but nonetheless struggle to perceive salient features such as a single voice in a crowded room. In fact, in a study of hearing aid wearers in lab and field settings, hearing-impaired participants preferred significantly reduced loudness for general use than normal-hearing participants [26]; for a review of related studies on preferred loudness/gain, see [27].

Hearing aids can be prescribed according to various strategies for avoiding discomfort involved with excessive loudness while optimizing detection of frequencies associated with human speech [28]. Even so, auditory information important to speech recognition and other functional outcomes involves temporal processing and the ability to discriminate between frequencies, which are not fully addressed by hearing aids [28]. Advancements in hearing aid technology are still accompanied by trade-offs requiring clinicians to address patients' individual priorities for effectiveness. Besides this, many patients avoid using hearing aids due to expense or stigma.

Cochlear implants are a revolutionary technology for patients with severe hearing loss who nonetheless retain some primary auditory neurons. Using an array of electrodes, the implant directly stimulates the cochlear neurons at various points along their tonotopic arrangement. Therefore, the implant bypasses the hair cells, permitting sound detection in the absence of functional hair cells. For this strategy to be effective, some cochlear neurons must be viable and responsive to the electrodes. This is problematic for implant candidates because cochlear neurons may degenerate over time in a deafened ear [29–31]. Regardless, cochlear implants use only a few dozen electrodes, drastically limiting the number of discernible frequencies within the spectrum of normal human hearing (20 Hz to 20 kHz) [32]. Spectral resolution is only one factor determining the success of cochlear implants, so even for the best candidates, increasing the number of electrodes does not necessarily improve speech recognition [33]. Additionally, the poor representation of music and poor perception of speech in noise are often-cited shortcomings of cochlear implants [32,34]. Addressing these

remaining challenges may necessitate the combination of cochlear implants with biological therapies.

An ideal strategy to restore hearing would address the root cause of sensorineural deafness by repopulating of the deafened auditory epithelium with hair cells. Hair cell regeneration occurs spontaneously in non-mammalian species including cold-blooded species and birds [35–38]. In general, spontaneous regeneration in adult mammals occurs only in the utricle, to a limited extent, through asymmetric division or direct transdifferentiation of supporting cells [39–41]. Recent evidence shows that a small percentage of supporting cells in the early postnatal mammalian cochlea can regenerate hair cells [42–46]. The Wnt target genes *Lgr5* and *Axin2* are proposed markers for supporting cells with regenerative potential, so-called inner ear stem cells [46–51]. Extensive further investigation will be necessary to harness this potential for therapeutic benefit [52]. In development, hair cells and supporting cells diverge from common prosensory precursors through Notch-mediated lateral inhibition [53]: Ligand expression on the surface of one cell activates the Notch receptor on an adjacent cell, triggering downregulation of the hair cell-specifying gene *Atoh1* [54]. As a result, the former becomes a hair cell and the latter a supporting cell. Inhibition of Notch signaling has been shown to promote hair cell transdifferentiation from supporting cells in early postnatal mouse cochleae [46,55,56]. However, the ability to respond to Notch inhibition decreases as Notch pathway components are downregulated with age [55]. Regardless, transdifferentiation is not ideal since it reduces the population of supporting cells, which are important components of sensory epithelia. Supporting cells may not be available for transdifferentiation to occur at all in cases of profound deafness in

which the organ of Corti has been reduced to a flat epithelium [57]. Without a ready source of endogenous stem cells in the mature cochlea, embryonic or induced pluripotent stem cells are a logical alternative to provide hair cells or hair cell precursors for transplantation into deafened epithelia.

Guided differentiation of stem cells towards hair cell fate has the potential to revolutionize the study and treatment of hearing and balance disorders. To date, several approaches to produce hair cells have been published (Table 1). They begin with aggregation of stem cells into spheres, or embryoid bodies, which initiates differentiation. From there, they diverge based on whether differentiation proceeds within a 2-dimensional (2D) or 3-dimensional (3D) culture. The 2-dimensional approach involves allowing the embryoid bodies to attach to a flat substrate. The substrate may be seeded with feeder cells to supply growth factors, or growth factors and small molecule morphogens may be supplied in liquid media. Ultimately, the adherent cells are screened for hair cell markers to assess differentiation. A 2-dimensional approach is attractive due to the increased level of control over the cells' environment. The physical properties of a substrate can be determined, for instance, by choosing materials with more or less tension or materials that bind to cells through different mechanisms. Also, control over the influence exerted by supplied morphogens is optimal in monolayer cultures since the medium has direct access to all cells. The simplicity of this approach is, however, also a major limitation given that the embryonic environment in which hair cells form is far more complicated. Supplying exogenous morphogens at appropriate doses and timing is only one piece of the complex puzzle of modeling development *in vitro*.

Table 1: Basic strategies and outcomes of stem cell protocols for hair cell production

	Stem cell type	*Initiation*	*Terminal differentiation*	*Indication of best average efficiency achieved*
Li et al. 2003 [58]	Mouse ESCs*	3D	2D	~5% Atoh1$^+$/Brn3.1$^+$ ~5% Atoh1$^+$/Myo7a$^+$ (immunostaining)
Oshima et al. 2010 [59]	Mouse ESCs and iPSCs**	3D	2D	0.36 ± 0.07% Atoh1$^+$/Myo7a$^+$/Espin$^+$ (immunostaining)
Chen et al. 2012 [60]	Mouse ESCs	3D	2D	<1% of otic epithelial progenitors develop apical projections and express espin (SEM and immunostaining)
Ouji et al. 2012 [61]	Mouse ESCs	3D	2D	17.2 ± 2.1% Atoh1$^+$/Brn3c$^+$ 26. 3 ±1.3%, Atoh1$^+$/Myo6$^+$ 16.1 ± 2.4% Atoh1$^+$/calretinin$^+$ (immunostaining)
Ouji et al. 2013 [62]	Mouse ESCs	3D	2D	12.8 ± 1.2% Myo6$^+$ 9.8 ± 1.3% Brn3c$^+$ 8.9 ± 0.8% α9AchR$^+$ (immunostaining)
Ronaghi et al. 2014 [63]	Human ESCs	3D	2D	≤9.03% of cells positive for 3 or more hair cell markers (single cell RT-PCR)
Ohnishi et al. 2015 [64]	Human iPSCs	2D	2D	0.01 ± 0.008% Myo7a+ (immunostaining)
Ding et al. 2016 [65]	Human ESCs	2D	2D	5.8% Espin$^+$ feeder-free or 6.7% on chicken utricle stromal feeder cells (immunostaining)
Kil et al. 2016 [66]	Human MSCs***	2D	2D	N/A
Ouji et al. 2017 [67]	Mouse ESCs	3D	2D	28.4 ± 4.7% Brn3c; 36.3 ± 6.1% Myo6 (immunostaining)
Koehler et al. 2013 / Koehler et al. 2014 [68,69]	Mouse ESCs	3D	3D	10-20% of aggregates with organoid(s) at day 20 1552.3 ± 83.1 Myo7a$^+$ cells per aggregate at day 20 (starting from 3000 cells/aggregate at day 0) (immunostaining)
DeJonge et al. 2016 (modification of Koehler et al. 2013) [70]	Mouse ESCs and iPSCs	3D	3D	~60% of aggregates with organoid(s) at day 20
Koehler et al. 2017 [71]	Human ESCs and iPSCs	3D	3D	19.7 ± 7.0% of aggregates with organoid(s) at days 60-100; 68-779 hair cells per organoid (average 226; 12 organoids assayed)
McLean et al. 2017 [51]	Lgr5$^+$ supporting cells	*In vivo*	3D	26.3% ± 2.5% of cells Atoh1$^+$

* ESCs = Embryonic stem cells
**iPSCs = Induced pluripotent stem cells
***MSCs = Mesenchymal stem cells

A novel hair cell regeneration method, the inner ear organoid protocol, using 3-dimensional cultures was published in 2013 [68]. It was developed on the foundation of central nervous system (CNS) and optic organoid studies using “serum-free floating culture of embryoid body-like aggregates with quick reaggregation,” or SFEBq [72,73]. With this method, 3-dimensional stem cell aggregates are guided through an initial ectodermal differentiation phase recapitulating early stages of embryonic development. Then, in the final maturation phase, the aggregates self-pattern with minimal input of exogenous factors. The earlier phase establishes tissue layers mimicking the embryonic germ layers ectoderm, endoderm, and mesoderm. As the intact aggregates continue to mature, the various cell types in these layers will exert influences on each other through contact cues and secreted factors. During the first half of the maturation phase, the epithelial ectodermal layer pinches off into the surrounding mesendodermal tissue to form vesicles. This process is analogous to the formation of the otic vesicle, the anlage of the inner ear, through invagination of the otic placode at E9-9.5 in mice. In the second half of maturation, the vesicle expands in size, resulting in a cyst lined with hair cells, with the apical side facing the lumen of the cyst as in the sensory epithelia of the inner ear. Therefore, 3-dimensional differentiation culture takes advantage of physical and chemical properties inherent in a heterogeneous aggregate, much like unique tissue types develop in context of a whole embryo. Heterogeneity is currently the limiting factor in terms of yield; however, steps have already been taken to begin optimizing the protocol to maximize production of otic tissue [70,74].

High-throughput, high-yield methods are essential to the goals of stem cell-based inner ear research. Understanding genetic causes of deafness and balance disorders,

discovering otoprotective drugs, studying hair cell physiology, and modeling auditory and vestibular development would all be facilitated by a sustainable source of hair cells. The results of initial experiments with the inner ear organoid protocol show its potential to become a powerful tool in a variety of applications. Aspects of the protocol that need further optimization include throughput and yield as well as reproducibility, functional maturation of hair cells, and control over hair cell type. Incorporating additional aspects of developmental biology may improve the protocol; in parallel, studying organoid differentiation may inform developmental studies. Through this reciprocal exchange of ideas, the inner ear organoid protocol be developed as a means of generating new hair cells to restore hearing and balance.

TAKING CUES FROM THE MAMMALIAN EMBRYONIC INNER EAR

Embryonic development is a profoundly complex biological process. The influences of secreted morphogens, contact cues, physical reorganization, and the extraembryonic milieu are spontaneously orchestrated so that a whole organism is born of a single zygote cell. Just as the relative levels and timing of various instruments are conducted in an orchestra, so too are the levels and timing of processes regulated in development. Dividing an entire composition into movements—or an entire developmental program into phases—is useful for its conceptualization.

The inner ear organoid protocol for stem cell differentiation is divided into two phases, as described in the previous section: ectodermal differentiation and maturation (Figure 2). Within the ectodermal differentiation phase are two applications of small molecules and growth factors. First, an inhibitor to the TGFβ pathway and bone

morphogenetic protein 4 (BMP4) are added at day 3. Second, a BMP pathway inhibitor and fibroblast growth factor 2 (FGF2) are added between day 4-4.5, with the timing optimized for the specific stem cell line used. Each addition recapitulates distinct events between germ layer formation in the gastrula-stage mouse embryo (~E6.5) and induction of otic progenitors (~E8.5) (Table 2).

Figure 2: General schematic of organoid differentiation

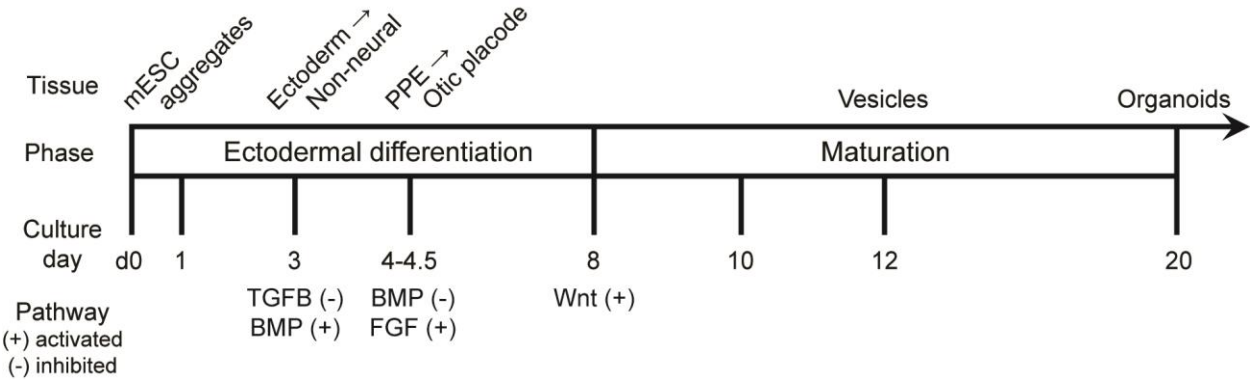

Early TGFβ inhibition favors ectodermal lineage by inhibiting formation of mesoderm and endoderm

The addition of a TGFβ pathway inhibitor on day 3 of the organoid protocol is based on the mechanism of ectodermal differentiation in the embryo. As the first step along an otic lineage, its efficiency is crucial to the ultimate production of hair cells in the organoids; each step in the organoid protocol establishes competence to respond to the next pro-otic cue. Therefore, understanding how TGFβ signaling is regulated in early embryonic patterning will ensure that the strategy used to manipulate this pathway *in vitro* is purposeful and effective.

Table 2: Developmental stages recapitulated in inner ear organoid protocol

Developmental stage	*Transition mediated*	*Embryonic day (mouse)*	*Embryonic mechanism*	*Inner ear organoid day*	*Inner ear organoid cue*
Germ layer specification	Presumptive ectoderm → Definitive ectoderm	E6.5 - 7	TGFβ inhibition	3	SB431542 [68]
Divergence of neural and non-neural ectoderm	Definitive ectoderm → Non-neural (surface) ectoderm	E7 - 7.5	BMP4	3	rhBMP4 [68]
Specification of preplacode and epidermis	Non-neural ectoderm → Preplacodal ectoderm	E7.5 - 8	BMP inhibition	4-4.5	LDN193189 [68]
Otic induction	Preplacodal ectoderm → Otic placode	E8 - 8.5	FGF3/10	4-4.5	rhFGF2 [68,70]
Otic prosensory domain specification	Otic placode → Prosensory domain	E8.5-E12.5	Wnt	8-14	CHIR99021 [70]
Hair cell differentiation	Prosensory domain → sensory hair cells	E12.5 (vestibular) or E14.5 (auditory)	Lateral inhibition	14-20 *Note: Atoh1 is upregulated as early as day 12* [75].	*Self-directed*

In the developing mouse embryo, TGFβ signaling plays a major role in establishing the anterior-posterior body axis (reviewed in [76,77]). This process is initiated just prior to gastrulation, a major rearrangement of epiblast that results in specification of the 3 germ layers that are precursors to all tissues of the body. Anterior-posterior patterning begins when distal visceral endoderm (DVE) shifts asymmetrically to form an anterior pole at E5.5 [76]. By E6.5, it has finished shifting and is redefined as anterior visceral endoderm (AVE) [76]. At this point, gastrulation begins with the formation of the primitive streak, an elongated groove through which epiblast tissue migrates to form layers of endoderm and mesoderm within the embryo. The anterior-most epiblast tissue that does not migrate through the primitive streak loses

pluripotency and specifies as definitive ectoderm [77]. This gives rise to neuroectoderm and to non-neural ectoderm, from which the inner ear derives, in a subsequent specification involving BMP signaling.

The effect of TGFβ signaling in gastrulation is to promote endoderm and mesoderm (reviewed in [78]). Accordingly, endogenous antagonists of TGFβ signaling promote ectoderm. TGFβ is one of a family of related ligands that also includes Activin and Nodal (Figure 3 and Table 3). Nodal expression is initially ubiquitous throughout the epiblast but becomes restricted towards the posterior pole during formation of the anterior-posterior axis [79]. The AVE secretes antagonists to Nodal, protecting the definitive ectoderm from its posteriorizing influence [80–84]. In mouse loss-of-function mutants for Nodal, the primitive streak and AVE do not form [80,85–88], which may result in premature differentiation and expansion of neural ectoderm [88]. Similarly, *in vitro* culture of anterior epiblast explanted prior to ectodermal commitment in the presence of SB431542—the same TGFβ signaling inhibitor used in the inner ear organoid protocol—results in upregulation of neural markers [89]. If these explants are

Figure 3: Simplified TGFB signaling pathway

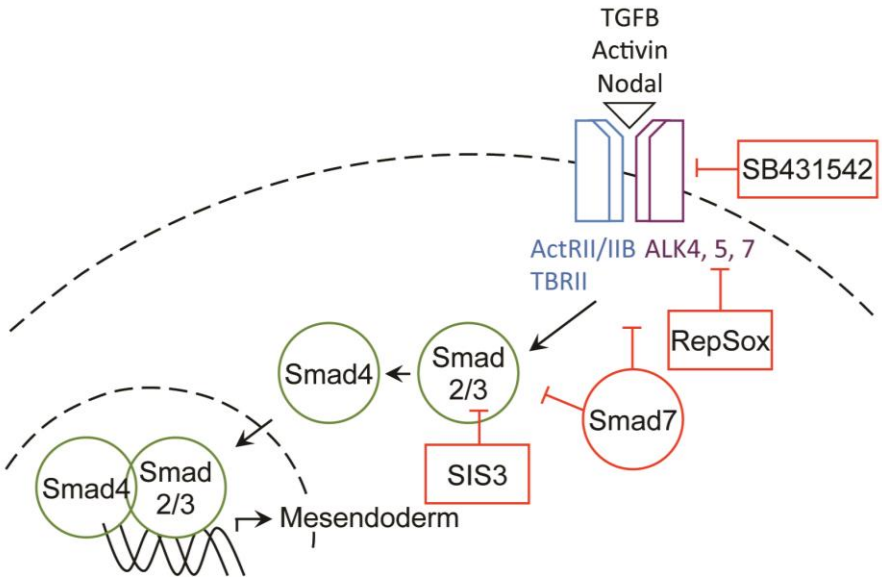

Table 3: Components and regulators of TGFβ superfamily signaling pathways

	TGFβ	*BMP*
Type I receptors	ALK4/5/7	ALK2, 3, and 6
Type II receptors	ActRII/IIB and TβRII	ActRII/IIB and BMPRII
Ligands (and their receptors) [90]	Activin (ALK4/5 and ActRII/IIB) Nodal (ALK4/7 and ActRII/IIB) TGFβ (ALK5 and TβRII)	BMPs (ALK2/3/6 and ActRII/ActRIIB/BMPRII)
Effectors	Smad2 and Smad3	Smad1, 5, and 8
Commonly-used inhibitors (and their targets)	LeftyA (Smad2), RepSox (ALK5), SB431542 (ALK4/5/7), SIS3 (Smad3)	Chordin (BMP2/4), Dorsomorphin (ALK2/3/6), Noggin (BMP2/4), LDN193189 (ALK2/3/6)

also cultured in the presence of BMP4, non-neural ectodermal markers are upregulated [89]. Conversely, Activin has been used in place of Nodal to induce mesoderm and endoderm in stem cell cultures [91–94]. However, its role in this process in embryonic development may not be conserved in mammalian species [94,95].

Given this evidence of the role of Nodal in development, TGFβ inhibitors have been adopted as efficient inducers of ectodermal lineage in stem cell differentiation protocols. SB431542 promotes neuroectoderm in cultures of mouse epiblast stem cells (EpiSCs) or human embryonic stem cells (hESCs) [96–98]. A protocol for telencephalon organoids that was a precursor to the SFEBq approach used LeftyA to inhibit Nodal and thereby promote neural specification [99]. BMP signaling, like TGFβ signaling, favors non-ectodermal germ fate during early patterning of the mouse embryo [100]. BMP4 expressed within extraembryonic tissue plays a role in reinforcing Nodal within the posterior epiblast, thereby maintaining the AVE [78,101]. Because TGFβ and BMP pathways are primary regulators of ectoderm specification, a dual inhibition strategy targeting both pathways (called dual-Smad-inhibition after the canonical

downstream effectors) has been used *in vitro* to derive CNS neurons from stem cell cultures [102].

SB431542 is also used as the pro-ectodermal morphogen for differentiation of inner ear organoids. The ectodermal lineage path toward CNS neurons diverges from the path toward inner ear fate, however, with the specification of neural and non-neural progenitors. BMP signaling is key to navigating this change in lineage paths in development; therefore, BMP4 is paired with SB431542 at day 3 of organoid differentiation.

Role of BMP4 in inhibiting default neural ectodermal fate, promoting non-neural ectoderm

Concomitant with its role in patterning the anterior-posterior axis, BMP4 is involved in patterning neural and non-neural fates along the dorsal-ventral axis. Prior to gastrulation, BMP4 secreted from surrounding tissue counteracts the tendency of anterior ectoderm to become neural [103,104]. This tendency toward neural fate in the absence (or rather antagonism) of BMP signaling is referred to as the “default model” of neural induction (reviewed in [105–107]). The importance of pre-gastrula BMP inhibition for anterior neural ectoderm in mammals was first shown in mice lacking the endogenous BMP antagonists Chordin and Noggin (Table 3) [108]. Forebrain tissue is severely lacking in the double mutants but is not completely absent. This suggests that inhibition of the BMP pathway is not solely responsible for neural induction [108,109]. Indeed, FGF and Wnt signaling are also implicated.

Of the 3 BMP type 1 receptors, BMPR1a (or ALK3) is the only one expressed in the epiblast [110,111]. Mice lacking BMPR1a show premature neural markers, expansion of neural tissue, and reduction of non-neural ectoderm [104,112]. This phenotype is similar to the Nodal knockout phenotype [88], which may be evidence of the role BMP4 plays in reinforcing Nodal expression as described in the previous section. The default model of neural induction was first established through studies of *Xenopus* and zebrafish; loss of non-neural ectoderm in BMPR1a-deficient mice provides support for it in a mammalian system.

Definitive ectoderm has the potential to become neural or non-neural depending on exposure to BMP4 [105]. It represents an intermediate stage between ectodermal commitment and differentiation of neural or non-neural derivatives. Though this developmental stage had long been established in non-mammalian vertebrates [105], it was only relatively recently demonstrated in a mammalian models. In 2013, a mouse study identified definitive ectoderm and highlighted its transient nature with anterior ectoderm explants prepared at E6.5, 7.0, or 7.5 [89]. In the presence of BMP4, the E6.5 explants were redirected toward mesoderm and endoderm fate, but this pluripotency was lost by E7.0. The E7.0 explants could be directed toward neural or non-neural fate depending on absence or presence of BMP4 but had committed to one or the other fate by E7.5. A similar experiment demonstrated a transient population of cells analogous to definitive ectoderm in mouse embryonic stem cells (mESCs) cultured under a neural induction paradigm with conditioned medium [113].

Other neural induction protocols use defined culture media components to differentiate stem cells. As mentioned, BMP signaling both reinforces TGFβ signaling in

germ layer specification and functions separately in regulating neural fate. Some studies have reported necessity of either BMP inhibition or TGFβ inhibition for inducing neural fate. For instance, Surmacz et al. first recognized the utility of the small molecule LDN193189 as an alternative to the animal-derived BMP inhibitors Noggin and Dorsomorphin [114]. Paired with SB431542, it was effective at upregulating Pax6, used in the study as a marker of neural fate, in their hESC differentiation paradigm. However, neither LDN193189 nor SB431542 was an effective neural inducer by itself. Surmacz et al. note that this contrasts with results from other groups showing that Dorsomorphin alone or SB431542 alone was an effective inducer of neural fate from hESCs [97,98,114,115]. Reconciling these differences, Kim et al. showed that stem cell lines of various origins have differential basal levels of activated Smad1/5/8 [116]. This explains differential requirements for BMP inhibition. Furthermore, they established that dual inhibition—using Dorsomorphin and SB431542 together in their study—was able to overcome inherent cell line differences for effective neural induction [116].

Two-step commitment to preplacodal fate: Elevation and subsequent attenuation of BMP signaling at the border between neural and non-neural tissues

The signals involved in segregating neural vs non-neural ectoderm precursors are then involved in medial-lateral patterning of neural plate, neural crest, preplacodal ectoderm (PPE), and epidermis [117,118]. BMP4 is elevated towards the lateral ectoderm where it promotes epidermis [118]. In non-mammalian species, FGF8 is implicated in counteracting BMP4 in medial ectoderm through phosphorylation of the Smad1 effector [119], thereby reinforcing neural fate choice [120]. Evidence suggests a

similar pro-neural capacity for FGF in mammals but is not conclusive as to whether the mechanism is direct through Smad1 regulation [121,122] or independent of BMP signaling [123,124]**.** Wnt signaling is also implicated in patterning neural and non-neural tissue. In chicken embryogenesis, Wnt expressed in lateral ectoderm blocks FGF-mediated antagonism of BMP4 and thereby permits non-neural fate[1] [128]. The integration of these signals results in neural crest and PPE. Although neural crest and PPE arise from a common "neural border region" between the future neural plate and epidermis, competence to become one or the other segregates with specification of neural vs non-neural lineages prior to patterning [129].

Towards the end of gastrulation, antagonism of BMP signaling mediates a refinement of non-neural (i.e., surface) ectodermal fate (Figure 4) [130]. Persistent BMP signaling results in epidermis from more ventral/lateral ectoderm, whereas complete attenuation results in PPE in the immediately adjacent border region [130]. PPE gives rise to the various cranial placodes, thickened regions of ectoderm that differentiate into cranial nerves and specialized sensory cells including those of the inner ear. As PPE-specific genes (e.g., *Eya1/2* and *Six1/4*) are upregulated, they positively auto-regulate so that PPE tissue is committed to its fate and its boundary with neural crest is refined [118].

Development of PPE has been recapitulated in embryonic stem cell cultures. Two protocols building on the dual-Smad-inhibition approach using SB431542 and Noggin to derive CNS neurons from hESCs were published in 2013 [131,132]. In one

[1] Wnt has been reported to block or promote neurogenesis in conflicting reports from non-mammalian studies (reviewed by [125]). However, the two models resulting from these conflicting reports may be reconciled by differences in the roles of Wnt at different developmental stages [126,127].

protocol, both inhibitors were removed on day 3, and preplacodal markers were observed on day 8 [131]. This report noted that endogenous BMP was necessary between days 3 and 5. In the other, only Noggin was removed on day 3, leaving only SB431542 in the media, to shift the fate from neural to preplacodal by day 11 through increased BMP signaling [132]. Both protocols resulted in a transient PPE stage that could be pushed to a specific placodal fate through additional exogenous factors. Another protocol parted from the dual-Smad-inhibition approach, pairing SB431542 with a Wnt inhibitor instead of Noggin, and observed PPE markers after 6 days [133]. After a series of additional factors applied together with FGF2, markers of otic placode were induced. Additional protocols for producing CNS neurons [134,135] as well as neural crest [136,137] and epidermis [138–141] from human or mouse ESCs have been published. Exact mechanisms leading from BMP, Wnt, and FGF signaling to PPE commitment are unclear, and much evidence supporting current models of PPE development is from non-mammalian research. However, the models presented by Groves and LaBonne attempt to reach consensus in the existing evidence across species [118]. Kwon et al. provide a concise model summarizing the proposed modifications to the original default model of neural induction and how the PPE lineage diverges from the neural, neural crest, and epidermal lineages in development (Figure 4) [130]. The model lays out a 2-step process in which BMP4 is initially required for non-neural ectoderm, and its complete attenuation is subsequently required for preplacode. In the inner ear organoid protocol, this stepwise transition is performed through initial application of BMP4 at day 3 and inhibition via LDN193189 24-36 hours later.

Figure 4: Spatiotemporal inhibition of BMP4 in patterning neural and non-neural ectoderm

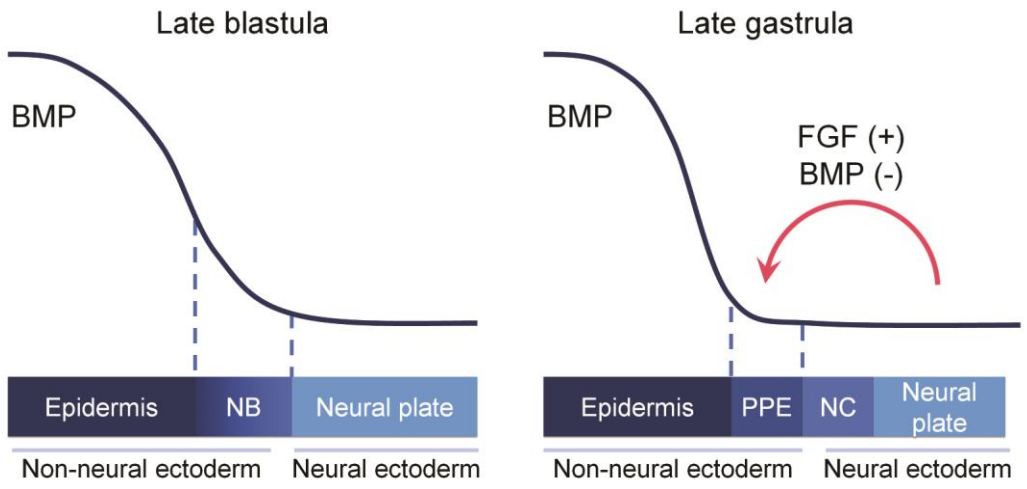

Figure redrawn from Kwon et al. 2010 [130]. In the late blastula stage of development (left), the domain that gives rise to PPE (and neural crest, NC) is characterized by an intermediate level of BMP signaling. By the late gastrula stage (right), attenuation of BMP signaling results in PPE specification.

FGF2 recapitulates the otic induction stage of development, when inner ear progenitors commit to otic fate

The next step in the inner ear organoid protocol is application of FGF2 at day 4.5. This is analogous to the upregulation of FGFs in tissues neighboring the presumptive otic ectoderm shortly after gastrulation. Around E8 in mice, FGF10 is upregulated in mesenchyme [142,143]. Shortly thereafter, FGF3 is upregulated in rhombomeres 4-6 of the hindbrain [142,143]. By E8.75, the expression pattern of FGF10 has already shifted so that FGF10 is found less in mesenchyme and more in the adjacent hindbrain [143]. FGF3 remains in rhombomeres 5-6 through E9.5, when the inner ear begins to take shape with formation of the otic vesicles [144].

The onset of FGF3 and FGF10 drives expression of the transcription factor Pax2 by E8.5, just after expression of Pax8 [143,145]. This event is generally considered

definitive of otic induction, or commitment to inner ear fate. *Pax2* and *Pax8* are closely-related genes [146] necessary for normal development of the inner ear [147–150]. Pax2 can largely compensate for Pax8, but Pax8 cannot completely compensate for Pax2 [150]. This may be explained by differences in timing since Pax8 expression only persists through early otic vesicle formation [151], whereas Pax2 is maintained in the ear through at least the first week postnatal [149,152].

Several studies have examined the necessity of FGF3 and FGF10 in inner ear development through characterization of mutant mouse strains [142,143,153–155]. The loss of FGF3[2] is more disruptive to otic vesicle formation and patterning than loss of FGF10 when assessed at E9.5: Vesicles are smaller, are positioned more ventrally, and show a dorsal-lateral shift in Pax2 from its normal ventromedial domain [143]. In addition, formation of the endolymphatic duct and cochleovestibular ganglion (cvg) is inhibited in FGF3 null mice [153,155], and expression of various dorsal otic vesicle markers is affected with regards to level or domain [155]. Mice null for both FGF3 and FGF10 form very small vesicles or no vesicles at all [142,143,156]. Furthermore, otic markers Pax2, Pax8, Gbx2, and Dlx5 are either severely reduced or lost from the placode [142,143]. These studies highlight the crucial role of FGF signaling in induction of otic markers and morphological development of the inner ear.

Another FGF ligand, FGF8, may contribute to inner ear development through its effect on FGF10 expression. Combined loss of FGF3 and FGF8, which is normally found in the endoderm surrounding the pre-otic ectodermal field, results in a similar

[2] Alvarez et al. report the lack of a phenotype from loss of FGF3 [142]. Hatch et al. suggest that various mouse genetic backgrounds or mutagenic strategies may underlie discrepancy in observed FGF3 null phenotypes [155].

phenotype to FGF3/10 double knockouts [157,158]. FGF10 expression in the mesenchyme adjacent to the otic field is reduced in FGF3/8 double mutant mice, suggesting that FGF3 and 8 may be involved in inducing or maintaining FGF10 [158,159]. Thus, the similarity in phenotypes in FGF3/8 double mutants and FGF3/10 double mutants may reflect overlapping functions and mutual positive regulation amongst these genes.

Even after FGF3/10 induces Pax2 expression, the borders of the otic domain are yet unresolved. The early otic placode is part of a larger $Pax2^+$ region called the otic-epibranchial progenitor domain (OEPD) [160,161]. Separation of otic and epibranchial placodes as well as separation of otic placode and epidermis are controlled by Wnt signaling. After FGF signaling sets up the OEPD, it upregulates Wnt8a in the adjacent hindbrain [156,159]. Wnt signaling then bolsters expression of otic genes (*Pax2*, *Pax8*, *Gbx2*, and *Sox9*) and restricts epidermal and epibranchial fates [162]. β-catenin is the primary effector of the canonical Wnt pathway. In a transgenic mouse, conditional expression of a stabilized β-catenin in $Pax2^+$ cells results in an enlarged otic placode via recruitment of prospective epidermal cells [162]. This mouse also supports a dorsalizing role for Wnt, counterbalanced by sonic hedgehog (SHH) from the ventral hindbrain and notochord [163,164]: The expression domains of dorsal markers Dlx5, Gbx2, and Msx1 are expanded ventrally throughout the enlarged placode at E9.5, yet Dlx5 and Msx1 are repressed in the medial portion nearest the ventral neural tube as the placode invaginates [162]. Conditional deletion of Wnt results in a smaller placode and otic vesicle and encroachment of $Foxi2^+$ epidermis into the normal otic field [162]. The Notch pathway reinforces the pro-otic role of Wnt [165]. Wnt upregulates

components of the Notch pathway, and in return, Notch signaling leads to increased Pax8 and the thickening of ectoderm that marks the otic placode [165].

Additional refinement of placodal boundaries occurs along the anterior-posterior axis: Anterior placodes (lens, olfactory, and adenohypophyseal) are characterized by Pax6 expression, trigeminal by Pax3, and posterior placodes (otic and epibranchial) by Pax2. These Pax genes repress one another and so contribute to the segregation of placodes. The importance of Pax2 and 8 in otic induction is underscored by the characterization of Pax2 null and Pax2/8 double null mouse embryos (Table 4). Furthermore, 55 different mutations in *PAX2* have been described in humans with renal coloboma syndrome, with 7% of patients exhibiting hearing loss [166]. However, even Pax2/8 double null mice develop an otic vesicle, although it does not develop past this stage [150]. This suggests that Pax2 and 8 are not master regulators initiating all subsequent events in inner ear development. Although Pax2 serves as a useful marker of otic lineage for inner ear studies, it is expressed in other tissues in the mouse embryo [167–169] and should be considered one of a panel of otic markers when characterizing differentiating stem cells.

The use of FGFs as otic inducers *in vitro* requires consideration of which ligand or ligands to use. Some stem cell differentiation protocols use FGF3 and 10 to produce hair cells as in the embryo [60,65], but others substitute FGF2 [51,58,59,63,64,68,71]. As ligands, FGF3 and 10 have highest affinity for the IIIb isoform of FGFR2 above all other FGF receptors [170,171], and FGFR2IIIb knockout mouse inner ears have a similar phenotype compared to FGF3 knockouts [172]. However, FGF2 activates various isoforms of FGF receptors with broad affinity, including the isoforms favored by

Table 4: Pax2 and Pax8 mutant mouse phenotypes

Genotype	*Mutation*	*Inner ear phenotype*	*Citation*
Pax2$^{Krd/+}$	Large deletion of chromosome 19	Normal auditory brainstem response (ABR)	Keller et al. 1994 [173]
Pax2^{1Neu}	Spontaneous 1-bp insert resulting in early stop codon, identified in 102 X C3H hybrid	Agenesis of cochlea (E14.5) Degeneration of spiral ganglion (E14.5) Enlarged ventral chamber in place of vestibular sensory portions (E14.5)	Favor et al. 1996 [147] *Note: This is the same insertion/frameshift mutation as was described in a family with human renal coloboma syndrome* [174].
Pax2$^{-/-}$	Deletion of 4kb including beginning prior to codon and extending through exon 2, 129sv background, described in Torres et al. 1995 [175]	Agenesis of cochlea (E17) Agenesis of spiral ganglion (E13.5) Normal vestibular development (E17)	Torres et al. 1996 [148]
Pax2$^{-/-}$	Obtained mice from Torres et al. 1995 [175], C57BL/6 background	Rudimentary cochlea (E15.5) Degeneration of cells normally expressing Pax2 in cochlea (E11.5) Degeneration of vestibular and spiral ganglia (E15.5) Distinct saccule often missing (E15.5) *Note: Severity of phenotypes varied amongst embryos.*	Burton et al. 2004 [149]
Pax2$^{-/-}$	LacZ inserted into Pax2, replacing exons 2 and 3, C3H/He background [176]	Absence of cochlear duct (E13.5) Degeneration of cochlear duct and adjacent mesenchyme (E13.5) Degeneration of spiral and vestibular neurons (E13.5) Agenesis of spiral ganglion (E18.5) Utricle, saccule, and cochlea combined into enlarged sack (E18.5)	Bouchard et al. 2010 [150]
Pax8$^{-/-}$	Cre inserted into Pax8 exon 3, C3H/He background [150]	Normal cochlea (E11.5) Normal spiral and vestibular ganglia (E13.5)	Bouchard et al. 2010 [150] *Note: Pax8 null mice are deaf due to athyroidism affecting synaptogenesis. See Christ et al. 2004* [177]
Pax2$^{-/-}$; Pax8$^{-/-}$		Arrest of inner ear morphogenesis at otic vesicle stage (E11.5) Arrest of neuronal development (E11.5)	Bouchard et al. 2010 [150]
Pax2$^{Egfp/Egfp}$	Egfp inserted into 5' regulatory sequence	Otic vesicle observed (E11.5) *Abnormal inner ear morphology observed in perinatal lethal embryo (Our unpublished observation)*	Soofi et al. 2012 [178]

FGF3 and FGF10 [170,171,179]. A study using explants of avian presumptive otic ectoderm showed that otic vesicles could form *in vitro* when attached to the adjacent section of hindbrain [180]. When the hindbrain was removed in this study, the ectoderm did not form vesicles except when FGF2 was added to the media at a high dose (200 ng/mL). In sum, the avian explant study highlights that an inductive cue from the hindbrain (i.e., FGF3) is necessary for otic vesicle formation. It also supports the use of FGF2 as a substitute for FGF3 and FGF10 in the inner ear organoid protocol.

SHH/Pax2 mediates cochlear duct outgrowth as Wnt/Sox2 regulates the prosensory domain

After day 8 of differentiation, otic vesicle-like structures that mature into organoids begin to form. Differentiation proceeds in a self-guided manner: The surrounding tissue presumably provides contact cues and secreted factors that help to differentiate and pattern the vesicles. Yet the nature of the endogenous factors secreted within the stem cell-derived aggregates has not been determined. So far, only one exogenous factor, a Wnt pathway agonist, has been added to the protocol to encourage otic vesicle formation [70].

At E9.0 in the mouse embryo, the otic placode invaginates, forming an intermediate otic cup that closes off to form an otic vesicle, or otocyst, by E9.5 [181]. At E10.5, the vesicle begins to elongate as dorsal vestibular structures and ventral auditory structures begin to take shape [181]. At the same time, neuroblasts delaminate from the ventral aspect, contributing to the cvg [182]. By E11.5, the cochlear duct starts to extend and turn simultaneously until completion of 1.5 turns by E17.5 [181]. During this

time, several major signaling pathways are regulating major morphological changes and specification of prosensory and non-prosensory cells in the inner ear, leading up to differentiation of Atoh1^{+} hair cells beginning around E12.5 in vestibular structures and E14.5 in the cochlea [6,183]. As mentioned, Wnt from the dorsal hindbrain and SHH from the ventral hindbrain and notochord drive dorsal-ventral patterning of the otic vesicle [163,164,184]. This mirrors the dorsal-ventral patterning mechanism well-characterized in the neural tube [185]. In the otic vesicle, SHH promotes ventral genes *Otx2* and *Pax2* and blocks the dorsal marker and Wnt target gene *Dlx5* [163]. In SHH$^{-/-}$ mice, Pax2 upregulated by FGF signaling is not maintained, and the cochlear duct, cvg, and vestibular sensory patches fail to form [163,186]. The effect on the cvg may be due to loss of SHH as a direct mitogenic cue and as a regulator of posterior Tbx1 expression, resulting in repression of the anterior cvg specifier Neurogenin 1 [187,188]. The overall phenotypes of SHH$^{-/-}$ and Pax2$^{-/-}$ mouse inner ears support the hypothesis that Pax2 plays a second role in inner ear development as an anti-apoptotic, proliferative factor promoting cochlear duct outgrowth [149,152,189].

Following otic vesicle formation and patterning, Wnt also takes on a new role as regulator of the Sox2^{+} prosensory domain [190]. In this capacity, it serves to promote specification, proliferation, and differentiation of hair cell progenitors. Deleting the downstream effector β-catenin through tamoxifen-inducible Cre recombinase at E11.5 in mice results in ablation of hair cells at E14.5, whereas expressing a constitutively-active form of B-catenin results in supernumerary hair cells [191]**.** *In vivo* and explant experiments indicate that Wnt activation can re-initiate cell division in post-mitotic progenitors at E13.5 and increase the number of hair cells [191].

Sox2 is also necessary for hair cells, supporting cells, and inner ear neurons to differentiate [192–194], and Wnt is required for normal expression of Sox2 in the developing ear [190]. In mice, Sox2 is first detected in the otic placode at E8.5 and preferentially marks the ventral side of the otic vesicle at E9.5 [192,195–197]. By E12.5, Sox2 (together with Jag1 [198] and $p27^{Kip1}$ [7]) marks the prosensory domain of supporting cell and hair cell progenitors [199]. It becomes downregulated in hair cells as they differentiate from E14.5 in the cochlea and is generally restricted to supporting cells soon after birth [16,199]. Misexpression of Atoh1 in the mammalian embryonic organ of Corti can induce formation of new hair cells from nonsensory cells primarily via transdifferentiation [193,200–202]; however, this does not occur in Sox2 knockout mouse explants [203].

Both β-catenin and Sox2 are able to interact directly with the 3' enhancer of Atoh1 [203–206]. When Sox2 is expressed at a sufficiently high level, its relationship with Atoh1 is mutually repressive [199,204]. Recent evidence from mouse cochlear explants supports the model that transient expression of Sox2 confers competence of prosensory cells to differentiate in response to Atoh1 [203]. Similarly, Wnt signaling at high or low levels may have distinct effects, promoting proliferation or differentiation, respectively [190]. This helps to reconcile the roles of Wnt in both proliferation and differentiation, which otherwise are seemingly at odds.

The extent to which Wnt depends upon Sox2 for its effects on the prosensory domain—and whether this is necessarily mediated through a Notch ligand Jag1 in a lateral induction model [198,207–210]—remains unclear. What is clear, however, is the complexity of signaling cues in inner ear development, especially at this stage when the

tapestry of cell types is weaving itself together. Many other pathways are acting concurrently to regulate the timing of differentiation throughout the ear [184]. These include SHH (promoting proliferation, delaying differentiation, and regulating medial-lateral cell patterning [187,211–215]), BMP (regulating medial-lateral cell patterning and prosensory competence [216,217]), Notch (regulating prosensory competence through proposed mechanism of lateral induction [198,207,218,219]), and FGF (first promoting proliferation and then differentiation [220,221]). Through these pathways, a complicated set of interactions takes place both within the sensory patches and between them and the surrounding tissues. The inner ear organoid protocol offers a useful framework for producing sensory patches in context of secreted and structural cues from other cell types. Discovering the nature of these cues is goal of future research. Continuing to pull apart the threads of embryonic development may also reveal a pattern of cues that can be replicated through artificial means, providing better control and improved yields.

Hair cell markers for monitoring *in vitro* differentiation yields

The developmental mechanism of hair cell differentiation from prosensory cells is lateral inhibition driven by Notch signaling [53]. Upregulation of Atoh1 drives expression of the Notch ligand Dll1, activating the Notch receptor on the surface of a neighboring cell, leading to its repression of Atoh1 [54]. This produces both $Atoh1^{+}$ hair cells and $Atoh1^{-}$ supporting cells. At the end of the inner ear organoid protocol, hair cells associated with supporting cells and neurons are evident. The ability to distinguish them depends on unique fate markers. However, definitive markers of inner and outer auditory hair cells, type I and type II vestibular hair cells, and the various supporting cell

types have been difficult to pinpoint. Markers that seem exclusive to one population of cells are generally also found in another population at a different time in development. Sox2 is a prime example: It is expressed in all prosensory progenitors but downregulated in hair cells, with the exception of a subset of vestibular hair cells that retain Sox2 into adulthood [222]. Another example is calretinin, which has been used as a marker of type II vestibular hair cells produced in organoids. Its expression is highly variable between P13 and adulthood and can be detected at times in each type of cochlear and vestibular hair cell [223].

Because clinical strategies to address severe deafness are currently inadequate, the need for a reliable means to regenerate inner hair cells is particularly acute. Directing differentiation towards inner hair cell fate is the focus of ongoing efforts through application of exogenous factors involved in otic vesicle patterning. To convincingly characterize outcomes, staining for a small set of cochlea-specific and inner hair cell-specific markers would be ideal. With the advent of high-throughput and single-cell transcriptomics techniques, comparing specific cell populations at timepoints throughout development is possible [224–226]. These kinds of analyses are expected to reveal new markers for cell types contained within inner ear organoids. Furthermore, RNA sequencing (RNASeq) is allowing stem cell researchers to assess the similarity of organoids to native tissues, predictive of their utility for transplantation [74,227–230]. In these ways, the field is moving toward clinical application of stem cell technology and restoration of function.

SUMMARY OF EXPERIMENTS

Inner ear organoids contain cells comparable to native hair cells with respect to several features. These include F-actin-rich stereocilia-like bundles, Myo7a expression, and markers of synapses with associated neurons. However, the derived hair cells appear to be immature and limited to vestibular phenotypes. Furthermore, the yield of derived hair cells must be improved to permit downstream applications of the inner ear organoid method. Given that the method was modeled on stages of embryonic development, we sought to harness developmental cues that could address these outstanding issues.

The experiments described in Chapter 2 were performed with a novel embryonic stem cell line modified with a reporter for Pax2, which is upregulated in inner ear progenitors following otic induction. We used this line to study parallels between otic induction during organoid formation and embryogenesis via cell and molecular biology. Our results supported a proposed mechanism involving ERK downstream of FGF receptor activation. We anticipate that these results will lead to experiments optimizing ERK activation to maximize the yield of otic progenitors capable of differentiating into hair cells. Additionally, our investigation yielded insight into the formation of organoid-associated neurons, another potential focus of future investigation.

The experiments described in Chapter 3 were focused on the TGFβ signaling pathway. We investigated the necessity of TGFβ inhibition for deriving otic progenitors and hair cells. We found that inhibition was necessary for organoid-stage hair cells but not for vesicle-stage progenitors. We also found evidence that the mechanism of TGFβ inhibition influenced the efficiency of vesicle formation. Using RNASeq, we performed a

comparative transcriptomics analysis of embryonic and derived otic vesicles; derived tissues were prepared with and without TGFβ inhibition at the first step of directed differentiation. Our analysis revealed differences between native and derived vesicles as well as between TGFβ-inhibited and uninhibited tissues. TGFβ inhibition is the first step in directing differentiation using the inner ear organoid protocol. Thus, understanding the influence of TGFβ signaling on hair cell fate has the potential to significantly improve outcomes.

From both investigations, potential targets for future experiments emerged. Manipulating developmental pathways guided by our results may lead to increased yields, improved maturation, or auditory rather than vestibular phenotypes. An overall discussion of the completed experiments and ongoing research in Chapter 4 describes how these improvements would significantly advance the hair cell regeneration efforts toward envisioned applications in research and medicine.

CHAPTER 2: Pax2^{EGFP} cell line illuminates key stages of development in mouse inner ear organoid model[3]

INTRODUCTION

Hair cells, the mechanoreceptors of the inner ear, are essential to auditory and vestibular function. In mammals, hair cell loss ultimately results in permanent sensory deficits: Cochlear hair cells do not spontaneously regenerate after loss or damage, and the regenerative capacity of vestibular organs is limited [232]. The advancement of therapies towards functional restoration is, consequently, an urgent goal of biomedical research.

Stem cells are heralded as the key to replacing damaged tissues as well as modeling disease states in the laboratory. To realize this potential, we must establish reliable routes from naïve pluripotency to mature cell fates. One approach is to follow cues from developmental literature, supplying signaling molecules as switches guiding differentiation along known pathways. During embryonic development, cochlear and vestibular organs and cochleovestibular neurons develop from thickened regions of surface ectoderm between the neural plate/crest and epidermis. These regions, the otic placodes, are influenced by morphogens secreted from surrounding tissues including

[3] This chapter has been accepted for publication as an original research report [231]: Schaefer SA, AY Higashi, B Loomis, T Schrepfer, G Wan, G Corfas, GR Dressler and RK Duncan (In press). From otic induction to hair cell production: Pax2^{EGFP} cell line illuminates key stages of development in mouse inner ear organoid model. Stem Cells Dev.

the underlying mesoderm (FGFs), neural plate (FGFs), dorsal neural tube (Wnts and BMPs), and ventral neural tube (SHH) (reviewed in [233]).

Koehler et al. recently pioneered a method for generation of inner ear sensory epithelia using a 3-dimensional stem cell culture paradigm [68,69]. Their protocol was built upon methods for making retinal and cerebral organoids from aggregates of mESCs in serum-free culture (i.e., SFEBq) [73,234,235]. The initial SFEBq methods were remarkably simple, belying the complexity of the tissues they produced and exploiting the tendency of dissociated mESCs to default to neural fates under serum-free conditions [107,236]. Two key modifications based on developmental mechanisms resulted in otic tissue: Differentiation was guided towards non-neural ectoderm via regulation of TGFβ/BMP signaling pathways [88,103] and subsequently towards otic placode via regulation of BMP and FGF signaling [130,142,143,237].

During formation of the otic placode, the specialized ectoderm from which all inner ear structures develop, FGF signaling upregulates the transcription factor Pax2 [143,161,238–240]. Although Pax2 is expressed in multiple embryonic tissues [167–169], it is commonly regarded as indicative of otic lineage in hair cell regeneration studies [58–60,63,68]. In this study, we produced inner ear organoids using mESCs with a reporter for expression of Pax2. We demonstrated the utility of such a reporter system in identifying vesicle formation in live cultures and the maintenance of marker expression through terminal hair cell differentiation. This allowed a direct relationship to be established between exogenous FGF2 dose and formation of otic vesicle-like structures. The dose of FGF2 also corresponded directly with ERK phosphorylation, suggesting that ERK mediates otic induction in this model system as in avian and

zebrafish embryos [241,242]. Finally, we compared neurons that arise in these organoids with embryonic neuroblasts and identified opportunities for future investigation of neurogenesis.

Overall, we draw parallels between several features of our organoids and developing inner ears. The efficiency of self-patterning in organoid cultures fluctuates, however, with multiple determinants in need of clarification. Therefore, since our evidence supports the use of inner ear organoids as a developmental model, we present insights into troubleshooting in hopes of advancing the field towards achieving the promise of stem cell technology.

MATERIALS AND METHODS

Mice

All mice were housed per institutional standards and used according to experimental protocols approved by the University of Michigan Institutional Animal Care and Use Committee.

We used mice carrying the *Pax2*^{EGFP} allele, in which enhanced green fluorescent protein (EGFP) coding sequence is inserted upstream of the Pax2 translational start site, and wild-type (WT) controls on the same genetic background [178]. Breeding cages with Pax2$^{EGFP/+}$ mice were set up to obtain embryos of all three genotypes; postnatal studies were performed only with WT and Pax2$^{EGFP/+}$ genotypes as the Pax2$^{EGFP/EGFP}$ genotype is perinatal lethal due to renal agenesis [178]. Genotyping was performed using the following primers: EGFP-F (5'-CTCGTGACCACCCTGACCTA-3'),

EGFP-R (5’-GTCCATGCCGAGAGTGATCC-3’), WT-F (5’-ACCGTATTACCGCCATGCAT-3’), WT-R (ACCTCTACAAATGTGGTATGGCT-3’). Amplification with EGFP primers results in a 525-bp PCR product, and WT result in a 230-bp PCR product. Presence of the 525-bp product represents the *Pax2*^{EGFP} allele.

To prepare images of marker expression at roughly equivalent developmental stages in comparison with differentiating mESC aggregates, timed pregnant C57BL/6 mice at E11.5 and E15.5 were obtained from The Jackson Laboratory. Embryos were collected at E11.5 and E15.5, fixed in 4% paraformaldehyde (PFA), cryoprotected with sucrose, and cryosectioned in OCT in transverse and parasagittal planes at 12 μm thickness. Staining of cryosections was performed according to the method described for mESC aggregates below.

Auditory brainstem response (ABR) recording

Mice were anesthetized with 65-120 mg/kg ketamine and 7 mg/kg xylazine, with or without 2 mg/kg acepromazine, administered intraperitoneally prior to the procedure. Mice were then placed on a heating pad inside the recording booth. Electrodes were then attached at the vertex of the head, beneath the test ear, and beneath the contralateral ear. Acoustic stimuli consisting of 4 ms tone bursts with 1 ms rise and fall times were delivered from a speaker at 30 bursts per second via a tube placed just outside the ear canal. Auditory evoked potentials were recorded at three tone frequencies: 8, 16, and 32 kHz. Data were acquired using the Tucker Davis Technologies System III, with up to 1024 responses averaged for each stimulus. Recordings began at 80 dB SPL, which was sufficient to elicit a response. Stimulus level was reduced systematically in 5-10 dB decrements. The minimum level eliciting a

reproducible waveform was determined to be the response threshold. The recording system was routinely calibrated in a closed system using a reference microphone and lock-in amplifier.

Derivation of Pax2^{EGFP} mouse embryonic stem cells

Blastocysts were flushed from the uterine horns of Pax2$^{EGFP/+}$ females 3.5 days after mating to Pax2$^{EGFP/+}$ males. Individual blastocysts were placed in wells of a 96-well culture plate seeded with irradiated mouse embryonic fibroblast (MEF) feeder cells in DMEM (high glucose, Gibco) supplemented with 15% fetal bovine serum (FBS; Harlan), 0.1 mM β-mercaptoethanol (Sigma), 50 IU/mL penicillin and 50 µg/mL streptomycin (Gibco), 1000 U/mL leukemia inhibitory factor (LIF; Chemicon), and 12.5 µM PD98059 (Sigma). Inner cell mass outgrowths were trypsinized and passaged sequentially until mESC lines were established in 35-mm cell culture dishes. For genotyping, mESCs were passaged on gelatin-coated dishes twice to eliminate feeder cells before being genotyped as described [178]. For expanding cultures, mESCs were maintained on irradiated MEF cells with media consisting of DMEM (Gibco), 15% FBS (Atlas Biologicals), 1X sodium pyruvate, 1X non-essential amino acids, 2X Glutamax, and 0.1 mM β-mercaptoethanol (all from Gibco), and 1000 U/mL LIF (ESGRO). Cells used in this study were frozen at passage 8, thawed, and expanded in feeder-free culture conditions before organoid formation.

mESC cultures

Embryonic stem cells from the Pax2$^{EGFP/+}$ mouse line were used to generate organoids between passages 13-17. Pluripotency staining was performed at passages

10 and 21. Colonies were maintained in feeder-free conditions on a 0.1% gelatin substrate with maintenance medium consisting of DMEM (high glucose, Gibco), 10% fetal bovine serum (Atlas Biologicals), 1.5 mM L-glutamine (Gibco), 5.4 mM HEPES (Gibco), 5.4 μM β-mercaptoethanol (Sigma), and 500 U/mL LIF (Gibco). At passage, colonies were dissociated to single cells using Cell Dissociation Buffer (Gibco) with 0.5 M EDTA solution (AccuGENE).

Differentiation protocol

Spherical aggregates of mESCs were differentiated according to the inner ear organoid protocol modified from Koehler et al. [68,69]. In brief, mESC colonies were dissociated to single cells and aggregated at 3000 cells per well in round-bottom 96-well Nunclon Sphera Microplates (Thermo Scientific) in 100 μL ectodermal differentiation medium. Medium consisted of GMEM, 10% KnockOut serum replacement (KSR), 15 mM HEPES, 1X non-essential amino acids, 1 mM sodium pyruvate (all from Gibco), and 0.1 mM β-mercaptoethanol (Sigma). Y-27632 (Calbiochem) was included in the medium at 10 μM on day 0 only.

On day 1, half of the volume was replaced with medium containing growth factor reduced (GFR) Matrigel (Corning) to achieve 2% final concentration. On day 3, 25 μL of medium containing SB431542 (1 μM, Stemgent) and BMP4 (10 ng/mL, Stemgent) was added to each well. On day 4.5, 25 μL of medium containing LDN193189 (1 μM, Stemgent) and FGF2 (0, 5, 25, or 100 ng/mL, Sigma) was added to each well. Aggregates were transferred into a new 96-well plate in 200 μL maturation medium containing 1% GFR Matrigel on day 8, with half of the medium exchanged daily for the remainder of the protocol. Maturation medium consisted of Advanced DMEM/F12, 1X

N-2 Supplement, 15 mM HEPES, and 1X Glutamax (all from Gibco). CHIR99021 (3 μM, Stemcell Technologies) was optionally added on day 8 as noted.

Modifications to the Koehler et al. protocol included our use of Y-27632, use of 10% KSR in the ectodermal differentiation medium instead of 1.5%, variation of FGF2 dose, and use of non-enzymatic dissociation buffer for passaging and forming aggregates from mESCs.

Immunostaining

Aggregates were collected, fixed 20 minutes to overnight in 4% PFA, and rinsed in phosphate-buffered saline (PBS) prior to further processing.

For staining of cryosections, fixed aggregates were cryoprotected via 30-minute incubations with increasing concentrations of sucrose up to 30% in PBS. Following overnight incubation in 30% sucrose at 4°C, aggregates were incubated 4-5 hours in a 1:1 mixture of 30% sucrose and OCT at room temperature, incubated 1 hour in OCT, and frozen in cryomolds on dry ice. A Leica 3050S cryostat was used to section tissue at 10-μm thickness. Slides were dried overnight, rehydrated in PBS for 15 minutes, and then transferred to humid chambers for the remainder of the staining procedure. Sections were blocked and permeabilized 15 minutes with 10% normal donkey serum (NDS) and 0.1% Triton X-100. Primary antibodies were applied overnight at 4°C in a 1:1 mixture of blocking/permeabilization solution with PBS. Alexa Fluor secondary antibodies were applied at 1:500 in PBS for 1 hour at room temperature with slides covered to prevent photobleaching. Nuclei were counterstained by 5-minute incubation with Hoechst 33242. Coverslips were added with ProLong Gold Antifade Mountant (Molecular Probes). For a list of antibodies used, refer to Table S1. Control tissues

stained without primary antibody were used to ensure that the Pax2^{EGFP} signal would not preclude use of green fluorophores.

For staining of whole-aggregate tissue, fixed aggregates were processed as described previously [69]. To prepare a custom imaging chamber, Sylgard 184 (1:10) prepared at approximately 1-mm thickness was cut to fit glass slides, and a metal punch was used to create a well to hold ScaleA2 solution containing a stained aggregate. A coverslip was placed across the well, and the imaging chamber was sealed with clear nail polish.

For staining of isolated organoids, fixed aggregates were transferred to PBS for microdissection of the hair cell-containing regions. Minutien pins were used to stabilize aggregates against 35-mm dishes of Sylgard while hair cell-containing cysts were dissected using iris scissors and fine forceps. The regions of protruding cysts distal to the aggregate bodies were cut open using scissors to expose the apical surfaces of hair cells, and the aggregate bodies were cut or teased away using scissors or forceps and discarded. The hair cell-containing epithelia were retained. Custom-made microwells were used to process single tissues in small solution volumes. Organoids were blocked and permeabilized in PBS with 5% NDS and 0.1% Triton X-100 for 15 minutes and incubated in primary antibodies in blocking/permeabilization solution overnight at 4°C. Alexa Fluor secondary antibodies (1:500) and phalloidin conjugates (1:100) were added in PBS for 1 hour at room temperature, and Hoechst 33242 was applied for 5 minutes at 1:2500 in PBS. Organoids were mounted using ProLong Gold.

For staining of mouse organs of Corti, 4-week-old WT and Pax2$^{EGFP/+}$ mice were decapitated under anesthesia (80 mg/kg ketamine and 20 mg/kg xylazine). Each

temporal bone was removed, and each inner ear was placed into 4% PFA. The cochlear duct was then perfused with 4% PFA by perforating the cochlear windows and apex. Following dissection, surface preparations of the apical turn were blocked and permeabilized in 5% normal donkey serum and 0.1% Triton X-100 in PBS for 1 hour at room temperature and incubated in primary antibody overnight at 4°C. After extensive washes, the preparations were stained with Alexa Fluor secondary antibodies (1:500) and Alexa Fluor 488 phalloidin (1:200) for 2 hours and counterstained by a 5-minute application of Hoechst 33242 (1:2500). After a final series of washes in PBS, preparations were mounted using ProLong Gold.

For pluripotency staining, colonies grown on gelatin-coated coverslips or in 6-well culture plates were washed with PBS and fixed with 4% PFA for 15 minutes. They were then blocked and permeabilized in PBS with 5-10% NDS and 0.1% Triton X-100 for 15 minutes. Primary antibodies were diluted in PBS or a 1:1 mixture of blocking/permeabilization solution for incubation at 4°C overnight. Alexa Fluor secondary antibodies (1:500) were diluted in PBS for incubation at room temperature for 1-2 hours. Hoechst 33242 was then applied for 5 minutes at 1:2500 in PBS. Brightfield and epifluorescence images were obtained using Leica DM IL and Olympus BX51WI microscopes. Confocal images were obtained using Olympus FluoView 1000, Leica TCS SP5, and Leica TCS SP8 confocal microscopes.

FM 4-64FX labeling

For live-imaging of FM 4-64FX dye labeling, a day 20 organoid (with distal portion of cyst removed to expose hair cells) was dissected away from the aggregate body, affixed to a collagen droplet in a 35-mm dish, and maintained through day 33.

After dissection, the culture was maintained in serum-free medium consisting of 1X Basal Medium Eagle (Sigma), 2.2 g/L sodium bicarbonate, 1X insulin-transferrin-selenium-ethanolamine (ITS-X, Gibco), 1% bovine serum albumin, 5 mg/mL glucose, and 8.8 U/mL penicillin G (Sigma). A stock solution of 2 mM FM 4-64FX in distilled water was prepared and stored at -20°C. The 5 μM working solution was prepared immediately before use by 1:400 dilution with low-calcium Hank's Balanced Salt Solution (LC-HBSS), prepared by adding 0.1 mM $CaCl_2$ to HBSS (Gibco) and filter-sterilizing. The organoid tissue to be labeled was rinsed in LC-HBSS, incubated 10 seconds in FM 4-64FX working solution at room temperature, and washed three times with LC-HBSS for 1 minute per wash. The time needed to add and remove the dye, taking care not to dislodge the tissue, and add the first wash totaled less than 30 seconds. Organoids were immediately imaged live in LC-HBSS.

Aminoglycoside treatment

Organoids were dissected and maintained on collagen droplets as described above. On day 33 of culture, gentamicin (Sigma) was applied to the media at 6 μM final concentration. After 72 hours, organoids were fixed in 4% PFA for 30 minutes at room temperature, and assayed for presence of stereocilia bundles via staining with rhodamine phalloidin (1:100, Thermo Fisher Scientific).

FGF assay

Solutions containing 1 μM LDN193189 and varying concentrations of FGF2 in ectodermal differentiation medium were prepared and added at day 4.5 of the differentiation protocol. After brief incubation at 37°C in a humidified culture incubator

with 5% CO2, aggregates were collected and rinsed twice with pre-chilled PBS with 1X Halt Phosphatase Inhibitor Cocktail (Thermo Scientific). Aggregates were lysed in RIPA Lysis and Extraction Buffer (Thermo Scientific) with 1X PI. For lysis, aggregates were incubated 15 minutes on ice and sonicated on ice in three 10-second pulses at 50% power. Lysates were centrifuged at 14000xg for 15 minutes and supernatants retained. Total protein concentration was assayed using BCA Protein Assay Kit (Thermo Scientific).

Western blotting

Lysates were diluted 1:1 with 2X Laemmli buffer from Bio-Rad (1610737) and denatured at 95°C for 5 minutes. 4-15% Bio-Rad Mini Protean TGX gels were loaded with equal amounts of total protein per well. Molecular weight standards from Bio-Rad (1610317) and Cell Signaling Technology (7720) were used. Proteins were transferred to nitrocellulose membranes, and membranes were blocked with 5% non-fat dry milk in TBS + 0.1% Tween (TBST) for 1 hour. Primary antibody incubations were performed overnight in TBST at 4°C. Horseradish peroxidase (HRP)-conjugated secondary antibody incubations were performed for 1 hour in TBST at room temperature. For a list of antibodies used, refer to Table S1. ECLs included SuperSignal West Pico (Thermo Scientific) and Amersham ECL Select (GE Healthcare). Images were obtained using a FluorChem SP system (Alpha Innotech). Densitometry was performed using Fiji software (version 2.0).

Vesicle and organoid quantification

The percentage of aggregates with at least one organoid, indicated by EGFP signal at the base of a protruding cyst, was quantified at day 20. The percentage of aggregates with at least one visible $EGFP^+$ otic vesicle-like structure was estimated at day 12 using epifluorescence. This analysis excluded vesicles not yet formed at day 12 or not visible due to orientation away from the camera. Since all organoids arose from vesicles, quantifying the percentage of aggregates with vesicles identified at day 12 *or* organoids at day 20 (referred to as "% vesicle- or organoid-positive") more accurately reflected the total number of vesicle-positive aggregates. Note that this percentage does not double-count aggregates in which both structures were identified.

Aggregate size measurements

Average long-axis diameter of 4 aggregates per timepoint was measured from brightfield images in Fiji software (version 2.0) [243]. Data were averaged across multiple cultures and plotted to track changes in aggregate size over time.

Statistical analysis

Statistical comparisons between two groups were performed using unpaired t-tests in Microsoft Excel. Comparisons amongst more than two groups were performed by one-way ANOVA with Tukey's post-hoc test using the XLSTAT plug-in.

RESULTS

Pax2$^{EGFP/+}$ mice develop normal inner ears

To develop a reporter system for monitoring otic induction during inner ear organoid formation, we derived mESCs from mice encoding EGFP between 5' regulatory elements and the endogenous Pax2 transcription start site in one allele (Figure 5A) [178]. Mice with a single copy of the allele (Pax2$^{EGFP/+}$) develop normal kidneys and midbrain-hindbrain tissues [178]. Moreover, they appear to form normal otic vesicles, with EGFP in the ventromedial domain where Pax2 is expressed (Figure 5B-D') [169], as do the majority of mouse lines carrying Pax2 loss of function alleles [148–150,178]. No apparent difference was seen in the gross morphology of cochlear and vestibular structures in Pax2$^{EGFP/+}$ mice compared to WT animals (data not shown). To investigate more closely, we stained whole-mount preparations of the organ of Corti from adult Pax2$^{EGFP/+}$ and WT littermates for markers of hair cells and neurons. Staining for Myo7a, an unconventional myosin characteristic of hair cells, and phalloidin-labeling of F-actin-rich hair bundles revealed the characteristic pattern of three rows of outer hair cells and one row of inner hair cells in both WT and Pax2$^{EGFP/+}$ mice (Figure 5E-F'). Tuj1 staining revealed robust peripheral projections extending towards the hair cells, with some continuing past the inner hair cells and into the outer hair cell region. In 1 of 3 Pax2$^{EGFP/+}$ embryos, we detected an aberrant pattern of innervation: Instead of extending radially towards the outer hair cells, multiple neurites traversed the tunnel of Corti at acute angles, occasionally parallel to the curvature of the organ of Corti. Auditory brainstem response (ABR) testing was performed on postnatal mice at 4 weeks of age to measure thresholds for response to auditory stimuli. Three frequencies, processed by different regions of the mouse cochlea, were presented: 8,

16, and 32 kHz. Average thresholds from WT and Pax2$^{EGFP/+}$ mice were not significantly different at any frequency (unpaired t-test, p>0.5, n=4 mice per genotype) (Figure 5G). Overall, our investigation of Pax2$^{EGFP/+}$ mice revealed normal auditory and vestibular function based on ABR testing for auditory-evoked potentials and absence of behavioral signs of vestibular dysfunction (e.g., circling, head bobbing, or torticollis). The *Pax2^{EGFP}* allele, therefore, reports a normal pattern of Pax2 expression and permits development of the inner ear from the otic vesicle to mature auditory and vestibular organs in heterozygotes. This supports the use of Pax2$^{EGFP/+}$ embryonic stem cells to produce inner ear organoids.

Pax2$^{EGFP/+}$ mESCs form inner ear organoids

Clonal mESCs were obtained from Pax2$^{EGFP/+}$ blastocysts (clone C5, Figure 2A). We transitioned these cells from MEF dependence to feeder-free maintenance on gelatin. At passage 10, Pax2$^{EGFP/+}$ cells were screened for the pluripotency marker Oct3/4, which was uniformly expressed throughout colonies (Figure 6B-B'''). To assay maintenance of pluripotency, cells were stained at passage 21 for a panel of pluripotency markers (Figure 6C-E'''). Oct3/4, Sox2, and Rex1 were uniformly expressed, but Klf4 and Nanog were variable with regards to staining intensity and the percentage of positive cells, suggesting that some cells in these populations may be switching between naïve and epiblast-like states.

Pax2$^{EGFP/+}$ cells at passages 13-17 were evaluated for capacity to generate inner ear organoids (Figure 7A). At day 0, mESC aggregates were formed, and their size expansion was tracked over the course of the protocol (Figures 7B and S1). When

1.5% KSR was included in the ectodermal differentiation medium as per the original protocol, aggregates expanded at a slower rate than expected and never reached the 1.5-2 mm diameter by day 12 described by Koehler and Hashino [69]. When 10% KSR was used, aggregates began at an average diameter of 320.3 ± 21.6 μm (n=21) at day 1 and expanded to 1054.3 ± 36.0 μm by day 8 (n=11) after 100 ng/mL FGF2 was applied at day 4.5. By day 20, aggregates treated in this way reached a final diameter of 1449.9 ± 81.7 μm (n=6). The final diameter of aggregates treated with 25 ng/mL FGF2 at day 4.5 (n=5) was not significantly different (p=0.201). Additionally, the inclusion of the Wnt signaling agonist CHIR99021 during early maturation did not appear to affect aggregate size. For all experiments going forward, the ectodermal differentiation medium contained 10% KSR, a departure from the original inner ear organoid protocol, which may reflect a unique requirement of this cell line.

Guided differentiation along the otic lineage was assessed via immunofluorescence staining of cryosections. Following treatment with BMP4 and an inhibitor of TGFβ signaling SB431542 (B/S) at day 3 to encourage differentiation of non-neural ectoderm and reduce mesoderm and endoderm, the aggregates formed a layer positive for E-cadherin (ECAD) and Tfap2a (AP2) (Figure 7C-F). This layer, detected at day 5-6, excluded staining for brachyury and N-cadherin (NCAD), markers of mesendoderm and neural ectoderm, respectively.

The addition of FGF2 and an inhibitor of BMP signaling LDN193189 (F/L) at day 4.5 guided non-neural ectoderm toward preplacodal and, specifically, otic placodal fate. By day 12, otic vesicle-like structures were easily visualized due to the upregulation of EGFP driven by the Pax2 promoter (Figure 3G-H). In trials of 1.5% KSR, we observed

Figure 5: Features of Pax2^{EGFP} reporter system and characterization of Pax2$^{EGFP/+}$ mice and WT controls at 4 weeks

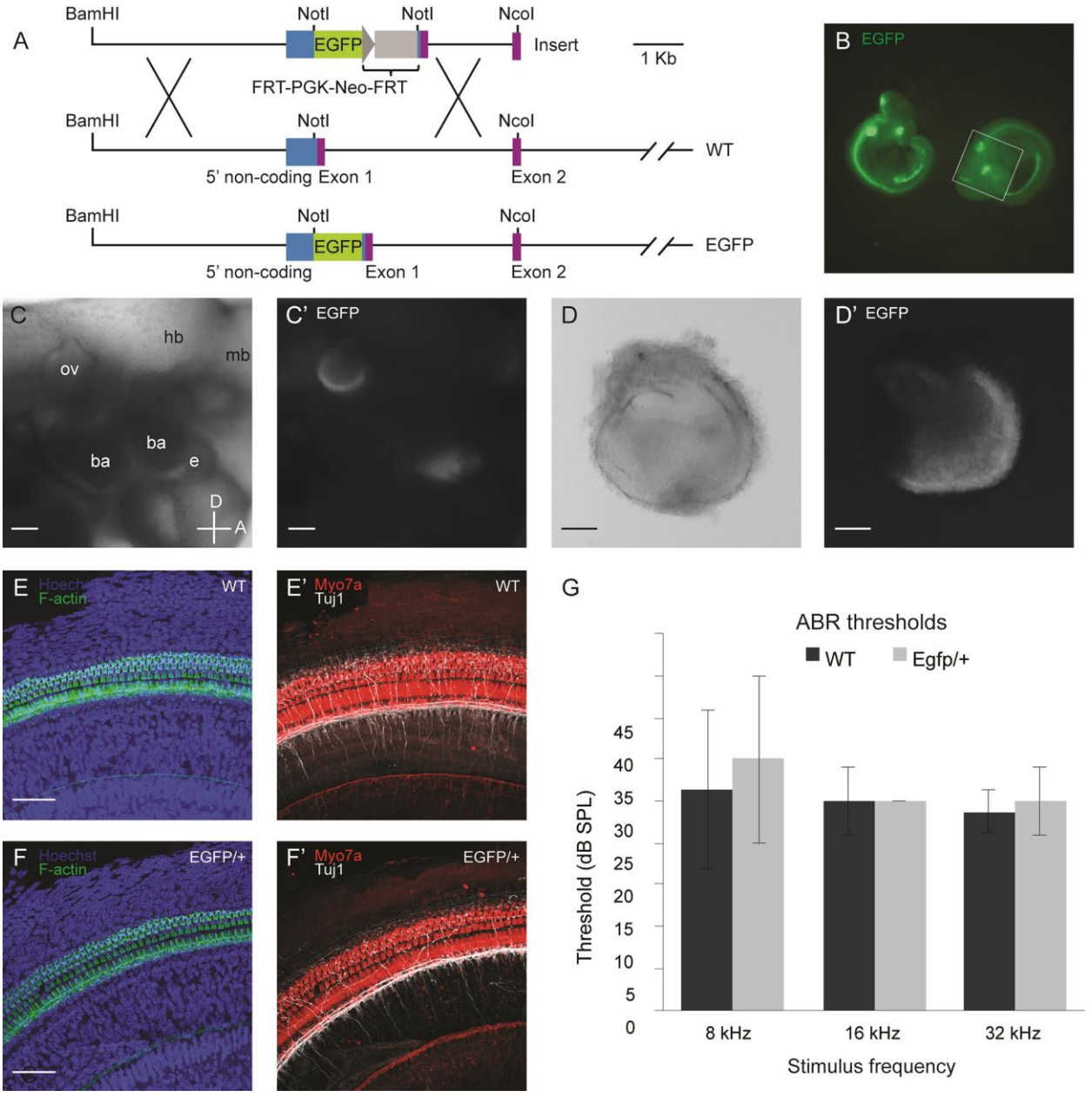

Features of Pax2^{EGFP} reporter system and characterization of Pax2$^{EGFP/+}$ mice and WT controls at 4 weeks postnatal. A: Schematic for creating the *Pax2^{EGFP}* allele, adapted from Soofi et al. 2012 [178]. BamHI-NotI and Not-NcoI arms homologous to 5' Pax2 sequence were ligated with an EGFP-PGK-Neo construct. This resulted in insertion of EGFP-PGK-Neo just upstream of the translation start site. Clones resistant to neomycin were obtained. Mice expressing this sequence were crossed with Flippase mice, removing the PGK-Neo fragment and resulting in Pax2$^{EGFP/+}$ mice. Both Pax2$^{EGFP/+}$ and Pax2$^{EGFP/EGFP}$ mESC lines were then derived. B: Epifluorescence image of Pax2$^{EGFP/EGFP}$ (left) and Pax2$^{EGFP/+}$ (right) embryos at E10.5. EGFP expression marks Pax2^{+} tissues including otic vesicles. C-C': Lateral, close-up view of Pax2$^{EGFP/+}$ embryo at E10.5. Box in panel B marks the region shown in panels C-C'. D-D':

Isolated otic vesicle from $Pax2^{EGFP/+}$ embryo. E-F': Immunofluorescence staining of Organ of Corti surface preparations from $Pax2^{EGFP/+}$ and WT mice. Mid-apical regions are shown. In both genotypes, stereocilia bundles rich in F-actin and cell bodies expressing Myo7a were present in the typical pattern: 1 row of inner hair cells and 3 rows of outer hair cells. Equivalent staining of neuronal projections marked by Tuj1 in $Pax2^{EGFP/+}$ and WT tissues suggested normal innervation as well. G: Thresholds for auditory evoked potentials measured by ABR testing of WT (dark bars) and $Pax2^{EGFP/+}$ (light bars) mice. No significant difference in sound response was found at any of the three frequencies presented (unpaired t-test, $p>0.5$, n=4 mice per genotype; mean ± standard deviation). Scale bars: 1 mm (B), 200 µm (C-C'), 100 µm (D-D'), 50 µm (E-F').

Figure 6: Establishment of Pax2$^{EGFP/+}$ mESC line

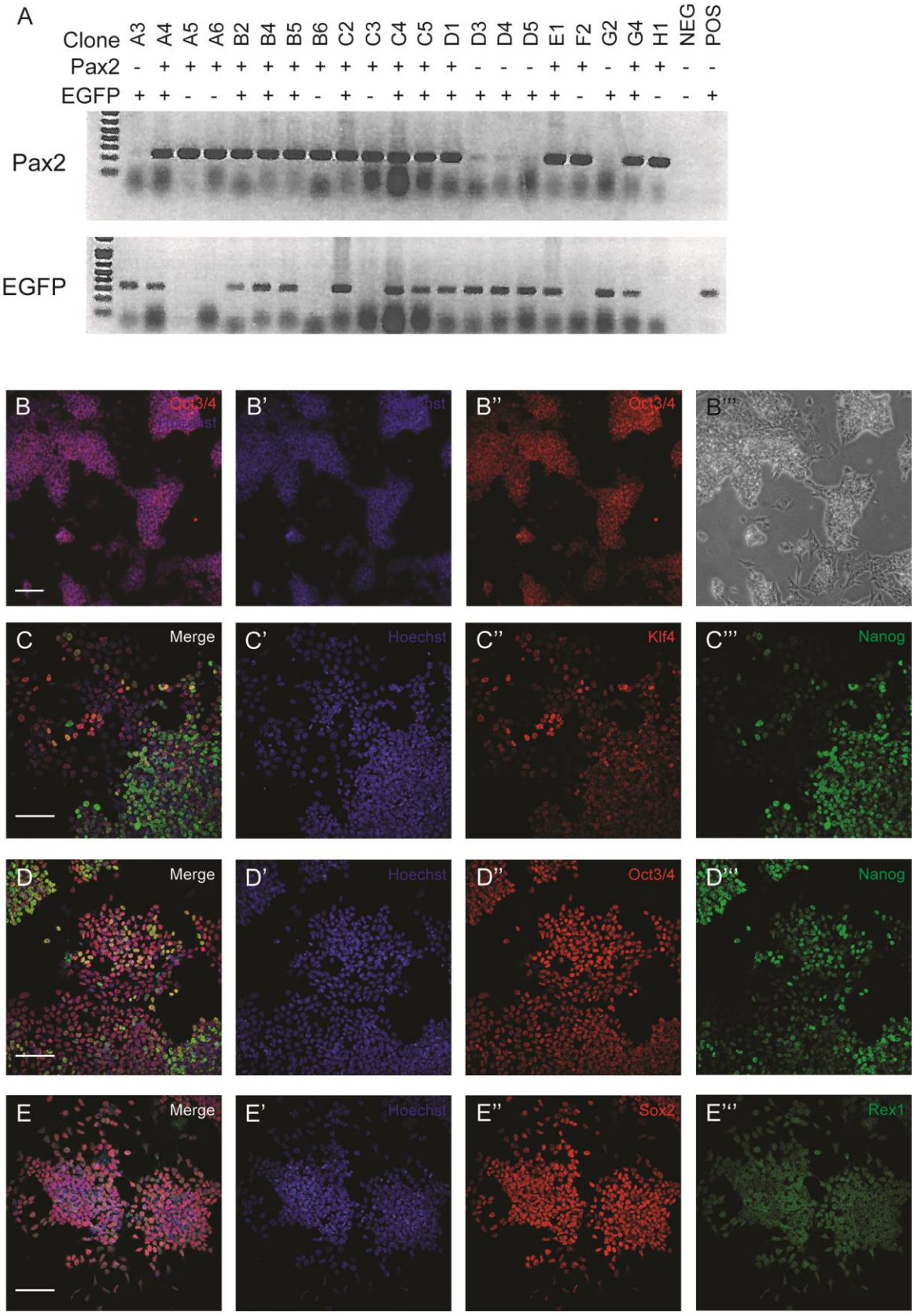

Establishment of $Pax2^{EGFP/+}$ mESC line. A: Genotyping mESC lines at the Pax2 locus. Blastocysts from a $Pax2^{EGFP/+}$ heterozygous cross were cultured in embryonic stem cell media and clonally isolated. DNA from individual clones were analyzed for the WT *Pax2* allele. PCR and primer pairs were as described previously [178]. The cells used in this study were from clone C5. B-B''': Brightfield and epifluorescence images of $Pax2^{EGFP/+}$ mESC colonies stained at passage 10. Oct3/4 staining throughout colonies supports characterization as pluripotent, undifferentiated stem cells. C-E''': Epifluorescence images of $Pax2^{EGFP/+}$ mESC colonies stained at passage 21 to assay maintenance of pluripotency. Note uniform expression of Oct3/4, Sox2, and Rex1 in D'', E'', and E''' but variable expression of Klf4 and Nanog in C'', C''', and D'''. Scale bars: 100 μm (B-E''').

Figure 7: Process of forming Pax2$^{EGFP/+}$ organoids

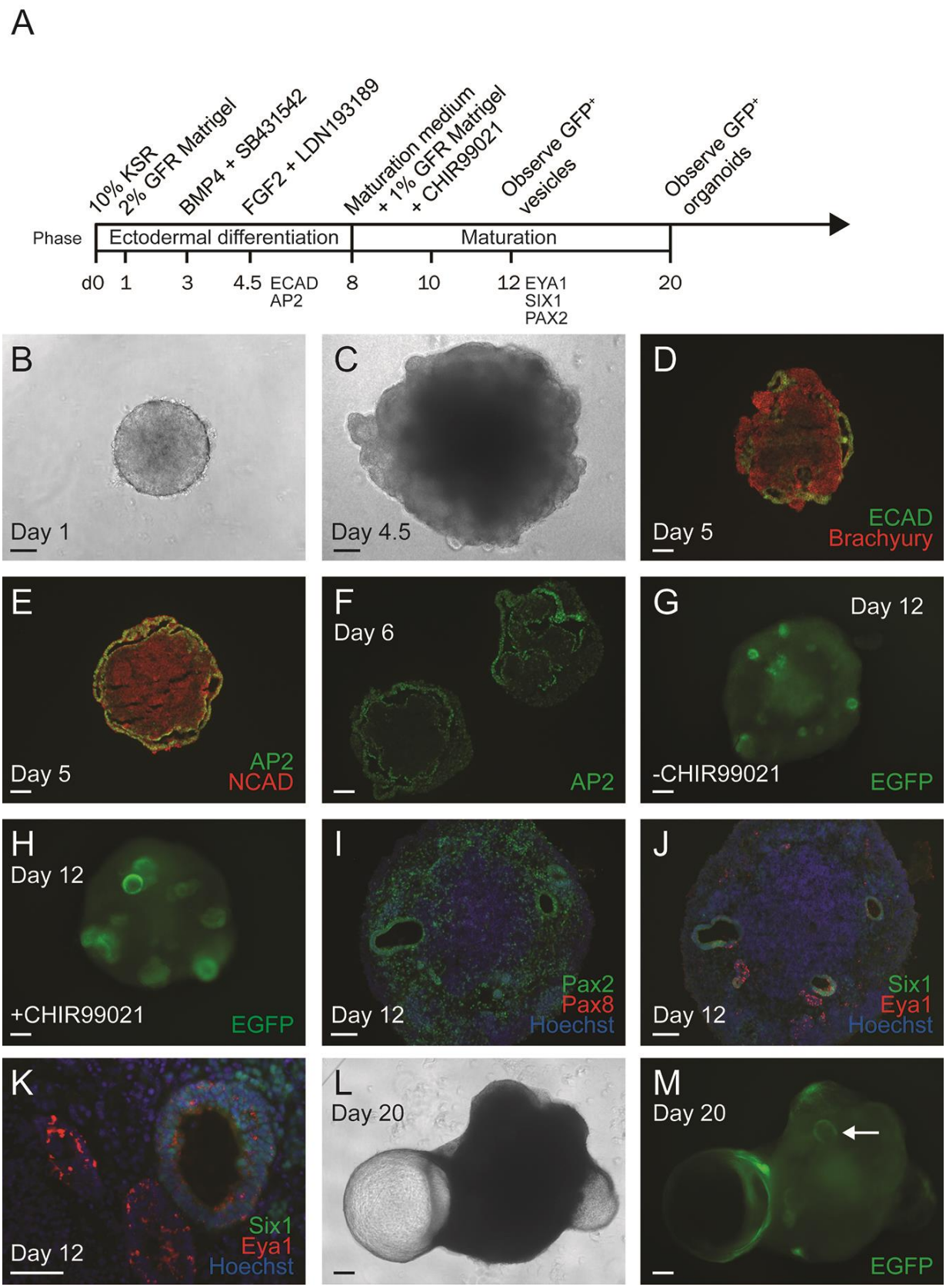

Process of forming Pax2$^{EGFP/+}$ organoids. A: Timeline of inner ear organoid formation. Additions of growth factor reduced (GFR) Matrigel and exogenous patterning molecules are indicated as well as milestones for successful cultures. Differentiation is guided via exogenous factors at day 3 and day 4.5; otherwise, organoid formation occurs through self-patterning. After the transfer of aggregates from ectodermal differentiation medium to maturation medium at day 8, 50% of medium is exchanged every other day, so the percentage of Matrigel becomes progressively dilute over time. The Wnt pathway agonist CHIR99021 (a GSK3β inhibitor) promotes formation of pre-organoid, otic vesicle-like structures when applied between days 8 and 10 [70]. It was not necessary for our cell line, however, and was not included in our cultures unless noted. B-M: Progression of aggregates through inner ear organoid protocol. Panels B-F and L-M exemplify aggregates treated with 25 ng/mL FGF2 at day 4.5 and without CHIR99021 at day 8. The aggregate in Panel G was treated with 100 ng/mL FGF2 at day 4.5 and without CHIR99021 at day 8. Panels H-K exemplify aggregates treated with 100 ng/mL FGF2 at day 4.5 and with CHIR99021 at day 8. B-C: Aggregates expand to over twice their original size and develop ruffled edges by day 4.5. D-F: Cryosectioning and immunofluorescence staining at days 5-6 reveal an outer layer expressing markers of non-neural ectoderm, E-cadherin (ECAD) and Tfap2a (AP2), and excluding markers of mesendoderm, Brachyury and N-cadherin (NCAD). G-H: Epifluorescence images of representative vesicle-positive aggregates at day 12. The *Pax2^{EGFP}* allele permits observation and tracking of vesicles as they form early during the maturation phase and later migrate and expand into organoid-containing cysts protruding from the surface. I-J: Adjacent cryosections stained for preplacodal markers Six1 and Eya1 or otic placodal markers Pax2 and Pax8. Pax2 signal is concentrated at vesicles, in accordance with epifluorescence imaging. Vesicles were also positive for Six1 and Eya1. Pax8 was not detected. L-M: Brightfield and epifluorescence images of a representative organoid-positive aggregate at day 20. Pax2^{EGFP} expression indicates the location of hair cells at the organoid region bordering the protruding cyst and the body of the aggregate. Note also the presence of a vesicle that did not expand and protrude, marked with an arrow. Scale bars: 200 μm (D-H, L-M), 100 μm (B-C, I-J), 50 μm (K).

markedly weaker EGFP epifluorescence than in trials of 10% KSR (not shown). In 10% KSR trials, EGFP signal increased gradually throughout the aggregates beginning on day 9 but was brighter in the vesicles compared to surrounding tissue. Staining for Pax2 confirmed the uniform expression of Pax2 in vesicle epithelia as well as scattered expression throughout the aggregates, whereas Pax8 expression was absent at this same time point (Figure 7I). Preplacodal markers Eya1 and Six1 were detected at the vesicle epithelia at day 12 (Figure 7J-K). Inclusion of CHIR99021 early in the maturation phase (days 8-10) appeared to increase the size and number of vesicles at day 12 (Figure 7H) [70]; however, this condition was not necessary for vesicle formation using $Pax2^{EGFP/+}$ cells and was not included unless otherwise noted. Aggregates were observed via epifluorescence microscopy until day 20, by which time the progressive expansion of vesicles into protruding cysts described by Koehler et al. was replicated in our cultures (Figure 7L-M) [68]. The EGFP signal became concentrated at the base of each protrusion, bordering the aggregate body, marking the “organoid” region where hair cells were expected. Overall, the $Pax2^{EGFP/+}$ mESC aggregates cultured with 10% KSR met major checkpoints for otic differentiation and reported on formation of $Pax2^{+}$ vesicles and organoids.

Otic induction during organoid protocol supports FGF-ERK-Pax2 mechanism

FGF signaling is a necessary step in the adoption of inner ear fate. We investigated whether a similar relationship existed between FGF2 dose and the efficiency of organoid production. Using a range of FGF2 doses (0, 5, 25, and 100 ng/mL) at day 4.5, we maintained cultures through day 20 and quantified the percentage of aggregates featuring at least one organoid as defined by an $EGFP^{+}$

border region at the base of a protruding cyst. A clear pattern of dose-dependency was observed: FGF2 was required for organoid formation, and increasing doses resulted in more aggregates forming organoids (Figure 8A-A''). The efficiency of vesicle production also corresponded with FGF2 dose, as expected based on our finding that all organoids arose from $EGFP^+$ vesicles (Figure 8A'-B). Using 25 ng/mL FGF2 resulted in a similar percentage of organoid-positive aggregates (24.1% ± 10.0) compared to the 10-20% reported previously [69]. The maximum dose tested, 100 ng/mL, resulted in an even higher percentage of organoid-positive aggregates (41.8% ± 19.8) (Figure 8B).

FGF receptors signal through multiple downstream pathways including those mediated by ERK, AKT, and PLCγ. Recent reports have demonstrated the necessity of ERK as a mediator of otic induction in chickens and zebrafish [241,242]. Further, the zebrafish study provided evidence that ERK is needed for hair cell development whereas AKT is involved in otic neurogenesis. Given the correlation between vesicle formation and FGF2 dose, we decided to investigate whether ERK activation would demonstrate the same relationship. We hypothesized that the process of otic induction in organoids would replicate the *in vivo* developmental mechanism, supporting the use of inner ear organoids as a model to study signaling mechanisms involved in early mammalian otic development.

To examine the activation of ERK downstream of FGF2, aggregates were harvested at 1 hour after application of LDN193189 and varying doses of FGF2 (0, 5, 25, and 100 ng/mL) at day 4.5. Lysates were prepared and screened for the activated, phosphorylated form of ERK (pERK). ERK phosphorylation increased in an FGF2 dose-dependent manner (Figure 8C). Interestingly, the strongest ERK activation was

induced by 100 ng/mL FGF2, a 4-fold higher dose than prescribed by the original organoid protocol [68,69]. These data reveal correlations between FGF2 and both organoid production and ERK phosphorylation, in agreement with developmental literature on otic induction [241,242].

Pax2$^{EGFP/+}$ organoids model several features of developing ear

Organoids were screened for Myo7a^{+} cells with F-actin^{+} apical structures, indicative of hair cells with stereocilia bundles. Myo7a^{+}/Pax2^{+} cells were found in the organoid regions where EGFP was observed (Figure 9A). Cryosectioning revealed the presence of internal organoids containing Myo7a^{+} hair cells arrayed in an epithelial layer with F-actin^{+} stereocilia-like bundles oriented inward towards the central lumen of each cyst (Figure 9B,B'). Protruding organoids were dissected and stained as isolated surface preparations. Imaging the apical face of the preparation revealed a variety of bundle morphologies, with some splayed and some tightly bundled stereocilia (Figure 5C). A network of thick F-actin-rich belts similar to those formed by supporting cells *in vivo* invariably marked the organoid regions where hair cells were found; this distinctive feature served as a useful marker by which to screen tissues for hair cells efficiently.

We screened for additional characteristics of auditory and vestibular organs to demonstrate the suitability of the Pax2$^{EGFP/+}$ cell line for inner ear organoid formation. The organoid hair cells were lined basally by a layer of Sox2^{+} cells similar to supporting cells of the inner ear. The hair cells themselves were positive for Sox2 as well (Figure 9D). This may be evidence of arrest at an immature stage as Sox2 is downregulated in auditory hair cells of neonatal mice [16,199]. Alternatively, it may point to a vestibular phenotype as particular vestibular hair cells express Sox2 into adulthood [222]. The

Figure 8: Evidence of ERK mediating FGF-driven otic induction in mouse organoid model

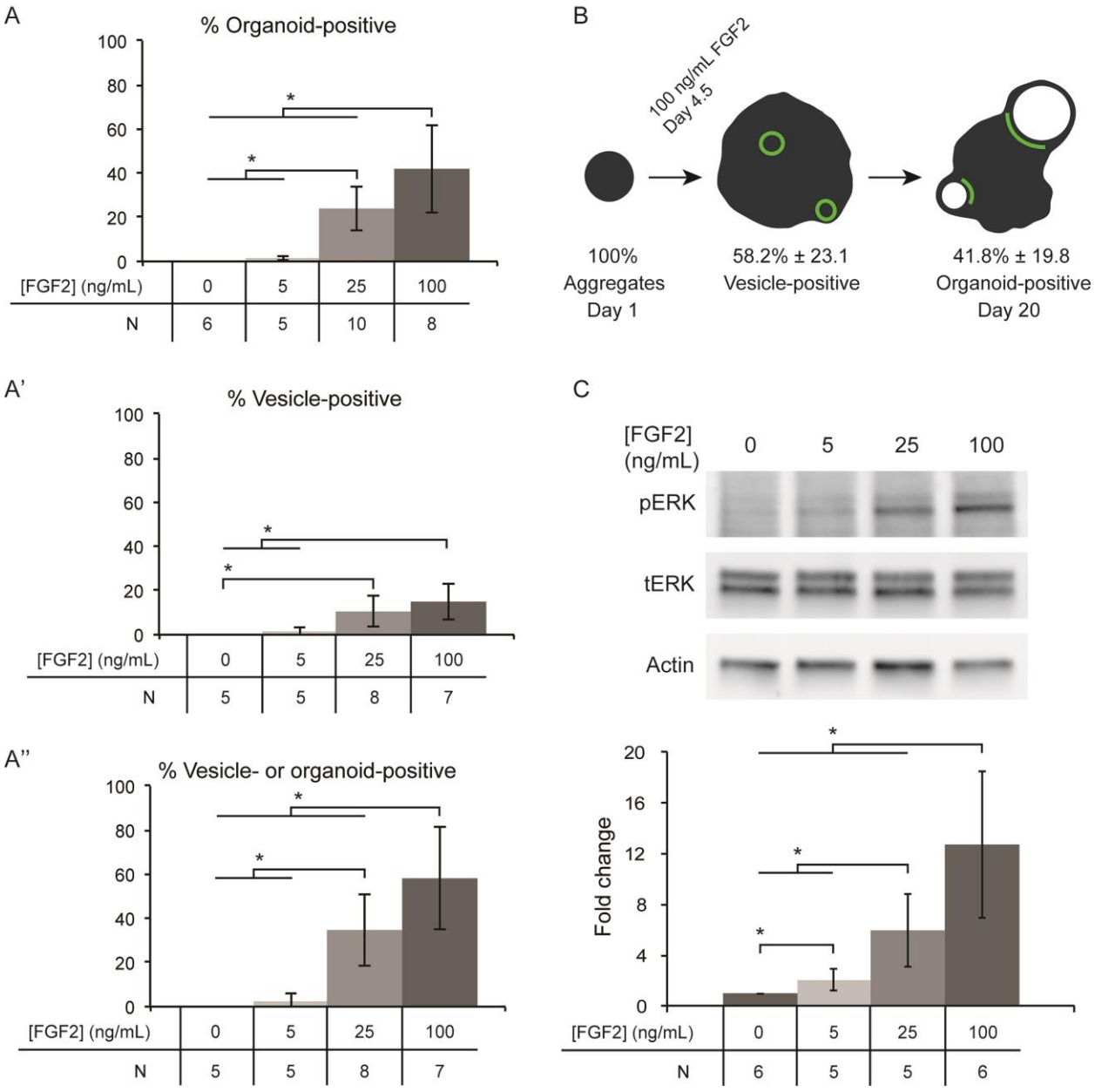

Evidence of ERK mediating FGF-driven otic induction in mouse organoid model. A: Quantification of aggregates with EGFP$^+$ organoid regions at the bases of protruding cysts at day 20. The percentage with organoids increased with higher doses of FGF2. A': Quantification of aggregates with EGFP$^+$ vesicles estimated via observation of live aggregates by epifluorescence. A'': Quantification of aggregates positive either for vesicles at day 12 or organoids at day 20. In panels A-A'', N indicates the number of cultures examined, and the data represent mean ± standard deviation (*$p<0.05$). B: Schematic illustrating percentage of original aggregates progressing to vesicle or organoid stages. Note that the vesicle-positive percentage is taken from Figure 5A'', since all organoid-positive aggregates progress through an intermediate, vesicle-positive stage. C: Western blotting for phosphorylated ERK (pERK), total

ERK (tERK), and actin. The proportion of phosphorylated-to-total ERK (pERK/tERK) increased with higher doses of FGF2. Fold change in pERK/tERK relative to 0 ng/mL FGF2 baseline is quantified (unpaired t-test, *$p<0.05$; mean ± standard deviation).

Figure 9: Characterization of Pax2⁺ inner ear organoids

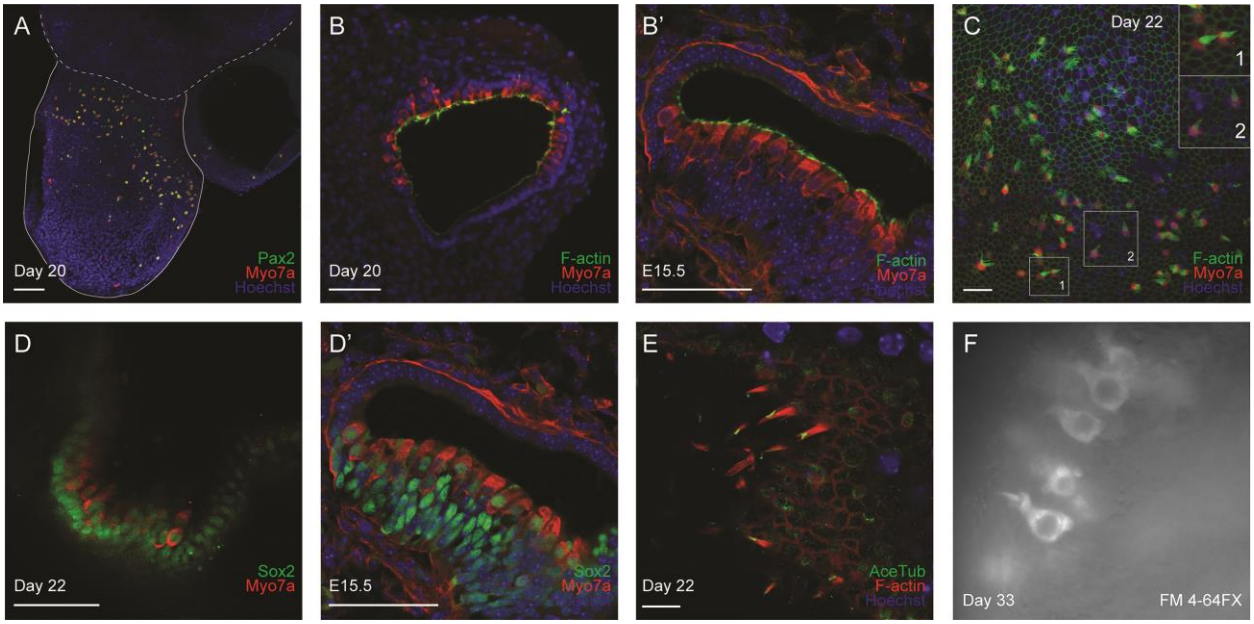

Characterization of Pax2⁺ inner ear organoids. A: Confocal z-projection showing whole-mount immunofluorescence of an aggregate at day 20. Note that Myo7a⁺/Pax2⁺ cells are found at the border between the aggregate (dashed line) and the protrusion (solid line). Following fixation and staining of tissues, the native EGFP signal was no longer observed, so fluorophores emitting green light could be used. B: Myo7a⁺ cells with F-actin-rich bundles arranged in an epithelial layer, shown via both cryosection and dissected organoid preparation staining. B': Vestibular hair cells stained for Myo7a and F-actin in E15.5 C57BL/6 control mouse embryo. C: Surface preparation of isolated organoid demonstrating variety of bundle morphologies. Vestibular-like bundles are shown in insets at higher magnification. D: Confocal image showing whole-mount immunofluorescence for Sox2⁺ cells reveals a supporting cell layer immediately below Myo7a⁺ hair cells. Because the hair cells are also Sox2⁺, they are evidently immature [16,199]. D': Vestibular hair cells and supporting cells in a C57BL/6 control embryo also express Myo7a and Sox2 at E15.5. E: Each stereocilia bundle in an organoid contains a single cilium positive for acetylated tubulin, reflecting a vestibular or immature cochlear phenotype. F: FM4-64FX dye, applied for 10 seconds before wash-out, is rapidly taken up by hair cells, presumably through mechanotransduction channels. Note the flask shape suggestive of type I vestibular hair cells [12]. Scale bars: 100 μm (A), 50 μm (B, B', D, D'), 20 μm (C), 10 μm (E). FGF2 doses: 25 ng/mL (C, F), 100 ng/mL (A-B', D, E).

presence of a single kinocilium, marked by expression of acetylated tubulin (AceTub), at each apical bundle supports characterization as either vestibular or immature auditory hair cells (Figure 9E).

To test for functional mechanotransduction channels, we applied the styryl dye FM4-64FX to an organoid that had been dissected at day 20 and cultured until day 33 adhered to a collagen droplet. Following 10-second application, the dye was washed out, and the organoid was imaged live. Positive labeling indicative of hair cells was observed (Figure 9F). Because the dye application was brief, entry presumably occurred through functional mechanotransduction channels rather than via endocytosis or uptake through other large pores such as those from P2X receptors [244]. To test for susceptibility to aminoglycoside-induced ototoxicity, additional organoids cultured on collagen to day 33 were treated with 6 μM gentamicin for 72 hours. Rhodamine phalloidin was used to screen for stereocilia bundles. Bundles were present in 3 out of 4 organoids in both treated and untreated conditions, indicating that the hair cells were not severely affected by aminoglycoside treatment (not shown).

Vesicle-associated neurons model features of embryonic inner ear neurogenesis

The incidence of neurons in inner ear organoids has been reported [68]. This prompted us to further investigate the source and synaptogenic potential of these neurons. We first examined whether the neurons in our organoids arose from neuroblasts associated with vesicles at day 12. Staining revealed cells expressing Islet-1/2 (Isl1/2) immediately adjacent to vesicles positive for Pax2 (Figure 10A). This pattern closely resembled Isl1/2^{+}/Sox2^{+} neuroblasts delaminating from otocysts in C57BL/6 mouse control tissue at E11.5 (Figure 6A'-A'') [245,246].

Figure 10: Comparison of immunofluorescence staining for Isl1 and SHH in day 12 aggregates and E11.5 embryos

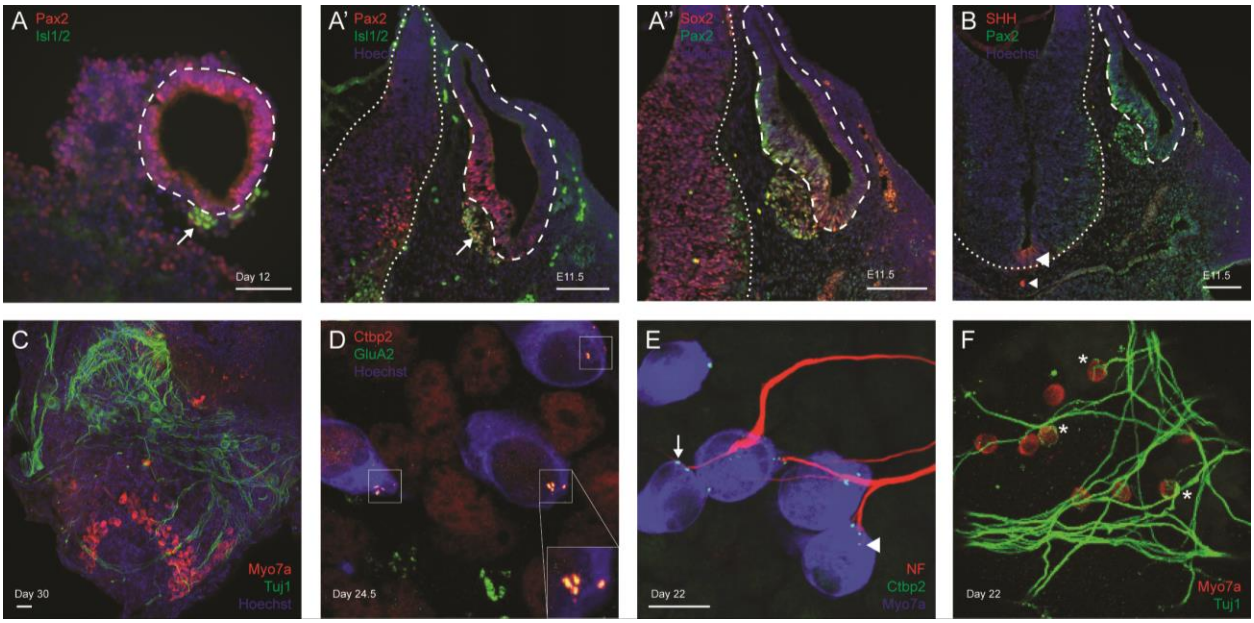

Comparison of immunofluorescence staining for Isl1 and SHH in day 12 aggregates and E11.5 embryos and evidence of organoid synapses. A-A'': Pax2 is enriched in otic vesicle of day 12 aggregate (treated with 100 ng/mL FGF2 at day 4.5 and 3 µM CHIR99021 at day 8) and E11.5 C57BL/6 mouse embryo relative to surrounding tissue. Isl1/2^{+} cells are found adjacent to the vesicles in both tissues, suggesting a process of delamination in aggregates similar to cvg formation in embryos. B: SHH staining is localized to specific sources in E11.5 control embryo at the level of the otic vesicle: the ventral neural tube (large arrowhead) and notochord (small arrowhead). In panels A-B, the otic vesicle is marked by a dashed line, the neural tube is marked by a dotted line, and neuroblasts or putative neuroblasts are marked by arrows. C: Dissected organoid preparation with neurons clustered near hair cells. Tuj1^{+} projections traverse through the hair cell region. D: Presynaptic Ctbp2 and postsynaptic GluA2 puncta are directly apposed at the base of hair cells. E-F: Some projections appear to terminate at hair cells, forming bouton endings (arrowhead in E) or calyceal endings (the latter suggesting type I vestibular phenotype, asterisks in F). Others continue past the hair cells, in some cases appearing to form *en passant* synapses (arrow in E). Scale bars: 100 µm (A-B), 20 µm (C), 10 µm (E). CHIR99021 treatment was included in panels D-E. FGF2 dose: 100 ng/mL (C-F).

In development, SHH signaling extrinsic to otic tissue impacts the specification of cochleovestibular ganglion (cvg) neuroblasts indirectly through Neurogenin 1, and SHH signaling intrinsic to otic tissue is necessary for cvg neuroblast proliferation and survival [187]. Given these relationships between SHH and with inner ear neurogenesis, we examined SHH expression in our day 12 aggregates through immunofluorescence staining. SHH signal was faint and non-specific (not shown). In contrast, SHH is readily detected at the ventral neural tube and notochord in E11.5 mice (Figure 10B).

Whether or not the specification of organoid-associated neurons involves SHH, their ability to form synaptic contacts with hair cells is important to evaluate as this could be exploited in disease modeling or regeneration studies. Tuj1^{+} neurons were found in clusters near regions of Myo7a^{+} hair cells within the isolated day 30 organoids (Figure 10C). These cells extended projections traversing the hair cell epithelia. Furthermore, these cells formed putative synaptic connections on hair cells as indicated by the co-localization of the presynaptic marker Ctbp2 and postsynaptic marker GluA2 in puncta at the basal aspect of hair cells (Figure 10D). This direct apposition of presynaptic and postsynaptic markers mimics the one-to-one pairing of these markers in the mature inner ear [21,247]. To characterize the interaction between neurons and hair cells in our organoids, we stained for neurofilament (NF) and Tuj1 and found projections with terminal boutons and calyces as well as *en passant* synapses (Figures 10E-F). Altogether, these results support the potential use of inner ear organoids as a model not only of hair cell development but also inner ear neurogenesis.

DISCUSSION

The generation of inner ear organoids from mouse and human pluripotent stem cells could transform *in vitro* disease modeling, drug discovery, and regenerative studies in auditory and vestibular research [68,71]. Adoption of the methodology is, however, lacking; to the best of our knowledge, all prior publications report efforts of a single laboratory. For our study, we applied the method to mouse embryonic stem cells derived from blastocysts of a heterozygous Pax2-reporter mouse line. The results reflect a dependence of otic vesicle induction on FGF concentration and support the vestibular-like characterization of the organoids. Variability in the efficiency of organoid production over time and passaging of cells suggests that further optimization is needed to make this protocol more robust and translatable to a broad range of pluripotent stem cell lines.

Here we demonstrated the utility of transcriptional reporter ESCs from an established mutant mouse line. Direct comparison between *in vivo* development and *in vitro* differentiation in the same genetic background is a prototype for organoid cultures as model systems. However, verifying that the reporter system recapitulates embryonic expression patterns and does not interfere with development is critical. We used mouse ESCs with an EGFP reporter driven by the endogenous Pax2 promoter sequence. In general, transcriptional regulatory elements are proximal to start sites, but some tissue-specific enhancer elements can be located far upstream. For example, enhancers within a 6.9-kb region upstream of the Pax2 transcription start site are sufficient to drive expression in mid-hindbrain domains, but a 30-kb 5’ region is required for expression in

the ear, kidney, and spinal cord [240]. Therefore, confirming that transcriptional reporter lines reproduce *in vivo* expression patterns is a necessary consideration when modeling development of specific tissues *in vitro*. Our results showed otic expression of the EGFP reporter *in vivo*, normal phenotypic hearing thresholds of $Pax2^{EGFP/+}$ mice compared to WT mice, and sustained expression of Pax2 from ESC-derived otic vesicles to sensory hair cell stages. Since Pax2 is a marker for otic vesicles and terminally differentiated sensory cells in mouse development [149,169,248], the $Pax2^{EGFP}$ allele is a potential asset for future studies of molecular events leading from progenitors to mature hair cells.

Our results were consistent with evidence that Pax2 heterozygosity on C57BL/6 background does not adversely affect formation of inner ear tissue [149]. Although Pax2 heterozygosity and C57BL/6 background (previously untested with this protocol) did not prevent organoid formation, we did find that modification of the original protocol was necessary. A higher concentration of KSR was required to induce aggregate growth to the expected size [69], raising the possibility that KSR influences proliferation rate. In two different mESC lines based on the 129 background strain, EB size did not change systematically with increasing KSR concentration [249]. Whether KSR affects proliferation during early stages of the inner ear organoid protocol and whether this is cell line-specific remain to be determined. Alternatively, KSR may affect differentiation or competence to adopt otic lineage. We found that higher KSR concentration was associated with stronger EGFP—and likely higher Pax2—expression within the vesicles and throughout the aggregates. From this we infer that some component of KSR influenced differentiation potential in addition to or independent of aggregate growth.

Differential requirements of organoid cultures for KSR concentrations ranging from 1.5% to 20% have been described and an unidentified caudalizing factor implicated [36]. One candidate is insulin, a weakly caudalizing factor in SFEBq cultures [250]. The uncharacterized influence of each component of KSR is an important consideration in optimizing protocols for independent cell lines. Though a higher concentration of KSR was advantageous for producing inner ear organoids with the $Pax2^{EGFP/+}$ cell line, its components could impact the efficiency of organoid formation in conflicting ways when added indiscriminately.

Inner ear organoid formation is largely dependent upon self-organization with limited input of exogenous patterning molecules during the maturation phase. In development, secreted factors Wnt (from the dorsal neural tube) and SHH (from the ventral neural tube and notochord) influence dorsal-ventral patterning of otic vesicles; their opposing gradients establish vestibular and auditory/neurogenic domains [163,164,186,187,251]. Day 12 aggregates lacked a particular source of SHH analogous to the ventral neural tube and notochord. In keeping with the absence of this ventralizing morphogen, the organoids expressed various features of vestibular-like end-organs. For instance, the presence of calyceal terminals was indicative of type I vestibular hair cells [45]. In addition to its role in ventralization and cochleogenesis, SHH signaling is required for maturation of the cvg, which becomes a source of SHH later in development [182,211,212,214,215]. In day 12 aggregates, $Isl1/2^{+}$ neurons did not themselves express SHH. Given the vestibular hair cell characteristics and the need for auditory hair cells in clinical applications, future inner ear organoid studies should evaluate directed patterning of vesicles through exogenous SHH. Additionally,

future studies should establish definitively whether Isl1/2^{+} cells originate from vesicles and give rise to the mature neurons found within the organoids. Resolving this issue is important if inner ear organoids are to be used as a model system for disease and developmental studies. Moreover, if these neurons are indeed otic in nature, then the protocol may ultimately provide sensory, non-sensory, and neural elements for inner ear repair and regeneration.

Additional differences between mESC-derived and embryonic inner ear tissues represent opportunities for optimization: For instance, our gentamicin treatment paradigm resulted in no obvious effect on derived hair cells. In contrast, treatment of neonatal mouse cochlea explants with 3.5 μM gentamicin for 72 hours results in a gradient of outer hair cell death, with nearly complete loss at the base of the cochlea [252]. We used 6 μM gentamicin based on experiments demonstrating severe loss of hair cells throughout cochlear explants (data not shown). Therefore, while the inner ear organoid protocol resulted in a close approximation of native hair cells with regards to molecular, structural, and functional characteristics, refinements are still needed to fully replicate hair cell physiology.

Another notable difference from embryonic tissue was absence of Pax8 staining in the newly formed, Pax2^{+} otic vesicles at day 12 of the protocol. Pax2 and Pax8 show overlapping expression in the ventral domains of otic vesicles of E9.5-10.5 mice [253], and Pax8 expression has been demonstrated previously using the organoid culture protocol [68]. The lack of Pax8 may indicate a unique feature of the cell line and may prompt experiments on the role of Pax genes in organoid formation. Pax2, Pax5, and Pax8 can compensate for one another in development, but Pax5 is not expressed in the

embryonic inner ear and was absent from our aggregates [150,176]. Therefore, the development of otic tissue *in vitro* relied solely on heterozygous Pax2 expression.

Tracking protocol efficiency is necessary for optimization

As mentioned, the adaptability of the inner ear organoid protocol to several distinct cell lines has been demonstrated. DeJonge et al. optimized FGF2/LDN193189 treatment timing for each cell line within a window of just 6 hours [70]. This showed that careful consideration of the relative efficiencies of different cell lines is crucial. Our experience suggested that cultures vary in efficiency not only with parameters defined by the protocol (e.g., timing or dose of drug treatments) but with additional parameters yet to be elucidated. We found that mESC passage number, reagent lots, and seasonal environmental fluctuations may influence outcomes. In addition, the reliance upon Matrigel, an animal-derived product that varies unpredictably in composition from lot to lot, is not ideal, though no reliable alternative has been established.

The data presented in this study were produced during a single period of cultures meeting criteria for “success” in generating otic cultures: At least 10% of aggregates were vesicle-positive, with some expanding into large, protruding cysts. During that time, non-otic cultures (lacking one or both criteria for success) corresponded to higher mESC passage numbers. It is important to note that subsequently, without changing materials or methods, our success rate dropped suddenly and without relationship to passage number for a prolonged interval. In contrast, hair cells were reliably identified in the organoid region at the base of each protruding cyst in our previous and subsequent cultures.

We present a summary of our culture attempts categorized by major variations to the original protocol tested (Figure S2) as well as a strategy we recommend for adopting the inner ear organoid protocol (Table 5). The summary corresponds to our trials with $Pax2^{EGFP/+}$ cells only, although we tested other cell lines (R1, R1/E, and E14Tg2a). As noted, our $Pax2^{EGFP/+}$ cell line required 10% KSR in the ectodermal differentiation medium. During the period when our cultures were consistently producing organoids, we performed drug treatments within ±3 hours from the timing prescribed by the original protocol with no adverse effects. The combinations of additional variables predicted to influence the success of inner ear organoid cultures are myriad; this presents a challenge even when using cell lines known to be amenable to the protocol.

The collective understanding of stem cell differentiation and pluripotency are still evolving, despite the fact that mESCs were first derived several decades ago [254,255]. Naïve and primed states of pluripotency have recently been distinguished, and pharmacological means of reverting primed cells to a naïve state are being discovered [256–258]. Although our outcomes did not correlate with passage number, maintenance of naïve pluripotency is a key consideration for stem cell cultures. Interestingly, human ESCs are more comparable to mouse epiblast stem cells (primed) than to mESCs (naïve), perhaps underlying the modifications that have been necessary to adapt mouse organoid protocols for human cells [71,259,260]. As our study demonstrated, the influence of cells surrounding target tissue in 3-dimensional stem cell culture paradigms—in terms of both secreted factors and physical cues—is relatively uncharacterized. In addition, the possibility that selecting for reporter cells may bias

outcomes toward higher efficiency has been suggested in retinal organoid literature [261]. Until we gain control over pluripotency states, environmental cues, and distinctions between cell lines, these remain necessary caveats for organoid researchers.

Efforts to understand, refine, and apply inner ear organoid technology are still in early stages. However, the potential value of reporter lines able to recapitulate endogenous expression patterns and restore function *in vivo* cannot be overstated. The many parallels between the $Pax2^{EGFP/+}$ organoids and true organs of hearing and balance are a strong impetus for continued investment in what may be a highly lucrative area of research.

Table 5: Recommended strategy to adopt inner ear organoid protocol

Optimized approach	**Evaluation**
Confirm pluripotency across multiple passages, and define a cut-off	Klf4, Nanog, Oct3/4, Rex1, Sox2, alkaline phosphatase
Test lot efficacy at checkpoints by omitting one at a time (B, S, B/S, B/S-F, B/S-L, B/S-F/L)	Differential aggregate morphology and staining for ECAD and AP2
Optimize dose and timing of B/S and F/L treatments	Staining for ECAD and AP2
Optimize % KSR in mEB media	Staining for Pax2 at early maturation phase
Screen for vesicles and organoids by cryosectioning	Track outcomes over time (seasonal effects), passage numbers, and lot numbers
Track outcomes over time (seasonal effects), passage numbers, and lot numbers	Compare against standards for acceptable outcomes
Track expiration dates and storage conditions of all drugs	Compare against standards for acceptable outcomes

CHAPTER 3: Early inhibition of TGFβ signaling is necessary for derived otic vesicles to achieve ultimate inner ear organoid fate[4]

INTRODUCTION

The potential of stem cells lies not only in their ability to adopt a full spectrum of cell fates but also in their promise to revolutionize medical interventions. The primary cause of sensorineural deafness is loss of inner ear sensory hair cells, which transduce mechanical sound stimuli into afferent electrical signals. Addressing the underlying cause by regenerating hair cells from patient-derived induced pluripotent stem cells is envisaged as a treatment to restore auditory function.

Interest in hair cell regeneration has exploded with the availability of stem cell lines. To translate results from the laboratory to the clinic, differentiation methods must be well-established and refined. A basic understanding of signaling mechanisms active in early embryonic development should serve as the foundation for differentiation protocols. Indeed, *in vitro* modeling of the environmental cues within a developing embryo is the focus of ongoing research. Additionally, the signaling cascades initiated at each stage in differentiation from stem cell to progenitor to mature cell must be

[4] This chapter represents a manuscript in preparation [74]: Schaefer SA, L Liu and RK Duncan A step in the right direction: Early inhibition of TGFB signaling is necessary for derived otic vesicles to achieve ultimate inner ear organoid fate.

understood to ensure efficiency and safety of medical applications. In addressing these challenges, stem cell and developmental research inform one another.

A differentiation protocol has been established for producing inner ear organoids from mouse embryonic stem cells (mESCs) [68,69]. It builds on the framework of serum-free floating culture of embryoid body-like aggregates with quick reaggregation (SFEBq) with a series of exogenous drug treatments [72,73,99]. The modifications are intended to mimic early developmental signaling pathways that lead to inner ear fate. Following the initial dissociation of mESC colonies and reaggregation into spheres, differentiation can spontaneously proceed towards any of the three germ layers, i.e., ectoderm, endoderm, or mesoderm [262]. With the first drug treatment, an inhibitor of the TGFβ pathway directs differentiation to favor ectoderm and limit endoderm and mesoderm [80,85–88,97,98]. Additional drug treatments further refine the lineage path toward non-neural, preplacodal, and otic placodal fate. The efficiency at each step is crucial to the final yield of organoids. Therefore, understanding and optimizing TGFβ inhibition is necessary to produce the large quantities of hair cells required for practical applications.

In this study, we examine the effect of TGFβ inhibition on generation of otic tissue using the inner ear organoid protocol. On day 3 of the protocol, the inhibitor SB431542 is applied, targeting TGFβ-family type I receptors ALK4, 5, and 7 [263]. Surprisingly, we find that TGFβ pathway inhibition is not necessary for derivation of intermediate, otic vesicle-like structures. Alternative drugs that inhibit TGFβ signaling via alternative mechanisms also permitted vesicle and organoid formation and only differed significantly from SB431542 in production of otic tissue at the vesicle stage. In

parallel, we compare the transcriptomes of derived vesicles with and without SB431542 treatment and the transcriptomes of E10.5 mouse otic vesicles at an equivalent point in development. We find that SB431542 overall induces a shift in transcription to better model native tissue, while persistent differences between derived and native vesicles represent opportunities for further optimization of the inner ear organoid protocol. These observations motivate future investigation of genes regulated immediately downstream of TGFβ receptor activation that establish competence to achieve otic fate.

MATERIALS AND METHODS

mESC cultures

The R1/E mESC line (from 129X1 x 129S1 mouse strain) was used for this study. Cells from passage 18-26 were used to generate inner ear organoids. For stem cell maintenance, colonies were cultured in feeder-free conditions on 0.1% gelatin in a medium consisting of a 1:1 mixture of Advanced DMEM/F-12 and Neurobasal, 0.5X B-27 (without vitamin A), 1X N-2 supplement, and 1X GlutaMAX (all from Gibco) supplemented with 1000 U/mL LIF (Gibco) and 2i inhibitors PD0325901 (1 μM Stemcell Technologies) and CHIR99021 (3 μM Stemcell Technologies) within 1 week of use. Colonies were dissociated to single cells with TrypLE Express (Gibco) for maintenance and for producing aggregates.

Differentiation protocol

mESC aggregates were cultured according to the previously described inner ear organoid protocol [68–70]. On day 0, following dissociation of colonies, cells were reaggregated in round-bottom 96-well Nunclon Sphera Microplates (Thermo Scientific). Cells were seeded at a density of 3000 cells in 100 µL ectodermal differentiation medium per well. The medium was composed of GMEM, 1.5% KnockOut serum replacement (KSR), 15 mM HEPES, 1X non-essential amino acids, 1 mM sodium pyruvate (all from Gibco), and 0.1 mM β-mercaptoethanol (Sigma).

On day 1 of the ectodermal differentiation phase, growth factor reduced (GFR) Matrigel (Corning) was applied at a final concentration of 2% in ectodermal differentiation medium by replacing half the volume in each well. On day 3, 10 ng/mL BMP4 (Stemgent) was added in 25 µL medium per well, with or without TGFβ inhibition. Inhibitors tested included SB431542 (1 µM, Stemgent), SIS3 (3 µM, Tocris), and RepSox (1 µM, Tocris). On day 4.25, 1 µM LDN193189 (Stemgent) and 100 ng/mL FGF2 (Sigma) were added in 25 µL medium per well.

To begin the maturation phase on day 8, aggregates were transferred into maturation medium consisting of Advanced DMEM/F-12, 1X N-2 supplement, 15 mM HEPES (Gibco), and 1X GlutaMAX, with 1% GFR Matrigel and 3 µM CHIR99021 (Stemcell Technologies). Half the volume of media was exchanged daily beginning on day 10. Aggregates were monitored for vesicle formation by day 12 and for organoid formation by day 20-22.

Quantification of vesicles and organoids

The rate of vesicle production was estimated by disrupting aggregates and counting the vesicles released. On day 12, 32 aggregates (from 4 columns chosen at random from each 96-well plate) were collected. Aggregates were washed with DMEM/F-12 (with HEPES, Gibco) to remove maturation medium and resuspended in DMEM/F-12 containing 1X collagenase/hyaluronidase (Stemcell Technologies) in 35-mm Nunclon Sphera dishes (Thermo Scientific). Dishes were placed at 37°C in a humidified 5% CO_2 culture incubator for 45 minutes. At 15-minute intervals, aggregates were triturated gently with cut 1-mL pipette tips to encourage gradual disruption and aid diffusion of the enzymes. After 45 minutes, an uncut tip was used to fully dissociate aggregates to a mixture of single cells, residual clumps, and intact vesicles. The mixture was filtered through a 40-μm cell strainer, which was then inverted and washed with DMEM/F-12 to retrieve vesicles and clumps into a fresh 35-mm Nunclon Sphera dish. Using a micropipette, vesicles were manually isolated from the clumps and transferred into a separate dish to prevent double-counting. The rate of vesicle production was then expressed as the number of vesicles counted within 20 minutes divided by the number of aggregates disrupted.

Organoids were identified through brightfield imaging by presence of translucent cysts between days 20 and 22. Cysts were either protruding or internal to the aggregates and must have a defined epithelial border to be considered an organoid. The rate of organoid production was expressed as the percentage of aggregates with at least one cyst meeting this criterion. At least 32 aggregates were screened per condition per trial.

Immunostaining

At day 12 (vesicle stage) or days 20-22 (organoid stage), aggregates were collected and fixed 1 hour in 4% PFA. Following fixation, aggregates were washed with phosphate-buffered saline PBS and stored at 4°C until further processing.

For cryosection staining, aggregates were incubated in sucrose at increasing concentrations up to 30% in PBS. Overnight incubation in 30% sucrose at 4°C was followed by incubation in a 1:1 mixture of 30% sucrose and OCT for at least 4 hours at room temperature or overnight at 4°C. Aggregates were then transferred to OCT in cryomolds for a 1-hour incubation prior to being frozen on dry ice. OCT blocks were sectioned using a Leica 3050S cryostat at 12-µm thickness. Sections were dried overnight at room temperature. Then, they were rehydrated with PBS for 15 minutes and transferred to a humid chamber for further processing. Slides were treated for 15 minutes with blocking/permabilization solution consisting of 10% normal donkey serum and 0.1% Triton X-100, then incubated overnight with primary antibodies in 1:1 PBS and blocking/permeabilization solution. Slides were incubated with Alexa Fluor secondary antibodies at 1:500 in PBS protected from light to prevent photobleaching. Hoechst 33242 was used for nuclear counterstaining at 1:2500 in PBS for 5 minutes. ProLong Gold Antifade Mountant (Molecular Probes) was used to apply coverslips. Table S1 provides a list of antibodies used in this study.

For dissected organoid staining, fixed aggregates with protruding cysts were transferred a 35-mm Sylgard dish with PBS. The hair cell-containing organoid epithelium at the base of a cyst was isolated using iris scissors and fine forceps and

placed into a custom-made microwell for staining. Blocking and permeabilization was performed by 15-minute incubation with 5% NDS and 0.1% Triton X-100 in PBS. Organoids were then transferred to a humid chamber and incubated overnight with Myosin 7a primary antibody (Santa Cruz, sc-74516) in blocking/permeabilization solution at 4°C. Alexa Fluor 568-conjugated donkey anti-mouse secondary antibody and Alexa Fluor 488 Phalloidin (Thermo Fisher Scientific) were applied at 1:500 and 1:100, respectively, in PBS for 1 hour at room temperature with tissues protected from light. Hoechst 33242 was applied at 1:2500 in PBS for 5 minutes, and organoids were mounted with ProLong Gold.

For brightfield and epifluorescence imaging, Leica DM IL and Olympus BX51WI microscopes were used. Additional imaging was performed using an Olympus FluoView 1000 confocal.

Statistical analysis

Comparisons between 2 groups were performed using unpaired t-tests in Microsoft Excel. Comparisons amongst more than 2 groups were performed with one-way ANOVA and Tukey's post-hoc test in the statistical analysis software package SPSS 24.

Isolation of derived vesicles for RNASeq

On day 12 of differentiation, R1/E aggregates were disrupted using collagenase/hyaluronidase as described. For RNASeq sample collection, the filtrate was collected in DMEM/F12 and transferred to a low-attachment dish on ice during

manual selection of vesicles under a dissection microscope. Vesicles were collected in Buffer RLT (Qiagen) in RNase-free tubes on ice and then frozen quickly on dry ice before being transferred to -80°C until RNA extraction. Selection was limited to 20 minutes to avoid RNA degradation. At minimum, 30 vesicles were collected from each biological repeat, and 3-4 biological repeats were performed per condition.

Dissection of embryonic vesicles

On E10.5, pregnant C57BL/6 dams were sacrificed, and uterine horns were removed and placed into PBS on ice. From this point, PBS was replaced frequently to keep tissues cold. Embryos were harvested under a microscope and then transferred to ice until dissected. Otic vesicles were harvested by creating a window in the epithelium adjacent to the second branchial arch using a scalpel blade. Vesicles were then teased away from periotic mesenchyme using fine forceps. Isolated vesicles were transferred to Buffer RLT in RNase-free tubes on ice and then frozen quickly on dry ice before storage at -80°C. Separate pregnant dams were used for each of the 4 biological repeats; each repeat comprised 2-6 otic vesicles from 1-3 embryos.

RNA sequencing

Total RNA was extracted using an RNeasy Mini Kit (Qiagen) and transferred to the UM DNA Sequencing Core for library preparation and sequencing. RNA input was assessed for quality and quantity using an Agilent Bioanalyzer 2100, Agilent 2200 TapeStation, and NanoDrop ND-1000 spectrophotometer (Thermo Scientific). The RIN scores ranged from 8-10. cDNA libraries were prepared from 100 ng total RNA per

sample using a TruSeq RNA Sample Prep Kit v2 (Illumina). Library quality was confirmed by TapeStation and qPCR before sequencing. The Illumina HiSeq-2500 platform was used to perform V4 single end, 50 bp sequencing of libraries. Samples were sequenced in duplicate, with each sample loaded in two separate lanes. Fastq output files generated by bcl2fastq software v2.17 (Illumina) were uploaded to the Galaxy web platform (http://usegalaxy.org/).

Data analysis

Data analysis was performed using Galaxy v0.4.3.1 [264]. Within Galaxy, the wrapper Trim Galore! v0.4.3.1 was used to assess the quality of base calls via FastQC v0.69 [265] and to trim and filter reads via Cutadapt v1.14. Trimming removed low-quality base calls (Phred < 20) before adapters, and then filtering removed short reads (<20 bp). Reads were aligned to the mm10 genome assembly with HISAT2 v2.0.5.2 [266]. The resulting BAM files were merged to combine data from duplicate lanes. Data were converted to raw counts (reads per transcript) with the HTSeq v0.6.1 script htseq-count using Ensembl annotations [267,268]. Raw counts were then normalized for differential expression analysis using DESeq2 v2.11.39 [269]. Normalized counts from DESeq2 were processed using Cluster 3.0 for preparation of heatmaps using Java TreeView Additional analysis such as gene ontology (GO) was performed on HTSeq counts by the UM Bioinformatics Core using iPathwayGuide ($p<0.05$ and $Log_2FC>0.6$).

Data availability

RNA sequencing data resulting from this study will be made available for download upon publication.

RESULTS

R1/E mESCs produce otic vesicle-like and organoid structures

To produce derived otic vesicles and inner ear organoids, we used the inner ear organoid protocol optimized for R1/E mESCs, with BMP4/SB431542 treatment at day 3 and FGF2/LDN193189 treatment at day 4.25 (Figure 11A) [70]. First, we established that the R1/E cell line recapitulated major checkpoints for inner ear organoid production in our hands, including formation of otic vesicle-like structures in the early maturation phase (Figure 11B-H'). At this time, R1/E-derived aggregates displayed translucent regions surrounding dense cores (Figure 11H-H'), in contrast to the overall dense aggregates of $Pax2^{EGFP/+}$ mESCs we have previously shown [231]. Otic vesicle-like structures could be visualized within the translucent regions by brightfield microscopy before the aggregates became opaque due to continued tissue expansion. These could be released from the surrounding aggregate by a combination of enzymatic and mechanical disruption as described in Materials and Methods (Figure 11I).

Within intact aggregates, the vesicles themselves expanded in size, becoming large-fluid-filled cysts by day 20-22 (Figure 11J). Immunofluorescence staining of epithelia dissected from these cysts revealed hair cell-like cells, indicating inner ear organoid fate (Figure 11K-L).

Figure 11: Formation of organoids from R1/E cell line

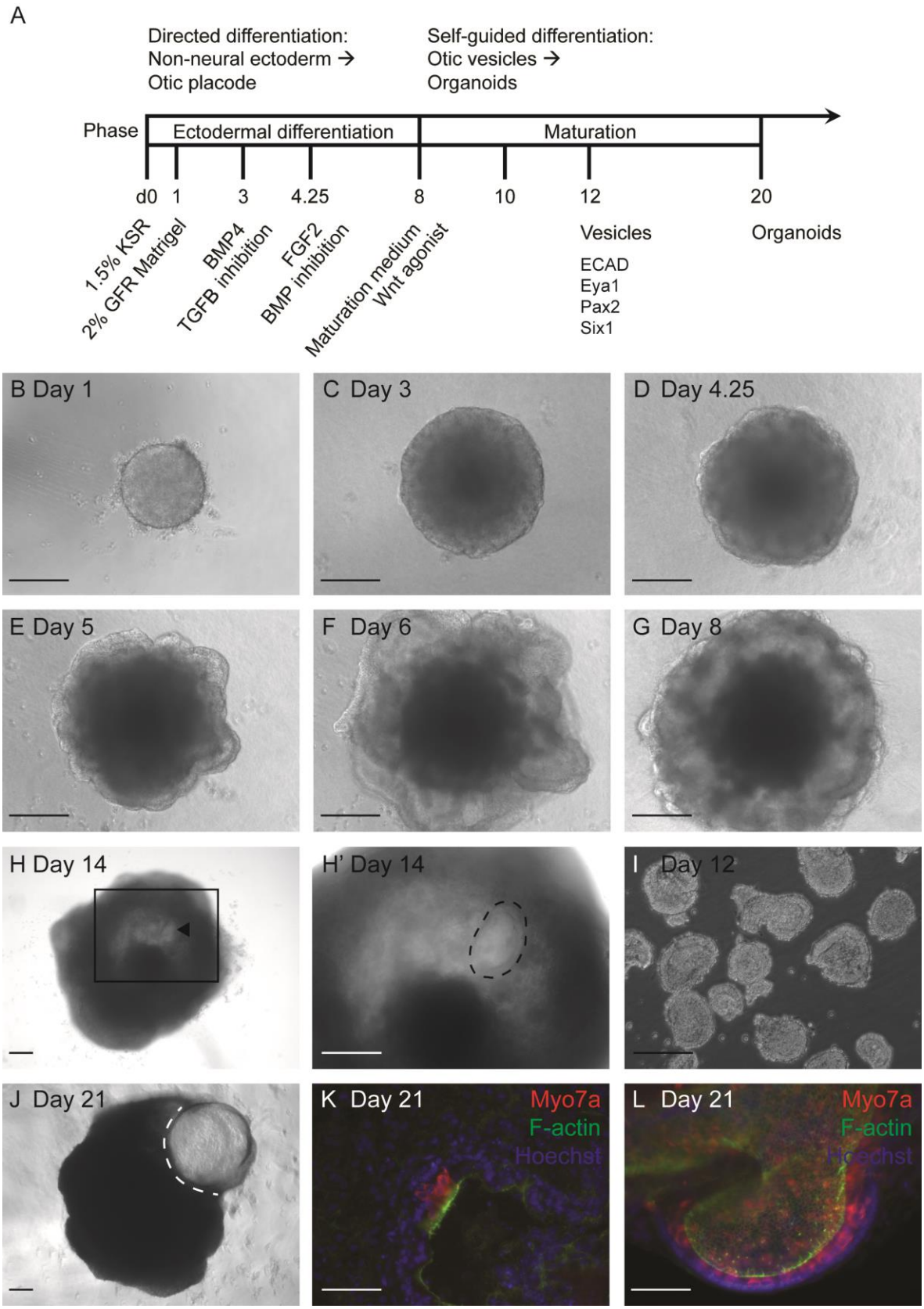

Formation of organoids from R1/E cell line. A: Modified timeline of inner ear organoid formation (compare to Figure 3). Changes from our previous experiments using $Pax2^{EGFP}$ mESCs include the following: In this study, FGF2 was always applied at 100 ng/mL, and the FGF2/BMP inhibitor (LDN193189) treatment was applied at day 4.25 instead of day 4.5. The Wnt agonist (CHIR99021) was always included during days 8-10. Although not shown in the figure, stem cell maintenance medium was changed from a classic formulation with serum and LIF to a newer 2i media formulation [270]. Ectodermal differentiation medium included 1.5% KSR rather than the 10% KSR required by $Pax2^{EGFP}$ aggregates. Y-27632 was omitted at aggregate formation. Finally, the reagent used to dissociate mESC colonies for was changed from non-enzymatic buffer to TrypLE Express. These changes were made to reproduce conditions used by Koehler et al. in the original inner ear organoid protocol and modifications made by DeJonge et al. for R1/E cells [68,70]. B-G: Changes in aggregate morphology in aggregates treated on day 3 with SB431542 as per the original inner ear organoid protocol. Extensive ruffling occurred by day 6 as described by Koehler and Hashino [69]; ruffling was was much more pronounced than observed in our prior cultures with $Pax2^{EGFP}$ mESCs. H-H' Vesicles are observed in translucent regions early in the maturation phase. H' shows a magnified view of a vesicle from panel H. I: Example of isolated vesicles. J: Organoid-stage aggregate with hair cell-containing region outlined. K-L: Immunofluorescence images of a cryosectioned (K) or dissected (L) organoid stained for hair cell markers Myo7a and F-actin. Scale bars: A-J: 200 μm, K-L: 50 μm.

TGFβ signaling inhibition by SB431542 is not necessary for derived otic vesicles

To investigate the role of TGFβ signaling in differentiation of otic tissue, we first examined SB431542-treated and untreated aggregates at day 12. In parallel, we sought to optimize TGFβ inhibition to ensure an optimal baseline of ectoderm for subsequent stages of differentiation. Therefore, we also examined aggregates treated with RepSox and SIS3, small molecules that inhibit TGFβ signaling via alternative mechanisms from that of SB431542 (Figure 12A). Whereas SB431542 and RepSox block signaling at the receptor level upstream of effectors Smad2 and Smad3, SIS3 specifically blocks activation of Smad3.

For quantification of vesicles formed by day 12, aggregates were disrupted and vesicles manually selected and counted. SB431542-treated and untreated aggregates produced vesicles at comparable efficiency; however, RepSox and SIS3 resulted in significantly more vesicles per aggregate ($p<0.05$) (Figure 12B). Despite differential efficiency in vesicle formation, the vesicles in all conditions were qualitatively similar as assessed by immunofluorescence staining. Day 12 tissues were cryosectioned and immunostained for 4 markers of embryonic otic vesicles: E-cadherin, Pax2, Six1, and Sox2. Fluorescence imaging revealed that the translucent regions observed early in maturation were spaces lined by epithelia from which otic vesicles pinch away, as shown previously in R1 aggregates [68,70]. Positive staining of vesicles for all 4 markers was observed in all aggregates regardless of TGFβ inhibition at day 3 (Figure 12C-F’’’).

Figure 12: Comparison of TGFβ pathway inhibitor effects at vesicle stage of differentiation

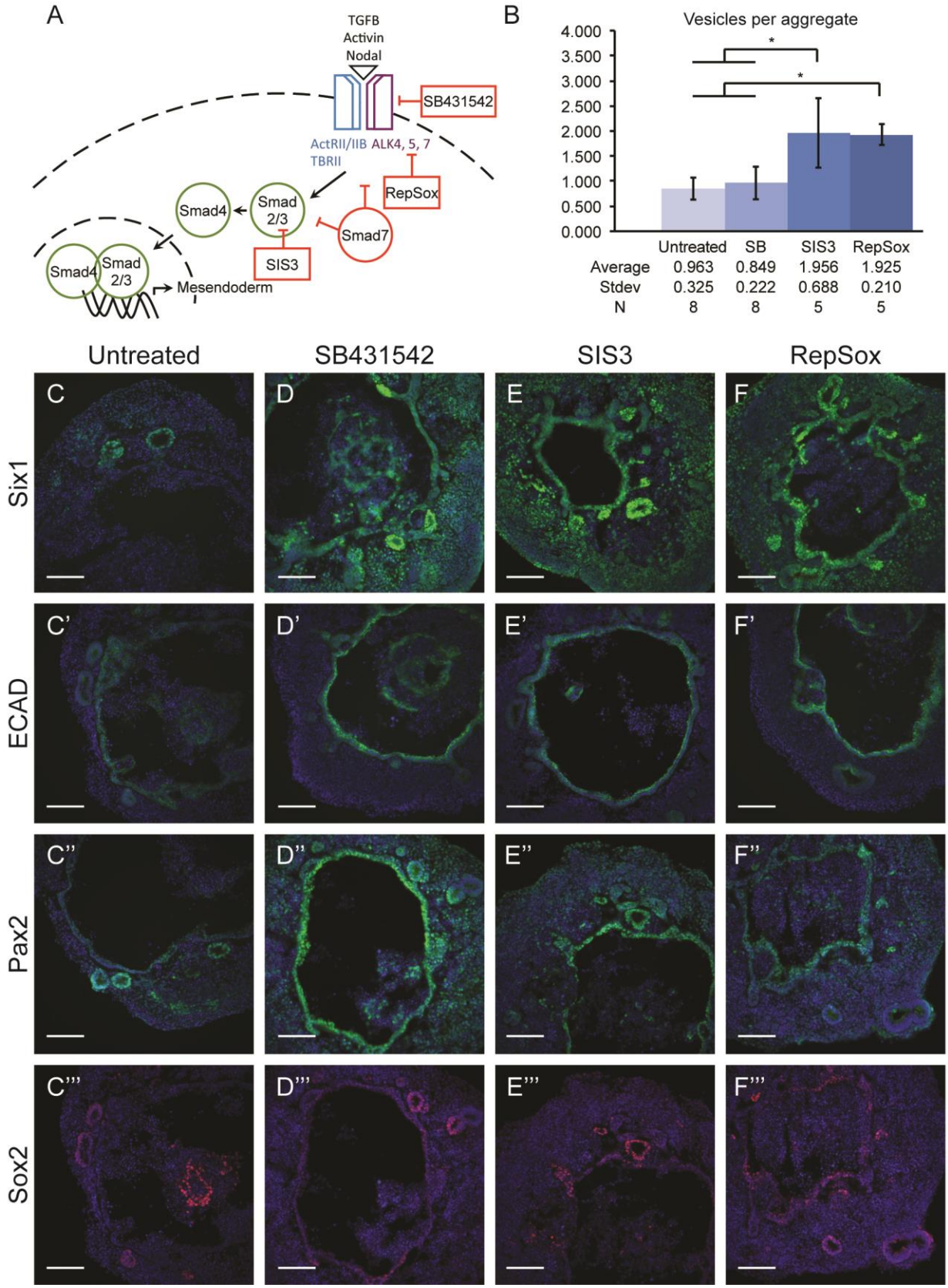

Comparison of TGFβ pathway inhibitor effects at vesicle stage of differentiation. A: Schematic showing mechanisms of TGFβ pathway inhibition. SB431542 targets type I receptors ALK4, 5, and 7. RepSox specifically targets ALK5. SIS3 specifically targets the effector Smad3. Smad7 is an endogenous inhibitor that regulates Smad-mediated signaling. B: Quantification of vesicles formed by day 12 in aggregates treated with differential TGFβ inhibition at day 3. Both RepSox and SIS3 produced more vesicles than SB431542 or untreated aggregates (unpaired t-tests, *$p<0.05$; mean ± standard deviation). C-F’’’: Immunofluorescence images of cryosectioned aggregates stained for otic vesicle markers. Positive staining was noted in all conditions. Scale bars: 100 μm (C-F’’’).

TGFβ signaling inhibition is necessary for inner ear organoids

Having observed improved efficiency of vesicle formation with the alternative inhibitors, we then investigated potential effects on organoid formation. Organoids form in the late maturation phase through the continued differentiation of vesicles; however, not all vesicles will necessarily become organoids. Thus, it was necessary to test the assumption that the alternative inhibitors RepSox and SIS3 may improve the yield not only of vesicles but of organoids as well.

We identified large, fluid-filled cysts indicative of organoids in the SB431542 (11/12 trials), RepSox (7/7 trials), and SIS3 treatment groups (6/7 trials). These cysts were either internal to the aggregates or protruding from their surfaces. The presence of hair cells was confirmed in both types via immunofluorescence staining in cryosections or dissected tissues, respectively. In all 3 TGFβ-inhibited groups, hair cells were Myo7a^{+} with apical F-actin^{+} stereocilia-like bundles and surrounded by thick F-actin belts as in native inner ear sensory epithelia (Figure 13A-C). The untreated group never produced either type of cyst (0/8 trials), and hair cells were not found in cryosections, which were screened in 3 of the 8 trials as a check on scoring organoid formation by visualization of cysts.

We then compared the influence of SB431542, RepSox, and SIS3 on aggregates' potential to form inner ear organoids. The percentage of aggregates with at least one cyst was quantified. No statistically reliable difference was observed amongst the 3 inhibitor groups (Figure 13D). RepSox, however, produced the highest average percent organoid-positive ($p=0.061$, t-test compared with SB431542) and with the least

Figure 13: Comparison of TGFβ pathway inhibitor effects at organoid stage of differentiation

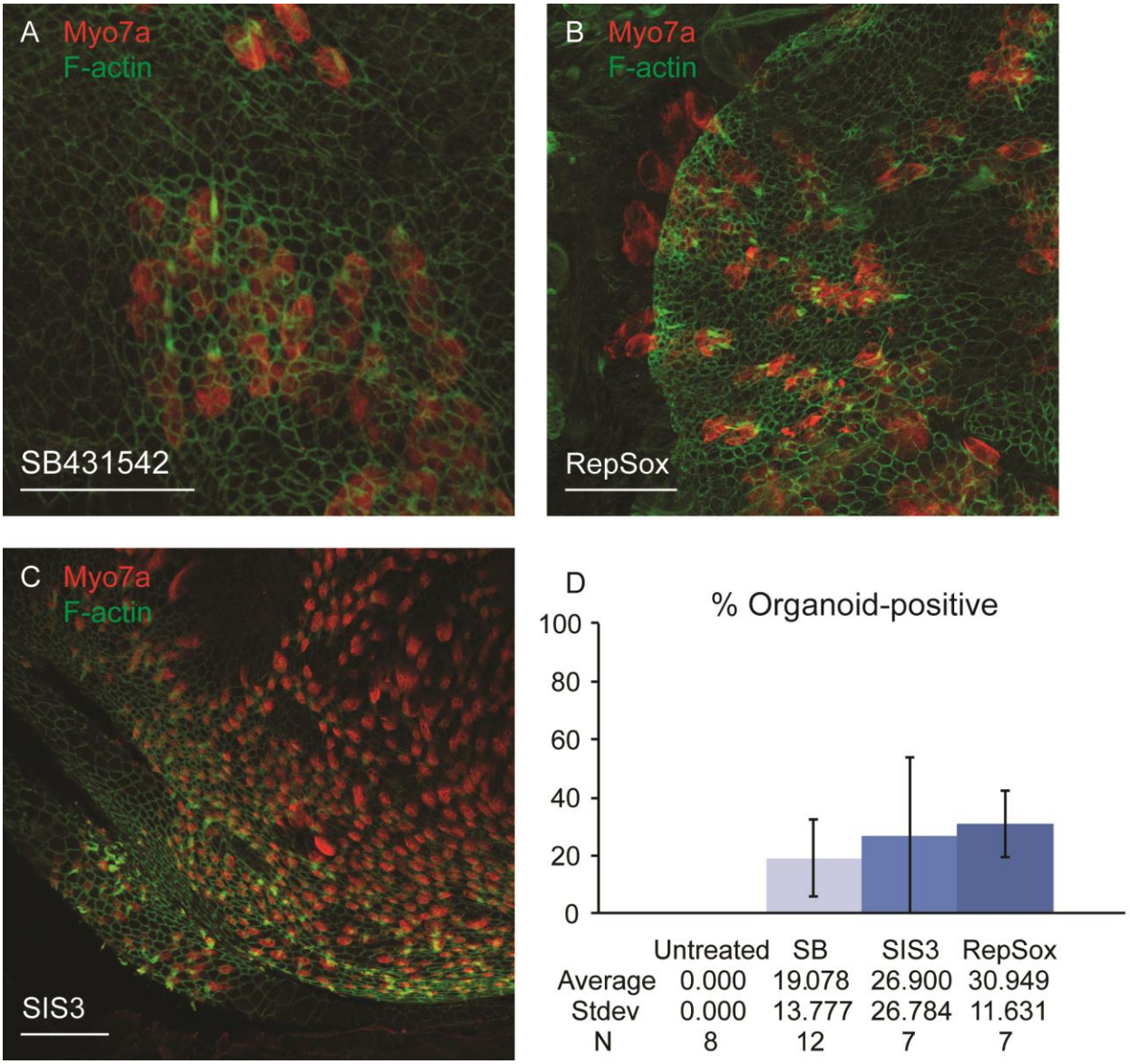

Comparison of TGFβ pathway inhibitor effects at organoid stage of differentiation. A-C: Confocal images of dissected organoids immunostained for hair cell markers Myo7a and F-actin. $Myo7a^{+}$ hair cells with $F\text{-}actin^{+}$ apical stereocilia bundles were noted in all tissues except those not treated with a TGFβ inhibitor (not shown). D: Quantification of hair cell-containing organoids. No significant difference was found, although RepSox was preferred for its tendency to produce more organoids with less variation in yield (unpaired t-tests, $p>0.05$; mean ± standard deviation). Scale bars: 50 μm.

variation between trials, making it a candidate for replacing SB431542 in future studies, pending further validation.

Vesicles derived from SB431542-treated cultures approach native otic vesicle transcriptome

To date, SB431542 has been used to promote non-neural ectoderm in all prior publications of mouse and human inner ear organoid protocols [68,70,71,75,231]. We sought to elucidate the long-term effects it exerts on derived otic vesicles and their competence to form hair cell-containing organoids. We also sought to discover new targets for modulation by exogenous factors to derive more native embryonic-like vesicles. In doing so, we would expect to model native otic vesicle differentiation more closely and efficiently and to achieve auditory—not just vestibular—hair cell fate. Day 12 vesicles were collected from the SB431542-treated condition, referred to as BSFL (BMP4, SB431542, FGF2, and LDN193189), and from the untreated condition, referred to as BFL. These were compared against each other as well as E10.5 otic vesicles harvested from C57BL/6 embryos in transcriptome analysis via RNASeq. Differentiation day 12 and embryonic day 10.5 were considered analogous as vesicles have just formed, and neuroblasts are in the process of delaminating [182,231].

First, the quality of RNA input and sequence reliability were assessed. The RNA integrity scores ranged from 8.0-10.0, and the mean quality score (Q) for each sequence was at least 36.14, corresponding to a 0.024% base call error probability (P). At least 93.03% of bases had a quality score of 30 or higher (Table 6). Analysis of sequences was performed using the Galaxy web platform [264]. The overall GC

content of the sequences was 49-50%, revealing no major bias. Only 0.1-0.2% of base pairs were trimmed due to lower quality (Q<20), and 99.1% remained in each sample after trimming and filtering (Table 7). The alignment of sequences to Ensembl annotated transcripts was performed using HTSeq Count, with at least 96.5% of reads per sample mapping to a feature (Table 8). The percentage of unique reads, indicating the mapped reads corresponding to a single feature, was at least 86.6%.

Gene expression profiles of otic vesicles produced by the 3 conditions were then analyzed in DESeq2 and iPathway Guide. A Venn diagram was generated to summarize the overlap between lists of differentially expressed genes generated from pairwise comparisons (Figure 14A). Differential expression was determined at $\log_2$(fold change)>0.6, and significance was determined at p-value (adjusted for false discovery rate)<0.05. In iPathway guide, 52636 total annotated features were examined. The number of genes unique to the E10.5 (native) vs BFL (derived) comparison was the highest at 1668, with 1083 unique to E10.5 vs BSFL and 236 unique to BSFL vs BSFL. Additional sets of genes appeared in the union of 2 or 3 comparisons. Principal component analysis (PCA) revealed the closeness of relationships between biological repeats and conditions by plotting their variation in two dimensions (Figure 14B). The biological repeats in each of the 3 conditions formed discrete clusters. In principal component 1 (PC1), which is the best representation of variation between samples, the relationship of BSFL and E10.5 clusters was closer than that of BFL and E10.5 clusters. Like the PCA plot, a correlation heatmap and hierarchical clustering illustrate that BSFL samples were closer to E10.5 than BFL samples were (Figure 14C). Samples were most closely related within each condition than across conditions, indicating relative

Table 6: Quality of RNA input and base call output

Sample	*Lane**	*Total RNA quality (RIN)*	*Barcode sequence*	*PF Clusters (reads)*	*% PF Clusters*	*Yield (Mbases)*	*% >= Q30 bases*	*Mean Quality Score (Phred)*
BFL-1	1	8.5	CTTGTA	24,280,297	91.05	1,578	93.33	36.2
BFL-1	2	8.5	CTTGTA	24,292,939	90.96	1,579	93.34	36.2
BFL-2	1	8.0	CCGTCC	21,681,310	91.01	1,409	93.03	36.14
BFL-2	2	8.0	CCGTCC	21,707,042	90.93	1,411	93.04	36.14
BFL-3	1	8.4	TTAGGC	24,874,381	91.12	1,617	93.05	36.14
BFL-3	2	8.4	TTAGGC	24,838,064	91.02	1,614	93.04	36.14
BFL-4	1	8.2	GATCAG	27,530,756	91.19	1,789	93.22	36.18
BFL-4	2	8.2	GATCAG	27,545,248	91.11	1,790	93.22	36.18
BSFL-1	1	8.6	ACTGAT	27,614,354	91.14	1,795	93.28	36.19
BSFL-1	2	8.6	ACTGAT	27,666,177	91.07	1,798	93.28	36.19
BSFL-2	1	8.8	ATTCCT	35,022,277	90.87	2,276	93.29	36.19
BSFL-2	2	8.8	ATTCCT	35,063,235	90.78	2,279	93.29	36.19
BSFL-3	1	8.0	GGCTAC	32,497,568	91.14	2,112	93.12	36.16
BSFL-3	2	8.0	GGCTAC	32,490,459	91.05	2,112	93.11	36.16
E10-1	1	9.7	ACTTGA	30,318,211	91.11	1,971	93.22	36.18
E10-1	2	9.7	ACTTGA	30,332,421	91.03	1,972	93.21	36.18
E10-2	1	9.8	CGTACG	27,370,770	91.02	1,779	93.16	36.17
E10-2	2	9.8	CGTACG	27,377,820	90.94	1,780	93.16	36.17
E10-3	1	10.0	AGTTCC	29,853,525	90.35	1,940	93.21	36.18
E10-3	2	10.0	AGTTCC	29,877,200	90.26	1,942	93.21	36.18
E10-4	1	9.1	GTTTCG	28,635,237	90.63	1,861	93.23	36.18
E10-4	2	9.1	GTTTCG	28,648,774	90.51	1,862	93.22	36.18

Table 7: Sequence quality determined by Fastqc and Trim Galore!

		Fastqc			*Trim Galore!*		
Sample	*Lane**	*Sequences flagged as poor quality*	*Sequence length before trimming*	*%GC*	*% Base pairs quality-trimmed***	*% Reads length-filtered after trimming****	*% Base pairs after trim/filter*
BFL-1	1	0	65	49	0.1	0.1	99.1
BFL-1	2	0	65	49	0.1	0.1	99.1
BFL-2	1	0	65	50	0.1	0.1	99.1
BFL-2	2	0	65	50	0.1	0.1	99.1
BFL-3	1	0	65	49	0.1	0.1	99.1
BFL-3	2	0	65	49	0.1	0.1	99.1
BFL-4	1	0	65	49	0.1	0.1	99.1
BFL-4	2	0	65	49	0.2	0.1	99.1
BSFL-1	1	0	65	49	0.1	0.1	99.1
BSFL-1	2	0	65	49	0.2	0.1	99.1
BSFL-2	1	0	65	49	0.1	0.1	99.1
BSFL-2	2	0	65	49	0.1	0.1	99.1
BSFL-3	1	0	65	49	0.1	0.1	99.1
BSFL-3	2	0	65	49	0.1	0.1	99.1
E10-1	1	0	65	49	0.1	0.1	99.1
E10-1	2	0	65	49	0.2	0.1	99.1
E10-2	1	0	65	50	0.1	0.1	99.1
E10-2	2	0	65	50	0.1	0.1	99.1
E10-3	1	0	65	50	0.1	0	99.1
E10-3	2	0	65	50	0.1	0	99.1
E10-4	1	0	65	49	0.1	0.1	99.1
E10-4	2	0	65	49	0.1	0.1	99.1

* Each sample was run in 2 lanes
** Phred score cutoff (per base quality) = 20
***After trimming adapters, discarded reads shorter than 20 bp

Table 8: Alignment of BAM file reads to annotated transcripts

Sample	*Total BAM file reads*	*% Mapped*	*% Mapped to forward strand*	*No feature (Reads mapped but no feature annotated)*	*Ambiguous (Reads with >1 feature at the mapped locus)*	*Not aligned (Reads not mapped to a locus)*	*Unique reads = Total BAM file reads - No feature - Ambiguous - Not aligned*	*% Unique reads*	*Alignment not unique (Total alignments of reads mapped to >1 locus)*
BFL-1	79115506	97.7	51.4	3653399	1506159	1794986	72160962	91.2	43138205
BFL-2	54629733	96.9	50.3	2959491	1767296	1725220	48177726	88.2	18155791
BFL-3	80257772	97.6	46.8	3168302	1574902	1970412	73544156	91.6	43494776
BFL-4	69198084	96.7	49.7	4505347	2160955	2287554	60244228	87.1	23029940
BSFL-1	68805580	96.5	47.5	4540231	2188093	2458247	59619009	86.6	22405056
BSFL-2	110773524	97.5	52.9	4624885	2225348	2770098	101153193	91.3	58510460
BSFL-3	81087825	96.6	49.5	4674452	2353780	2809619	71249974	87.9	26574097
E10-1	73969184	97.3	61.1	3324875	2357667	2036344	66250298	89.6	21903917
E10-2	67353052	97.3	46.6	3077971	2180446	1858195	60236440	89.4	20592341
E10-3	73832198	97.3	49.9	3138940	2458663	2027702	66206893	89.7	22917308
E10-4	70149841	97.3	53.4	3219652	2219175	1922924	62788090	89.5	21108960

uniformity in biological repeats (Figure 14C). A heatmap of significantly differentially expressed genes separated into 3 clusters: E10.5-enriched (C1), BFL-enriched (C2), and BSFL-enriched (C3) (Figure 14D). Specific markers of otic vesicles (OV), neuroblasts (N), and signaling pathways (Sig) and other tissues relevant to otic development were identified among the 3 groups.

GO analysis of differentially expressed genes returned generic terms related to organismal and developmental processes with hundreds of genes per term; the top 10 results per comparison are shown (Table 9). Filtering the results to ear-related terms did reveal differences from the broad category of ear development (in all 3 comparisons) to the specific categories of inner ear receptor cell development and stereocilium organization (BSFL vs BFL). The BSFL vs BFL comparison returned the largest number of ear-related terms (10 terms compared to 5 in E10.5 vs BFL and 4 in E10.5 vs BSFL). The identities of genes related to inner ear development were examined as shown in BFL vs. BSFL and BSFL vs. E10.5 comparisons (Figure 15).

DISCUSSION

In this study, parallels between early stages of inner ear organoid formation and mouse otic development were explored. The role of the TGFβ pathway in body axis patterning and germ layer specification is conserved across vertebrate and invertebrate species [271]. Likewise, its inhibition promotes an ectodermal lineage in mESC aggregates on the path toward otic fate through the inner ear organoid protocol. Efficiency of each step in differentiation depends upon the efficiency of the preceding step. Because of this, TGFβ signaling on day 3 of the protocol is pivotal in the

Figure 14: Differential expression analysis of day 12 derived and E10.5 embryonic otic vesicles

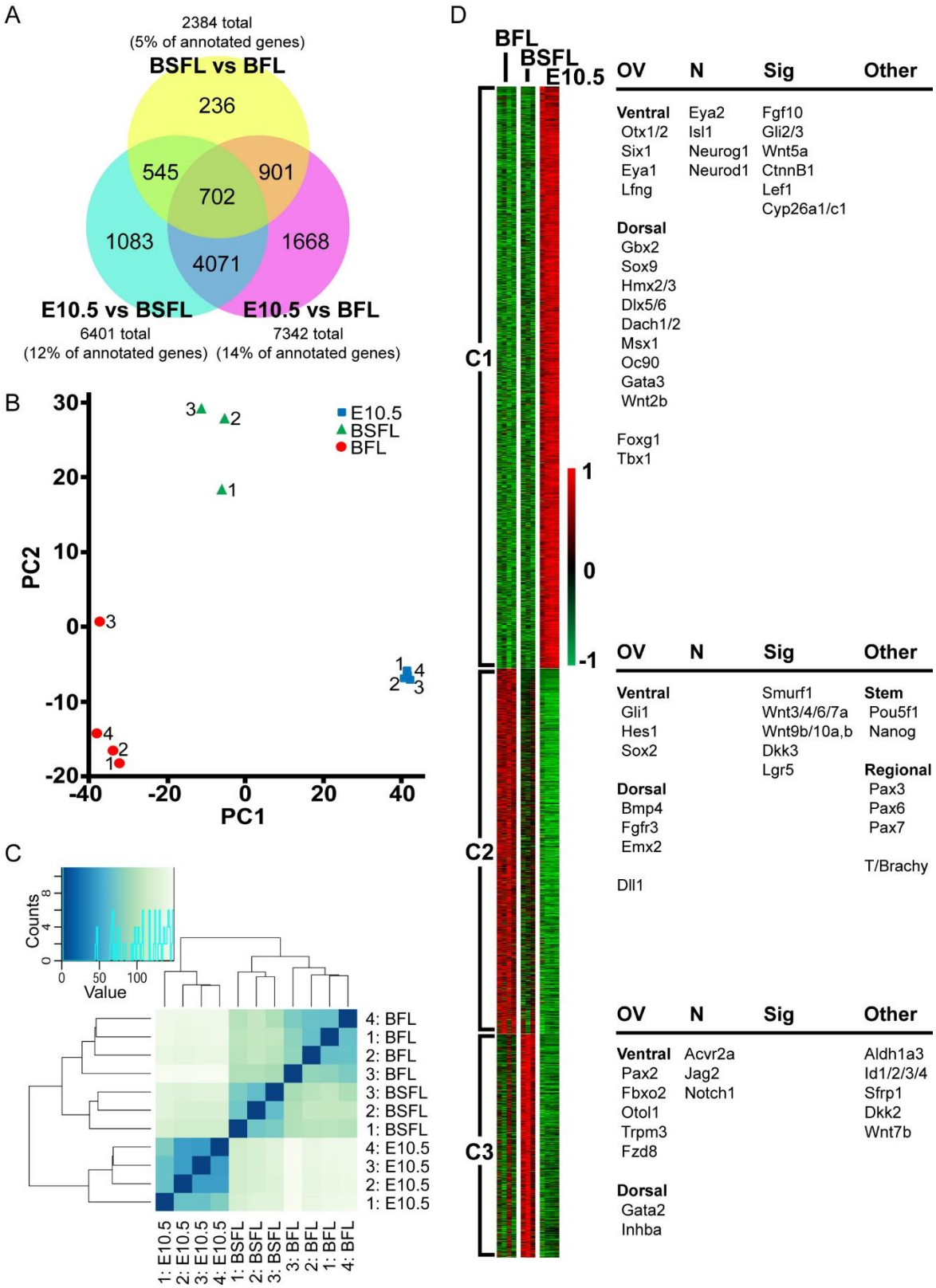

Differential expression analysis of genes with $\log_2$(fold change)>0.6 and p<0.05. A: Venn diagram illustrating overlap in differential expression lists from pairwise comparisons between conditions. B: PCA illustrating closeness of relationships within and between conditions. C: Correlation heatmap and hierarchical clustering showing levels of relatedness between individual samples. D: Heatmap of differentially expressed genes separated into 3 clusters (C1, C2, and C3) based on enrichment in each of the 3 conditions over the other 2. Expression data were normalized to maximum and minimum, giving a range of values from -1 to 1 with mean of 0. Particular genes of interest are highlighted to the right.

Table 9: GO analysis of biological processes of differentially expressed (DE) genes

	BSFL VS BFL			E10.5 VS BFL			E10.5 VS BSFL		
TOP 10	GO term	#genes (DE/ALL)	p-value	GO term	#genes (DE/ALL)	p-value	GO term	#genes (DE/ALL)	p-value
1	multicellular organismal process	**1052** / 5532	1.00E-24	multicellular organismal process	**2407** / 5663	1.00E-24	multicellular organismal process	**2081** / 5663	2.10E-23
2	single-multicellular organism process	**978** / 5131	1.00E-24	single-multicellular organism process	**2230** / 5235	1.00E-24	single-multicellular organism process	**1930** / 5235	5.90E-22
3	animal organ development	**613** / 2796	1.00E-24	anatomical structure development	**2039** / 4839	1.37E-22	anatomical structure development	**1770** / 4839	7.20E-18
4	system development	**769** / 3811	1.00E-24	single-organism developmental process	**2143** / 5118	1.37E-22	positive regulation of biological process	**1698** / 4625	9.80E-18
5	single-organism developmental process	**940** / 5028	1.00E-24	developmental process	**2163** / 5172	1.37E-22	developmental process	**1876** / 5172	2.40E-17
6	developmental process	**945** / 5082	1.00E-24	tissue development	**779** / 1625	2.41E-22	single-organism developmental process	**1858** / 5118	2.60E-17
7	anatomical structure development	**896** / 4754	1.00E-24	animal organ development	**1269** / 2852	6.37E-22	single-organism process	**3630** / 10678	4.50E-17
8	multicellular organism development	**828** / 4302	1.00E-24	cell differentiation	**1499** / 3451	2.26E-21	multicellular organism development	**1610** / 4378	6.10E-17
9	anatomical structure morphogenesis	**533** / 2434	1.00E-24	multicellular organism development	**1853** / 4378	3.08E-21	animal organ development	**1090** / 2852	3.40E-16
10	animal organ morphogenesis	**264** / 923	1.00E-02	system development	**1661** / 3876	3.37E-21	response to stimulus	**2228** / 6291	1.20E-15
EAR-RELATED	GO term	#genes (DE/ALL)	p-value	GO term	#genes (DE/ALL)	p-value	GO term	#genes (DE/ALL)	p-value
1	ear development	**76** / 215	5.47E-15	ear development	**121** / 217	2.44E-07	ear development	**93** / 217	0.01
2	inner ear development	**64** / 186	4.55E-12	ear morphogenesis	**77** / 127	1.27E-06	inner ear development	**81** / 188	0.018
3	ear morphogenesis	**49** / 125	1.40E-11	inner ear development	**104** / 188	3.68E-06	ear morphogenesis	**58** / 127	0.018
4	inner ear morphogenesis	**40** / 103	2.37E-09	inner ear morphogenesis	**63** / 105	2.61E-05	inner ear morphogenesis	**48** / 105	0.038
5	middle ear morphogenesis	**11 / 24**	0.001	middle ear morphogenesis	**19** / 24	7.51E-04			
6	inner ear receptor cell differentiation	**21** / 70	0.002						
7	inner ear receptor stereocilium organization	**12 / 33**	0.007						
8	outer ear morphogenesis	**5 / 9**	0.026						
9	regulation of inner ear receptor cell differentiation	**5 / 9**	0.026						
10	inner ear receptor cell development	**14** / 50	0.03						

Figure 15: Genes from GO term inner ear development

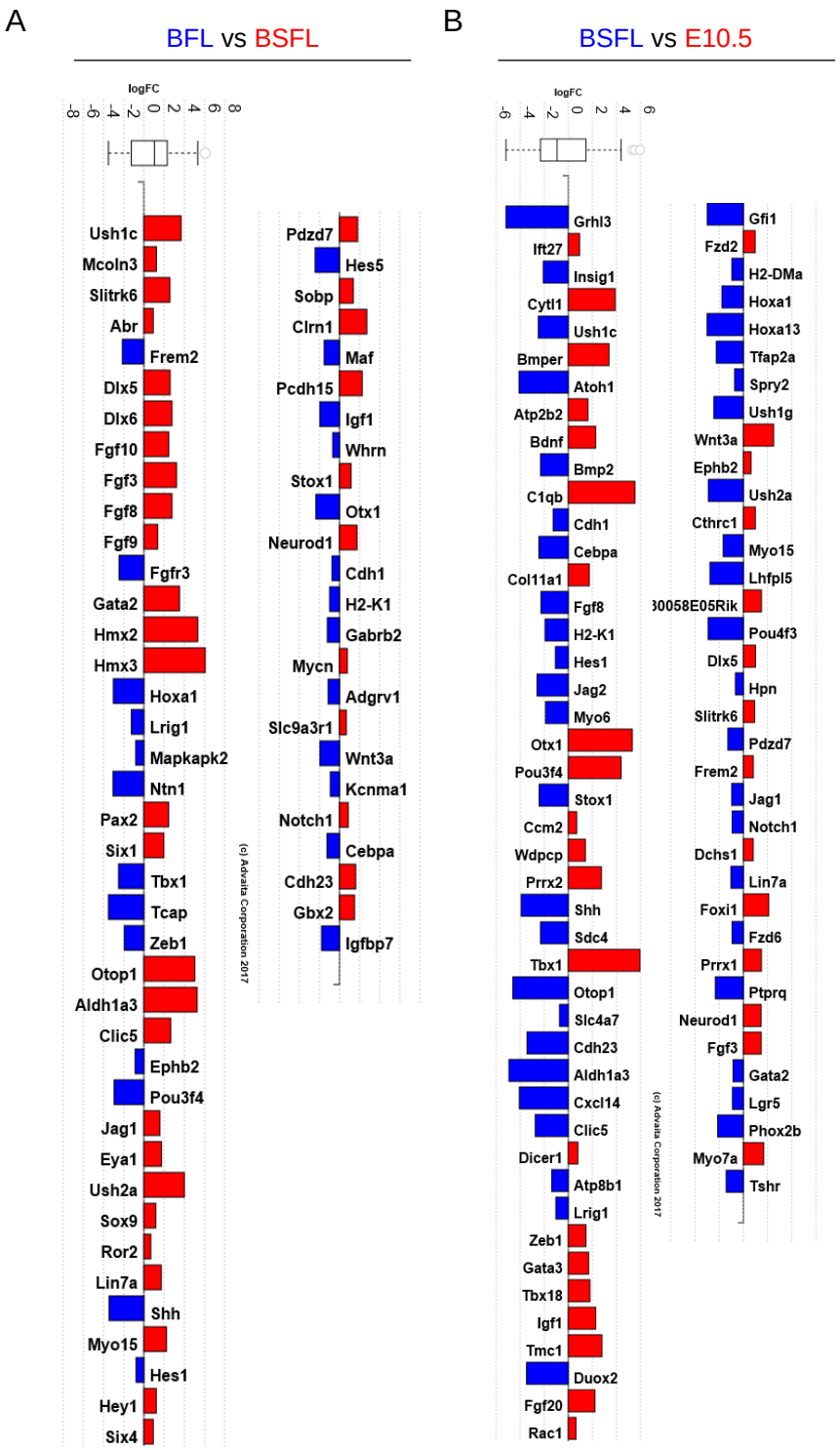

Differentially-regulated genes related to inner ear development from GO analysis. A: BFL (blue) vs BSFL (red) in left 2 columns. B: BSFL (blue) vs E10.5 (red) in right 2 columns.

production of vesicles and organoids that emerge several days later. Given the fundamental role TGFβ signaling plays in embryos and in early differentiation of stem cells, it was a logical target to begin optimizing the inner ear organoid method to reach its full potential.

In our cultures, TGFβ inhibition was necessary for vesicles to mature into hair cell-containing organoids. However, derived otic vesicles were observed in the maturation phase with or without of TGFβ inhibition in the earlier ectodermal differentiation phase. Vesicles were similar in expressing all 4 otic vesicle markers assayed. Exclusion of SB431542 had no discernible impact on vesicle formation or character. This was surprising given that attenuation of TGFβ signaling by endogenous antagonists is thought to be necessary for formation of anterior ectoderm in developing mouse embryos [80–84]. Epiblast explants from mice lacking Nodal, a ligand for TGFβ receptors, are biased towards anterior ectodermal differentiation, and the embryos fail to produce mesendoderm [80,85–88]. If TGFβ inhibition maximizes differentiation along a non-neural ectodermal lineage path and restricts mesendoderm, then the incidence of otic vesicle-like structures at similar rates with and without SB431542 is unexpected. One explanation is that our panel of otic vesicle markers may be too narrow or the immunostaining approach not sensitive enough to detect subtle changes in expression functionally significant for further differentiation.

Another explanation would be that stem cell aggregates are not fully equivalent to embryos, so their ability to model all aspects of embryonic development is limited. Several stem cell studies have demonstrated neural differentiation through TGFβ pathway inhibition, however, indicating sufficiency in modeling this particular aspect of

development. SB431542 has been used as a neuralizing factor in cultures of mouse epiblast stem cells and human embryonic stem cells [97,98,272]. LeftyA, an inhibitor to Nodal, was used to promote differentiation towards telencephalon fate in mESC aggregates [99]. Finally, Koehler et al. showed a reduction in Brachyury (a marker of mesoderm) and upregulation of TFAP2α (a marker of non-neural ectoderm) in establishing the original inner ear organoid protocol with SB431542 [68]. Our aggregates may have a lower baseline of TGFβ signaling at day 3 as suggested by the similar morphologies between our untreated and SB431542-treated aggregates from Koehler et al. at points during the ectodermal differentiation phase (Figure S3) [68]. In that case, our uninhibited cultures would represent an intermediate level of TGFβ signaling, sufficiently low for vesicle formation but too high for maturation of organoids. Differential baseline levels of activated Smad1/5/8 downstream of BMP receptors have been reported previously for various human stem cell lines [116]. This results in differential requirements for BMP4 inhibition in neural induction from hESCs [114]. A similar cell line-dependent variability in baseline TGFβ signaling could necessitate optimization of TGFβ inhibition in the inner ear organoid protocol.

The improved efficiency of vesicle formation per aggregate with RepSox and SIS3 supports these inhibitors as useful alternatives to SB431542. However, the increased percentage of aggregates with organoids was not statistically significant, although RepSox resulted in the highest percentage and least variance. The discrepancy in outcomes between vesicle and organoid stages raises interesting possibilities: More vesicles may form within the same percentage of aggregates, or more aggregates may produce vesicles with fewer of the vesicles competent to become

organoids. Given that increased yields of otic tissue will be necessary for downstream applications of the inner ear organoid protocol, the mechanism by which RepSox leads to increased yields of otic tissue merits further investigation. RepSox was named for its ability to replace Sox2 in generating induced pluripotent stem cells (iPSCs) through the Yamanaka factor approach [273,274]. It does so by upregulating Nanog, which has been shown to restrict differentiation of neuroectoderm and mesendoderm [272]. Whether this mechanism could have shifted ectodermal tissue toward the non-neural lineage, causing increased formation of derived otic vesicles, remains to be determined.

Ligands for TGFβ receptors have been shown to produce differential outcomes despite activating the same effectors, Smad2 and Smad3 [275,276]. TGFβ signaling is subject to complex regulatory processes from ligand traps and accessory receptors at the cell surface to nuclear shuttling and transcriptional cofactors (see review [277]). Even though the TGFβ family type I receptors ALK4, 5, and 7 all signal through Smad2/3, targeting one of these receptors (or its corresponding ligand) is not necessarily expected to produce the same outcome as targeting another or all 3. This was demonstrated simply in a study of Activin and Nodal in P19 cells: Treatment with Activin caused a significantly shorter duration of Smad2 activation than did Nodal treatment [278].

In our cultures, all 3 TGFβ inhibition strategies tested had observable effects in our cultures; thus, we infer some baseline of TGFβ signaling. Using SB431542 broadly inhibits TGFβ receptor heterotetramer complexes whether they incorporate the type I receptor ALK4, 5, or 7 [263]. RepSox, on the other hand, only targets complexes incorporating ALK5 [279]. Since ALK5 complexes are activated by Activin and ALK7

complexes by Nodal, RepSox would therefore allow endogenous Nodal signaling to proceed uninhibited [90]. The fact that RepSox and SIS3 increased vesicle yields above SB431542 may be related to Smad2 activation, due either to persistent Nodal signaling (with RepSox) or to selective inhibition of only Smad3 (with SIS3 [280]). SB431542, in contrast, inhibits receptors that activate both Smad2 and Smad3. Our initial hypothesis was that SIS3 may have more noticeable effects on vesicle or organoid formation relative to SB431542 because its mechanism of action is uniquely at the effector level. However, the idea that targeting ALK5 via RepSox would lead to observable differences compared to inhibiting all 3 ALK receptors via SB431542 is reasonable given the many layers of regulation on top of the simplified ligand-receptor-Smad model of TGFβ signaling.

Since uninhibited aggregates ultimately failed to produce organoids, the impact of TGFβ inhibition was ostensibly delayed until after the vesicle stage. This suggests an epigenetic mechanism. In development, epigenetic changes have been suggested to explain the delay between onset of competence factors and preplacodal markers, with most of gastrulation occurring in the interim [130]. Embryonic stem cells show global DNA demethylation so that progressive epigenetic changes may underlie commitment to lineage paths; in addition, epigenetic mechanisms may play an active role in fate decisions [281,282]. Investigating epigenetic changes in the derived vesicles resulting from TGFβ activation several days prior is a possibility with the myriad novel epigenomics approaches [282]. This not only could inform optimization of the inner ear organoid protocol by revealing targets for demethylation to re-open blocked lineage

paths, for instance, but could also provide new insights into mechanisms involved in early embryonic development.

In our gene expression analysis, PCA and heat mapping revealed that, relative to untreated derived vesicles, SB431542-treated vesicles represented an overall shift towards the native E10.5 transcriptome. In the expression levels of some genes, however, SB431542-treated vesicles were still more “derived” than “native-like,” as evidenced by the closeness of the BSFL cluster to the BFL cluster along PC1. Achieving a more native-like vesicle through additional optimization of the inner ear organoid protocol is a goal of ongoing studies. Focusing on genes differentially expressed between native and derived vesicles and unaffected by TGFβ inhibition via SB431542 may reveal new targets for additional exogenous factors (Table S3).

With the rise of organoid approaches in regenerative medicine and developmental modeling, our ability to define molecular fingerprints for unique cell types is likely to become more sophisticated. Already the stem cell research community is shifting towards larger sets of markers to distinguish stages of differentiation. Our RNASeq dataset clearly shows differential regulation of genes between TGFβ-inhibited and uninhibited tissues several days after treatment of these cultures diverged. From this subset of genes, a new set of criteria may emerge for defining otic vesicles that captures their potential to achieve hair cell fate. Because our analysis is restricted to persistent mRNA transcriptome-level changes, targets of acute differential gene regulation remain to be discovered.

Some of the most striking differences in expression were in a set of genes related to retinoic acid (RA) signaling. RA is implicated in patterning the anterior-

posterior axis of the otic vesicle [184]. The otic placode epithelium is exposed to opposing gradients of RA producing and degrading enzymes as the placode invaginates to form the otic cup [283]. By the time the otic vesicle has fully formed, the epithelium is no longer responsive to RA, yet RA is crucial to establish anterior (e.g., Lfng and NeuroD) and posterior (e.g., Tbx1) marker domains within the otic vesicle [283]. Opposing roles for RA in regulation of Tbx1 have been reported. In the posterior OV, RA appears to promote Tbx1 [283]. This relationship has also been implicated in anterior-posterior patterning of placodal tissues in general [284]. In other, non-placodal tissues, RA and Tbx1 are mutually repressive (Figure 16) [285,286]. Our data, surprisingly, fit with this non-placodal model. Our analysis shows *Tbx1* in a category of genes expressed more in native vesicles than in derived vesicles (Table S3). Conversely, retinoic acid receptor beta (RARb) expression was higher in derived vesicles, and RA producing enzyme Aldh1a3 expression was elevated in BSFL derived vesicles. RA catabolizing enzymes Cyp26a1 and Cyp26c1 were expressed more in native than derived vesicles. These observations suggest that Tbx1 suppression in derived vesicles may relieve inhibitory regulation of RA. As further

Figure 16: Model of relationship between RA, Tbx1, and Otx1

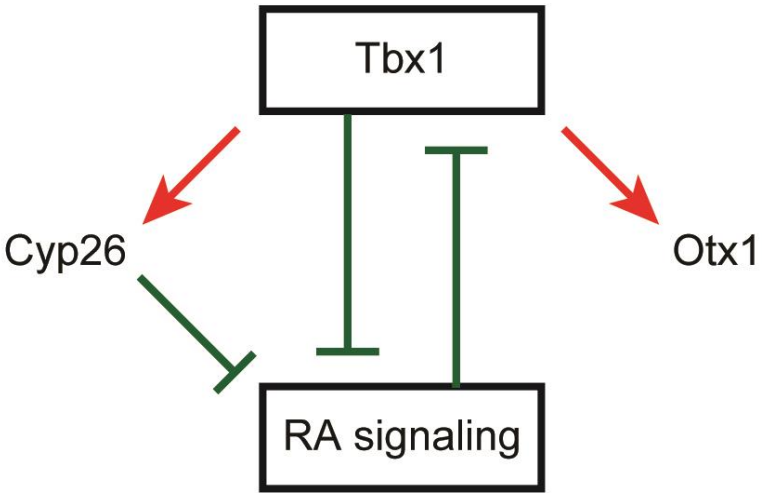

Figure adapted from Yutzey et al. 2010 [285]. Tbx1 and RA are mutually repressive, and Tbx1 is necessary for Otx1 expression in the ventral otic vesicle. Cyp26, RA degrading enzyme, is also downstream of Tbx1.

evidence, Otx1 expression was higher in native vesicles vs derived vesicles. Tbx1 is necessary for expression of Otx1 in the ventral otic vesicle [287], and both Tbx1 and Otx1 are necessary for morphogenesis of the inner ear [288,289]. A shift in anterior-posterior patterning with SB431542 treatment would be logical given the major role of TGFβ in establishing the anterior-posterior body axis early in embryogenesis [76,79,80]. Interestingly, the expression of anterior placodal genes *Pax3*, *Pax6*, and *Pax7* is highest in BFL; this is unexpected as embryonic TGFβ signaling promotes posteriorization but may suggest dysregulation of anterior-posterior cues in derived otic tissues. Altogether, our results suggest that RA signaling may be too active in derived vesicles. Inhibition of RA or input of other anterior-posterior patterning molecules could be advantageous to promote formation of otic tissue and improve yields.

An additional goal of our ongoing studies is to achieve auditory hair cells rather than vestibular. In development, auditory hair cells arise from ventral otic vesicle progenitors whereas vestibular hair cells arise from dorsal progenitors. Thus, we propose to induce a shift in patterning from dorsal to ventral character in our vesicle-stage aggregates. Since our vesicles are more dorsal—in that they give rise to vestibular-like hair cells—and since native vesicles are patterned with dorsal and ventral aspects, our RNASeq data may reveal targets for ventralizing morphogens. Although opposing gradients of Wnt and SHH from the dorsal and ventral hindbrain stand out as drivers of dorsal-ventral patterning in otic vesicles, they do not control patterning of all genes differentially required for dorsal or ventral structures. For instance, Hmx3 is required for development of the vestibular inner ear [290]. Otic vesicles of E9.5 mice show normal dorsolateral Hmx3 expression regardless of SHH knockout or constitutive

activation of the Wnt effector B-catenin [162,163]. Notably, Hmx2 and 3 are significantly upregulated in our BSFL and native samples compared to BFL (Table S3). This suggests that TGFβ signaling is related to suppression of Hmx2/3. To our knowledge, whether TGFβ signaling contributes directly or indirectly to otic vesicle patterning in concert with Wnt and SHH has not been explored.

Another motivation for studying downstream targets of TGFβ signaling is the idea that TGFβ pathway inhibition could promote regeneration in the inner ear. This is inspired by an interesting parallel between inner ear and kidney development: Both require expression of the transcription factor Pax2. Evidence suggests that TGFβ signaling is inhibitory to regeneration of kidney tubule cells following renal ischemia. After such an event, Pax2 is re-expressed in proliferative renal cells as damaged tissue is regenerated [291]. Activin, a ligand for TGFβ receptors that is also upregulated in ischemic renal tissue, regulates proliferation by suppressing Pax2 [291]. Revealing an analogous role for Pax2 in the ear, Pax2 knockout mice form otic vesicles, but their cochlear ducts fail to extend due to reduced proliferation and increased apoptosis [148–150]. In sum, the idea that TGFβ inhibition may be useful in inner ear regeneration, supported by evidence in the kidney, is worth exploring by elucidating targets of TGFβ signaling.

Overall, the large sets of differentially-regulated genes in our analysis reflect the foundational role of germ layer specification early in embryonic development. Neural tube, neural crest, and placodal derivatives all originate from definitive ectoderm. Therefore, our study may facilitate future research focused on modeling development of these tissues. Understanding TGFβ signaling will be especially beneficial to inner ear

research as it may lead to generating large quantities of hair cells for *in vitro* studies and for developing *in vivo* hair cell replacement therapy.

CHAPTER 4: Discussion of key findings and ongoing studies

The preceding two chapters presented results of experiments addressing key questions about modeling inner ear development with a 3-dimensional stem cell-based approach. Our questions focused on the role of FGF and TGFβ signaling pathways. Ultimately, our observations—both directly and indirectly related to these pathways—prompted many follow-up questions for future research. We also recognized the utility of the inner ear organoid protocol for asking novel questions not necessarily related to embryonic development. In this chapter, our major findings and the potential for direct follow-up studies will be discussed. Finally, this chapter will describe the pilot studies we have initiated in developmental modeling and other applications of the organoid technology.

DISCUSSION OF KEY FINDINGS

In Chapter 2, we demonstrated that mESCs modified with the *Pax2*^{EGFP} allele were valuable in investigating otic induction during formation of inner ear organoids. Nascent derived otic vesicles could be monitored easily using epifluorescence microscopy. Epifluorescence imaging of live tissues and immunofluorescence staining of cryosections indicated diffuse Pax2 expression throughout the aggregates; however, the EGFP signal was clearly brightest at the vesicles. The vesicles could then be observed over time in live culture as they developed into large, hair cell-lined cysts. The

Pax2^{EGFP} reporter is additionally useful in selecting vesicles isolated using the collagenase-hyaluronidase method described in Chapter 3, providing quick confirmation that the selected vesicles express Pax2. Future studies may include disruption of vesicles to single cells, followed by fluorescence-activated cell sorting to purify otic progenitors for additional downstream assays or applications. Establishing the utility of this cell line is significant alone: ES lines derived from C57BL/6 mouse strains had not previously been tested, and stem cell lines can vary in their responses to differentiation cues. As we observed, Pax2$^{EGFP/+}$ aggregates differed from R1/E aggregates in terms of morphology; this was important to note since morphological features from R1 cells were previously described as criteria for successful inner ear organoid cultures.

Using Pax2$^{EGFP/+}$ aggregates, we showed that within the hour after FGF2 is applied on day 4.5 to promote otic fate, ERK phosphorylation occurs. This supports the mechanism of ERK-mediated, FGF-driven otic induction proposed in avian and zebrafish developmental literature [241,242]. Strengthening this evidence was the dose-dependent relationship we found between FGF2 and ERK phosphorylation. To establish that activated ERK is necessary for otic induction, future work should include inhibition of the ERK pathway using a pharmacological agent such as PD98059, which targets MEK, the kinase that phosphorylates ERK. If this pathway is necessary for hair cell formation, then inhibition of parallel pathways involving AKT and PLCγ, which are also activated downstream of FGF receptors, may be beneficial: Since AKT is implicated in otic neurogenesis, it may direct cells away from hair cell fate toward otic neuronal fate. Inhibiting this would, in theory, maximize the population of progenitors directed to become hair cells.

The fact that the inner ear organoid protocol produces both hair cells and neurons can be considered a feature since it opens the possibility of modeling synapse formation and function. The origin of inner ear organoid neurons had not previously been studied. To address the nature of these neurons, we asked whether they originate from derived otic vesicles. Indeed, we found Islet1/2^{+} cells adjacent to the vesicles, evocative of delaminating neuroblasts in embryonic development. Future investigation using a fate-mapping approach could be used to settle this question by marking cells originating from vesicles. Nonetheless, finding evidence of an additional parallel with embryonic inner ears suggests additional utility of the protocol in developmental modeling of otic neurogenesis. Furthermore, it may lead to high-throughput generation of auditory and vestibular neurons for academic and clinical use.

By dissecting the organoid region away from an aggregate, we were able to demonstrate uptake of the styryl dye FM4-64FX by derived hair cells after a brief, 10-second application. This suggested mechanotransduction channel expression [244], motivating more intensive future investigation through simultaneous deflection of stereocilia bundles and electrophysiological recording. While improving efficiency is an important step in extending this protocol to the clinic, so, too, is ensuring that derived hair cells are functionally equivalent to native hair cells.

Remarkably, the inner ear organoid protocol reproduces many features of an inner ear sensory epithelium. However, our experiences also exposed limitations of the current protocol and opportunities for improvement. Though the protocol can generate organoids at high efficiency (in terms of % organoid-positive aggregates), this depends upon competence of the tissue to respond to differentiation cues at each step. Some

indications of competence are readily assayed. For instance, stem cells should express markers of pluripotency, and the non-neural ectodermal layer should express E-cadherin and AP2. We found that successful formation of organoids could be prevented by some factor or factors that we and others using the protocol have been unable to predict. In time, the issue seems to resolve, suggesting the influence of a seasonal variable such as temperature or humidity. These variables could directly affect the culture environment, resulting in inconsistent evaporation rates and therefore inconsistent concentrations of media components. They could also affect the production of animal-derived reagents (e.g., Matrigel). To move forward, we outlined best practices for monitoring and, when possible, ensuring success of the protocol in Table 5. Testing of synthetic reagents may help to resolve additional issues as new products are constantly being developed, some intended for use with the profusion of novel organoid approaches.

Other unpredictable features of the cultures represent opportunities rather than roadblocks for future research. The maturation phase of the inner ear organoid protocol occurs with vesicles developing into organoids in context of surrounding tissues that presumably provide physical and molecular signaling cues. We envision isolating vesicles using the enzymatic and mechanical approach we devised and culturing them separately in defined conditions. Vesicles could be embedded in an extracellular matrix or tunable hydrogel allowing for adjustment of stiffness. Reagent-soaked beads could then be positioned to supply diffusible factors in directional gradients. This would allow modeling the otic vesicle patterning that produces dorsal (vestibular sensory), ventral

(auditory sensory), and antero-ventral (neural) populations of vesicle-derived tissue. Additional cues could be tested for their potential involvement in patterning as well.

Of particular interest to us is recapitulating the gradient of SHH that favors ventral inner ear fates. In our aggregates, we were unable to demonstrate a distinct source of SHH analogous to the ventral neural tube or notochord. This suggests that the aggregates do not recapitulate otic vesicle patterning in a self-directed manner. SHH signaling may still occur at a level permissive of neuroblast formation, but the directionality that normally contributes to dorsal-ventral patterning appears to be absent. Mimicking the spatial arrangement of signaling cues will likely be necessary to produce specific hair cell types or to favor differentiation and survival of neurons, and this will likely require a directed approach during the maturation phase.

In Chapter 3 of this thesis, we showed that otic vesicles were derived with or without TGFβ inhibitor treatment on day 3. This was unanticipated, prompting questions about the role of the TGFβ pathway in early embryonic germ layer specification. The idea that it promotes mesoderm and endoderm while inhibiting ectoderm may be an oversimplification. One possibility is that TGFβ receptor activation results in epigenetic effects that restrict terminal differentiation of ectodermal derivatives without preventing the formation of definitive ectoderm or ectoderm-derived progenitors. Thus, our untreated aggregates could have produced ectoderm competent to form otic vesicles that were, then, not competent to achieve hair cell fate due to an epigenetic modification. Testing this hypothesis is a potential focus of investigation that could reveal important insight into developmental mechanisms involving the TGFβ pathway and epigenetic restriction of fates. Alternatively, our unanticipated observation may

reflect cell line-specific differences in basal TGFβ signaling. This would be akin to cell-line specific baseline levels of activated Smad1/5/8, the effectors of BMP signaling, revealed in various stem cell lines [116].

One goal of our future work is to isolate otic progenitors from day 12 vesicles for implantation into a deafened auditory epithelium. We hypothesize that *in situ* signaling cues will encourage integration and differentiation to repopulate the sensory epithelium. The increased efficiency of vesicle production (in terms of number of vesicles per aggregate) makes SIS3 and RepSox tempting alternatives to SB431542 for implantation. While we preferred RepSox for its tendency to produce organoid-positive aggregates with less variable efficiency, neither RepSox nor SIS3 resulted in a statistically reliable increase in organoid production above SB431542. One possible explanation is that although more vesicles are present, the surrounding tissue is not providing the correct types or levels of cues conducive to hair cell differentiation. Another explanation is that the vesicles themselves are less responsive to those cues. Thus, we must consider whether the increased number of vesicles produced by RepSox would be responsive to *in situ* signaling cues following implantation. Therefore, additional work is necessary to evaluate the vesicles produced by RepSox-treated cultures. We propose adding a RepSox condition to our RNASeq comparative analysis.

The fact that the mechanism of TGFβ signaling inhibition impacted otic differentiation, at least at the vesicle stage, argues for a closer investigation of TGFβ signaling. This pathway can involve multiple receptors, effectors, and regulatory proteins at each point between the ligands and transcriptional targets. Understanding the signaling processes involved in inner ear development is important as we attempt to

recapitulate these in stem cell cultures. Optimizing TGFβ signaling inhibition, the first step of directed differentiation in the inner ear organoid protocol, will contribute to ultimate efficiency of organoid production. It may also contribute to producing otic progenitors that are most competent to respond to later stages of differentiation and maturation.

Our RNASeq study represents the first transcriptome-level comparison of stem cell-derived and native otic tissue. Of the thousands of differentially expressed genes between derived and native samples, we focused on those with relatively high fold changes to ascertain major differences that could be targeted in a refined approach. Several of the highest fold changes were related to RA signaling. RA is involved in anterior-posterior patterning of the otic vesicle [283]. Genes positively related to RA signaling (i.e., those encoding receptor RARb and synthesizing enzyme Aldh1a3) were enriched in derived samples, whereas genes negatively related (i.e., those encoding the catabolizing enzymes Cyp26a1 and Cyp26c1) were enriched in native samples. Interestingly, the RA target gene *Tbx1* (a marker of the posterior OV) and its downstream target *Otx1* were less expressed in the derived samples. Overall, this suggests an inhibitory relationship in derived tissues, with RA reducing expression of Tbx1 and, therefore, Otx1. Mutual repression of Tbx1 and RA has been described in non-placodal tissues such as the neural crest and pharyngeal arches [285,286]. This model, however, is at odds with one proposed for RA signaling in placodal tissues [284], including the otic placode [283]: In these tissues, RA is thought to promote Tbx1. Thus, our derived tissues unexpectedly fit with a non-placodal model of retinoic acid signaling.

In embryonic development, otic tissue loses responsiveness to RA as the otic cup invaginates and the otocyst forms [283]. Furthermore, the RA-synthesizing and catabolizing enzymes influential for the anterior-posterior patterning effects are not localized to the otic tissue but rather expressed in adjacent mesoderm and ectoderm, respectively [283]. Thus, apparent differences in native and derived expression could be biased by carryover of adjacent tissue. To directly assess the potential influence of elevated RA signaling in our derived tissues, we propose to use mESCs modified with a reporter for a response element of RA. If our vesicles are, in fact, influenced by excessive RA signaling, then inhibiting this pathway would better model native embryonic conditions.

The overall highest fold changes we found were in *Hmx2* and *Hmx3* expression, with significant enrichment in SB431542-treated derived and native vesicles compared to uninhibited vesicles. This suggested a relationship between TGFβ inhibition and upregulation of these genes. *Hmx2* and *Hmx3* are expressed in the dorsolateral otic vesicle and required for vestibular inner ear development [162,163,290]. To our knowledge, direct involvement of TGFβ signaling in otic vesicle patterning has not previously been described. This evidence underscores the importance of optimizing our first step in directed differentiation through SB431542 or alternative inhibitors. As noted above, in addition to its early role in germ layer specification, TGFβ could potentially induce epigenetic changes that restrict the adoption of specific cell fates in later stages of differentiation. For instance, by regulating Hmx2/3, it may bias precursors on the path toward vestibular hair cell fate. Determining the mechanism of later-stage effects

of TGFβ inhibition (after initial specification of ectoderm) is a subject of interest. The long-term nature of these effects suggests investigation using epigenomics approaches.

ONGOING STUDIES

Even with the conclusion of these experiments, the potential of inner ear organoids is only beginning to be realized. *In vitro* modeling of mammalian embryonic development is a tractable, scalable, and overall more convenient alternative to *in vivo* studies. Aggregates throughout the inner ear differentiation protocol could be used to work out the multiple roles that molecules like SHH, Wnt, Sox2, Pax2, and others are suggested to play in mammalian inner ear development. Modeling damage or disease through ototoxic drugs, genetic aberrations (potentially through introducing mutations with CRISPR), or other challenges to inner ear physiology would be a highly valuable for biomedical research. Organoids could be used to test Notch pathway inhibitors to promote transdifferentiation of $Sox2^{+}$ supporting cells or to test additional regeneration strategies. These long-term goals necessitate optimization of the inner ear organoid protocol. Modifications to the protocol to tailor it to auditory vs vestibular fates and to improve overall yields are a major focus of ongoing efforts.

Opportunities for follow-up studies to our experiments were delineated above and in the preceding chapters. In addition, our lab has pioneered studies illustrating the broad range of future directions for inner ear organoid research:

1) Coculturing organoids with sections of mouse brainstem at the level of cochlear nuclei to study synapse formation in collaboration with Dr. Michael Roberts (KHRI, UM). The inner ear organoids are associated with neurons that may, as our imaging data suggests, delaminate from the vesicular epithelium and that do

appear to form synaptic contacts with the derived hair cells. We are interested in investigating whether these neurons can establish the next synaptic connection in the afferent pathway toward central auditory processing in the brain. Therefore, we obtained slices from mouse brainstem at the level of the cochlear nucleus and established conditions to culture these adjacent to isolated organoids (Figure 17A-D). We observed outgrowth of processes from the organoids, extending toward the brainstem slices (Figure 17E-F). Notably, in the absence of a brainstem slice, processes extending from the organoid explant did not extend radially but rather encircled the explant. Future experiments would investigate synaptic connections, for example, using fluorescent tracer such as Fluoro-Ruby to illuminate network structure or using a calcium indicator for network activity. This system could be used to model reinnervation of a deafened epithelium, examine

Figure 17: Preliminary testing of brainstem coculture

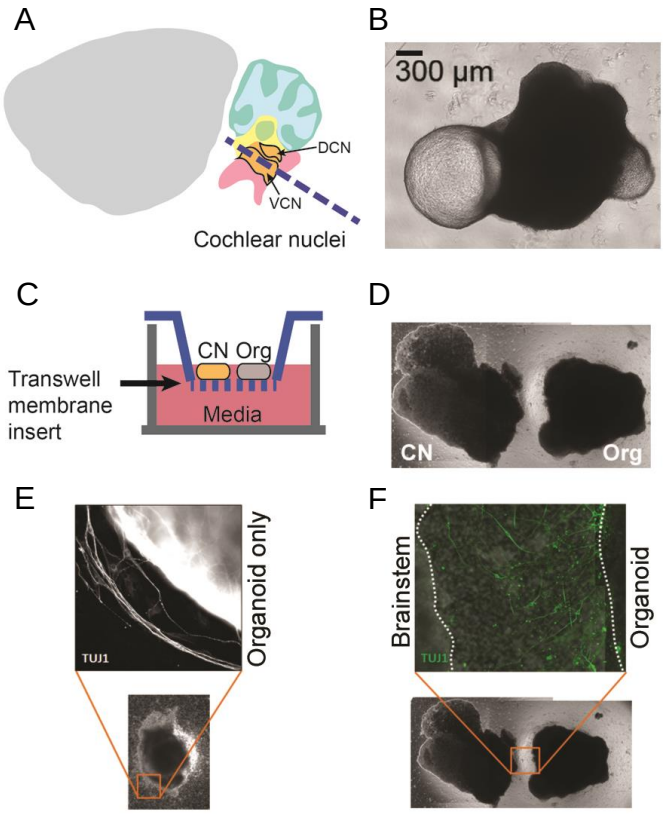

A: Preparation of cochlear nucleus (CN)-containing brainstem slice. B: Preparation of isolated organoid. C: Schematic of coculture system on Transwell membranes. D: Example of brainstem slice (left) and organoid (right) in culture on Transwell membrane. E: Tuj1 staining of organoid showing outgrowth of neuronal processes. F: Tuj1 staining showing both brainstem and organoid, with Tuj1^{+} processes traversing the space between them.

synapse formation, predict integration of regenerating tissue with the CNS, or to improve outcomes with cochlear implants through regrowth of peripheral processes to be stimulated by the electrodes.

2) Implanting organoids under kidney capsule in mice to promote maturation in a physiological environment, as has been performed with lung and intestinal organoids, in collaboration with Dr. Jason Spence (CDB, UM). The Spence lab has demonstrated that human intestinal organoids, derived from hESCs in vitro and engrafted under the mouse kidney capsule, undergo significant expansion and maturation of intestinal cell types [292]. Our labs collaborated to test this approach to maturation of our inner ear organoids, since the hair cells seem to arrest at an immature state. We recovered the tissue after a maximum of 5-6 weeks and sectioned and stained for hair cell markers. Locating hair cells within the tissue was extremely challenging, and evidence from our coculture experiments suggested that the organoids may not thrive when exposed to serum. If the number of hair cells per organoid prior to engraftment can be optimized by other means, then this strategy or a similar strategy for maturation would be worth revisiting. The Spence lab has also used a synthetic scaffold as an alternative to support culture and maturation of lung organoids, which also do not thrive when engrafted into the kidney [293]. This might provide a suitable environment for maturation of our organoids as well.

3) Implanting derived otic progenitors obtained from vesicle-stage aggregates into guinea pig ears to repopulate deafened auditory epithelia in collaboration with Dr. Yehoash Raphael (KHRI, UM).

Figure 18: Implantation of R1-EGFP mESCs and derived otic progenitors into deafened guinea pig cochlea

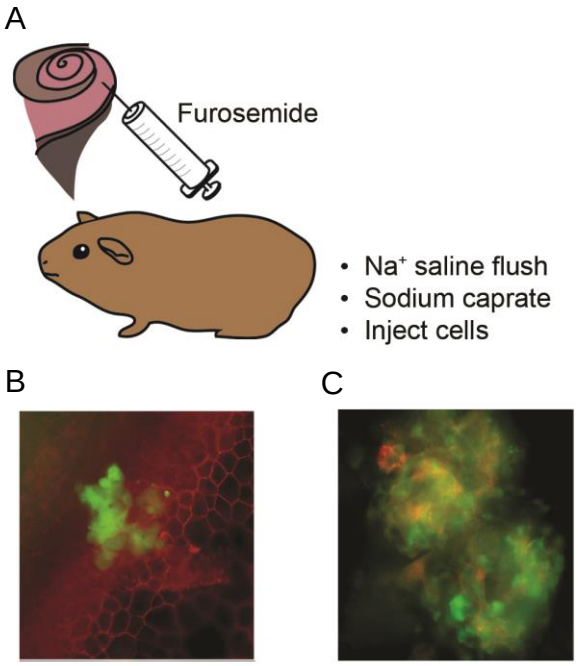

A: Preparation of guinea pig to receive implanted cells. The scala media is prepared using furosemide and extracellular medium to disrupt the normally harsh high-potassium environment. Sodium caprate is used to promote cell integration of cells into the flat deafened epithelium. Cells are then injected into the scala media. B-C: $EGFP^+$ cells from undifferentiated ES stage (B) or otic progenitor stage (C) are found after 24 hours.

Towards the goal of regenerating a sensory epithelium in a deafened ear, we have performed pilot experiments using R1 mESCs stably expressing EGFP. These were implanted into the scala media as single cells either at the stem cell stage or the otic progenitor stage (from day 12 vesicles derived using the organoid protocol, disrupted using enzymatic and mechanical means). The scala media is first prepared by injection with the loop diuretic furosemide to poison potassium pumping mechanisms and by flushing out the harsh, high-potassium endolymph with a standard extracellular medium. Sodium caprate is then used to break tight junctional barriers in the deafened auditory epithelium to promote integration of the implanted cells (Figure 18A). 24 hours after implantation, we observed clusters of $EGFP^+$ stem cells (Figure 18B) and of $EGFP^+$ derived otic progenitors

(Figure 18C). These pilot experiments provide encouraging evidence of cell survival. Our goal is to repeat this approach over a longer period to allow time for the cells to integrate and differentiate in context of a pro-otic environment.

4) Treating aggregates with additional morphogens such as SHH to induce ventralization of vesicles and produce auditory hair cells. Ongoing experiments in the lab are investigating the effect of SAG, an agonist to the SHH receptor Smoothened, and SANT-2, an antagonist to the same receptor, on the dorsal-ventral patterning of derived otic vesicles (Figure 19A). These cues are provided between day 10-12 of the organoid protocol, and vesicles are collected for qPCR

Figure 19: Evaluation of gene expression changes with SHH pathway modulators in derived otic vesicles

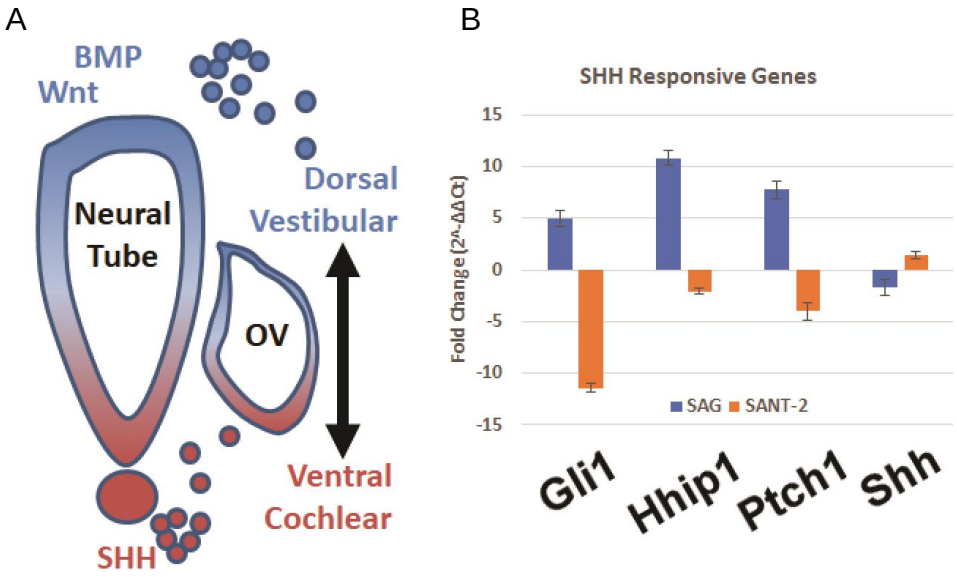

A: Schematic of endogenous factors implicated in dorsal-ventral patterning of the mammalian embryonic otic vesicle. B: Results of preliminary qPCR testing, showing differential regulation of SHH-responsive genes in vesicles from cultures treated with a SHH pathway agonist (SAG) or antagonist (SANT-2).

analysis of dorsal and ventral markers and SHH-responsive genes (Figure 19B). So far, we have observed upregulation of SHH pathway markers Gli1, Hhip1, and

Ptch1 resulting from SAG. Correspondingly, we have observed downregulation of these markers resulting from SANT-2. Additional analyses of dorsal-ventral markers and, at later stages, vestibular and auditory markers will be performed.

Considerations for widespread adoption of the organoid protocol include cell line differences that necessitate fine-tuning the doses and timing of drug treatments. This has been demonstrated by the optimization of FGF2/LDN193189 application within a 12-hour window [70]. Better modeling of the embryonic environment with a less variable product than Matrigel would be advantageous; toward this end, we have tested an alternative called BME2 (Amsbio) but found it to be no more effective than Matrigel. In adapting strategies from development for stem cell differentiation, the use of synthetic molecules is preferred due to their relative stability and affordability. These must be tested to ensure they replicate mechanisms of endogenous molecules without unintended effects. Many other labs have attempted to produce organoids without success; basic knowledge of stem cell pluripotency and priming are still catching up with labs aspiring to perform in translational research. Yet, the results presented here are some of the most promising examples of hair cells derived entirely *in vitro* compared to others published thus far. Since these results are possible and the downstream applications would be so lucrative, the reliable production of inner ear organoid cultures is a worthwhile pursuit.

Appendix

Supplemental Figures and Tables

Figure S1: Tracking increase in aggregate diameter during ectodermal differentiation phase

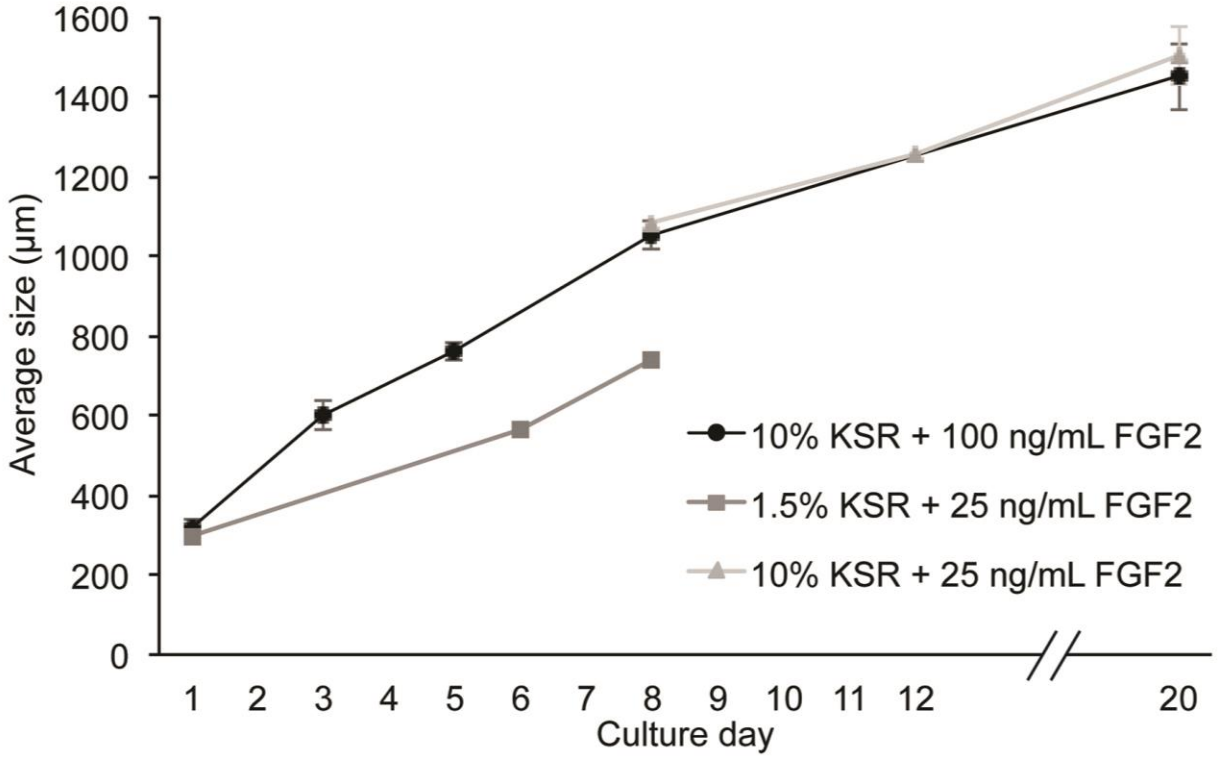

Tracking increase in aggregate diameter during ectodermal differentiation phase. Measurements of long-axis diameter were made from 4 random aggregates and averaged across multiple cultures. Aggregates cultured with 10% KSR and treated with 100 ng/mL FGF2 were measured at day 1, 3, 5, 8, and 20 (n=21, 6, 7, 11, and 6, respectively; mean ± standard deviation). Treatment with 25 ng/mL did not result in a difference in aggregate size as shown by measurements at days 8, 12, and 20 (n=1, 1, and 5, respectively; mean with ± standard deviation shown for day 20). Aggregates cultured with 1.5% KSR and treated with 25 ng/mL FGF2 were measured at day 1, 6, and 8 (n=2 each; mean).

Figure S2: Tracking inner ear organoid culture success rate with Pax2$^{EGFP/+}$ mESCs

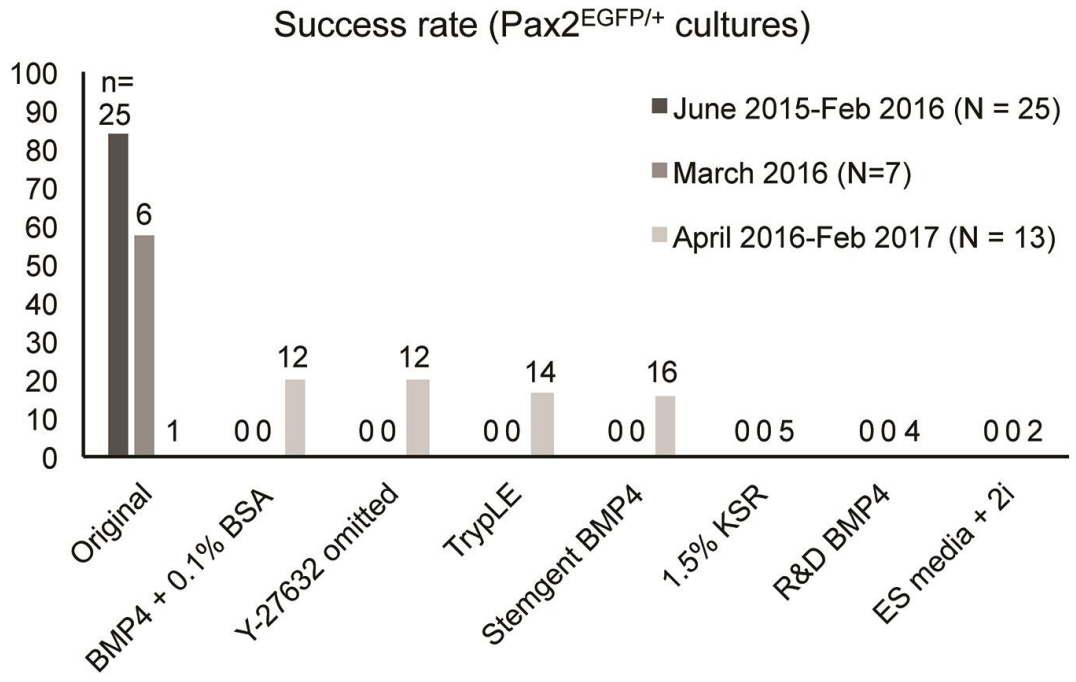

Tracking inner ear organoid culture success rate with Pax2$^{EGFP/+}$ mESCs. Major changes to the protocol tested during troubleshooting efforts are indicated. Results are separated into 3 groups: those obtained during a period of reliably successful cultures (from June 2015-Feb 2016), those obtained during a brief period of mixed otic and non-otic cultures (March 2016), and those obtained during a subsequent prolonged period of non-otic cultures with few, qualified successes. A culture was considered successful if at least 10% of aggregates formed vesicles and at least some of these became large, protruding cysts. Early cultures reliably contained hair cells in the organoid regions. In contrast, of the 2 cultures after March 2016 that resulted in cysts (of 13 total cultures), neither resulted in detectable hair cells. Changes to the protocol tested during this period included preparing BMP4 with 0.1% BSA as a carrier, omitting Y-27632 from ectodermal differentiation medium at the time of aggregate formation, using TrypLE to dissociate mESC colonies rather than non-enzymatic dissociation buffer, using 1.5% KSR in ectodermal differentiation medium, and including 2i (1 µM PD0325901 and 3 µM CHIR99021 [270]) in the mESC maintenance medium. These changes were made to faithfully replicate the methods of Koehler et al. An additional strategy was to test a different supplier of BMP4 on the basis of anecdotal evidence of variation in BMP4 potency between lots. The attempts shown in this figure are not independent, but the low percentage of qualified success during the April 2016-Feb 2017 period highlights that none of the changes made was a sole determinant of success.

Figure S3: Early aggregate morphologies with and without SB431542

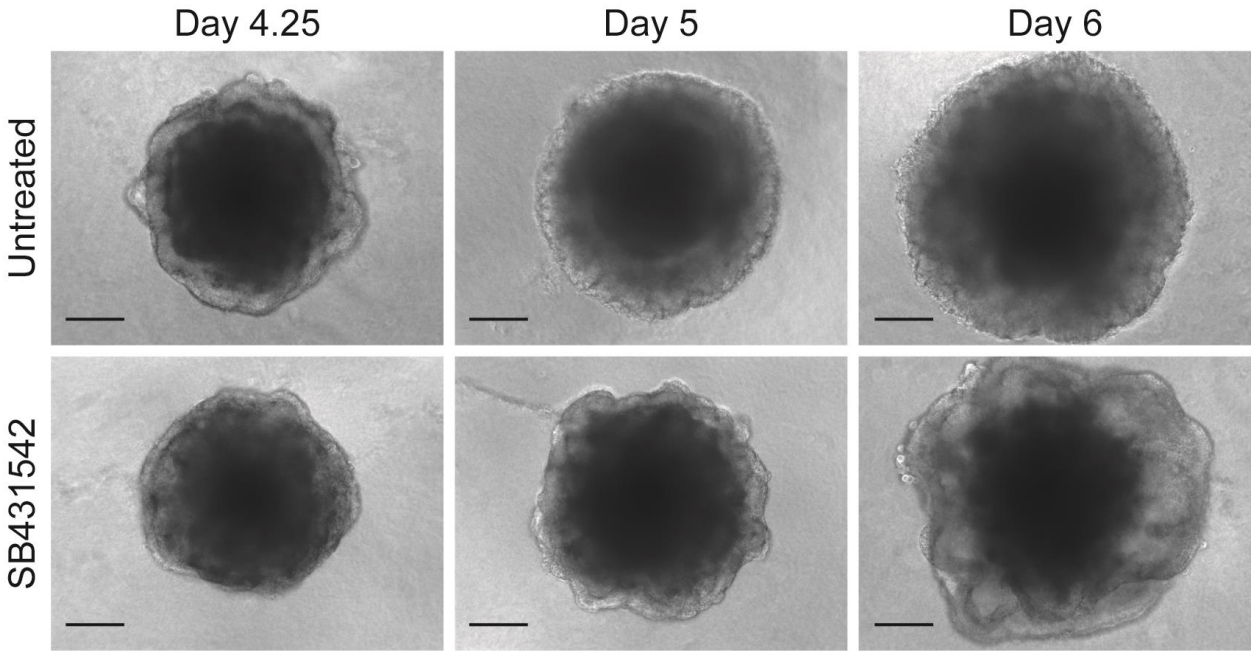

Early aggregate morphologies with and without SB431542. Brightfield images of aggregates at days 4.25, 5, and 6. Similarity between our untreated aggregates at days 4.25-5 and Koehler et al's SB431542-treated aggregates at days 5-6 prompted further investigation of the role of this pathway in our cultures [68]. Scale bars: 50 µm.

Table S1: Antibodies and stains used in Chapter 2

Immunostaining				
Target	**Supplier**	**Catalog number**	**Host**	**Dilution**
Acetylated Tubulin*	Sigma	T7451	Mouse	1:500
AP2	Developmental Studies Hybridoma Bank	3B5	Mouse	1:50
Brachyury	R&D	AF2085	Goat	1:20
Ctbp2	BD Transduction Labs	612044	Mouse	1:100
E-cadherin	Cell Signaling	3195	Rabbit	1:200
Eya1	Santa Cruz	sc-15094	Goat	1:50
F-actin (Alexa Fluor 488 Phalloidin)	Thermo Fisher Scientific	A12379		1:100
F-actin (Rhodamine Phalloidin)	Thermo Fisher Scientific	R415		1:100
FM 4-64FX	Thermo Fisher Scientific	F34653		5 µM
GluA2	EMD Millipore	MAB397	Mouse	1:1000
Hoechst 33242	Invitrogen	62249		1:2500
Islet-1/2	Developmental Studies Hybridoma Bank	39.4D5	Mouse	1:500
Myosin 7a	Santa Cruz	sc-74516	Mouse	1:100
Myosin 7a**	Proteus	25-6790	Rabbit	1:100
N-cadherin	BD	610920	Mouse	1:100
Neurofilament***	EMD Millipore	AB5539	Chicken	1:1000
Pax2	Biolegend	901001	Rabbit	1:200
Pax2	Invitrogen	71-6000	Rabbit	1:150
Pax8	Santa Cruz	sc-81353	Mouse	1:50
SHH	Developmental Studies Hybridoma Bank	5E1	Mouse	1:10
Six1	Sigma	HPA001893	Rabbit	1:1000
Sox2	Santa Cruz	sc-17320	Goat	1:100
Tuj1	Covance	MRB-435p	Rabbit	1:300
Tuj1**	Sigma	T2200	Rabbit	1:200
Pluripotency assay				
Klf4	R&D Systems	AF3158	Goat	1:200
Nanog	Abcam	ab80892	Rabbit	1:100
Oct3/4	Santa Cruz	sc-8628	Goat	1:50
Rex1	Thermo Fisher Scientific	PA5-27567	Rabbit	1:200
Sox2	Santa Cruz	sc-17320	Goat	1:100
Western blotting				
Actin	Cell Signaling Technology	4967	Rabbit	1:1000
pERK	Cell Signaling Technology	9106	Mouse	1:500
tERK	Cell Signaling Technology	9102	Rabbit	1:1000

Table S2: Antibodies and stains used in Chapter 3

Target	**Supplier**	**Catalog number**	**Host**	**Dilution**
ECAD	CST	3195	Rabbit	1:200
F-actin (Alexa Fluor 488 Phalloidin)	Thermo Fisher Scientific	A12379		1:100
Hoechst 33242	Invitrogen	62249		1:2500
Myosin 7a	Santa Cruz	Sc-74516	Mouse	1:100
Pax2	Invitrogen	71-6000	Rabbit	1:150
Six1	Sigma	HPA001893	Rabbit	1:1000
Sox2	Santa Cruz	Sc-365823	Mouse	1:100

Table S3: Analysis of genes with fold change at least 1.5 and p<0.05

Key
SB431542 effect: + moves towards E10.5; - moves away from E10.5; 0 no significant effect
Significant upregulation
Significant downregulation

SB431542 effect	Gene	E10.5 Native vs BSFL Derived					E10.5 Native vs BFL Derived					BSFL Derived vs BFL Derived				
		Normalized Counts	Log_2(FC)	StDev Log_2(FC)	Fold Change (FC)	Adjusted p-value	Normalized Counts	Log_2(FC)	StDev Log_2(FC)	Fold Change (FC)	Adjusted p-value	Normalized Counts	Log_2(FC)	StDev Log_2(FC)	Fold Change (FC)	Adjusted p-value
	BFL<BSFL<E10.5															
+	Dlx5	1082.0430384	1.0016129	0.2915010	2.0022372	0.0024851	1082.0430384	3.5977571	0.2763758	12.1068958	1.29E-36	1082.0430384	2.5961442	0.2966919	6.0466842	3.91E-16
+	Dlx6	427.4307160	0.5825812	0.2418042	1.4975262	0.0426798	427.4307160	3.3637530	0.2397872	10.2941514	1.88E-42	427.4307160	2.7811718	0.2564522	6.8741045	1.12E-24
+	Gbx2	858.4925449	1.7550033	0.5073362	3.3752709	0.0023046	858.4925449	3.2557521	0.4786998	9.5516641	1.32E-10	858.4925449	1.5007488	0.5094202	2.8298956	0.0277036
+	Msx1	1181.2823809	1.2010196	0.4297955	2.2990209	0.0164510	1181.2823809	2.9116162	0.4036866	7.5246069	8.07E-12	1181.2823809	1.7105966	0.4314710	3.2729615	0.0012027
+	Fgf10	1312.0564228	0.6621421	0.3177355	1.5824305	0.0865892	1312.0564228	3.1264413	0.2988347	8.7327819	6.63E-24	1312.0564228	2.4642992	0.3206830	5.5185879	1.60E-12
+	Fgf3	211.3636322	1.4709597	0.5366012	2.7720622	0.0188965	211.3636322	4.6970806	0.5276391	25.9395336	1.56E-17	211.3636322	3.2261210	0.5577883	9.3574860	0.0000003
+	NeuroD1	1687.6534029	1.4642134	0.5069799	2.7591300	0.0128041	1687.6534029	3.2046501	0.4775323	9.2192548	2.38E-10	1687.6534029	1.7404367	0.5080387	3.3413630	0.0072102
	E10.5<BSFL<BFL															
+	Anterior placodes	499.9804254	-1.9741714	0.4848992	**-3.9290252**	**0.0002608**	499.9804254	-3.8376829	0.4548255	**-14.2974193**	**7.53E-16**	499.9804254	-1.8635115	0.4804135	**-3.6389228**	**0.0016320**
+	Anterior placodes	203.5351929	-2.9862551	0.3915262	**-7.9241441**	**7.31E-13**	203.5351929	-6.1914481	0.3865588	**-73.0821963**	**2.53E-61**	203.5351929	-3.2051930	0.3080102	**-9.2227243**	**9.91E-23**
+	Neural crest	438.4768356	-2.1644091	0.5556017	**-4.4828279**	**0.0005036**	438.4768356	-4.6979471	0.5235290	**-25.9551172**	**8.43E-18**	438.4768356	-2.5335380	0.5484302	**-5.7898982**	**0.0000905**
+	OV and CVG marker	8825.3564575	-8.0393451	0.2242598	-263.0776982	5.08E-277	8825.3564575	-8.8632239	0.2119935	-405.4060645	0.00E+00	8825.3564575	-0.6238787	0.1970281	-1.5410127	0.0154256
+	SHH-related	870.1184062	-3.9175251	0.7099760	-15.1109773	0.0000004	870.1184062	-7.3651819	0.6811436	-164.8696401	1.77E-25	870.1184062	-3.4476569	0.6966394	-10.9105875	0.0000212
+	Wnt-related	337.7112953	-2.4758973	0.5496578	-5.5631320	0.0000453	337.7112953	-4.5179298	0.5180932	-22.9103844	7.29E-17	337.7112953	-2.0420324	0.5410380	-4.1182529	0.0023516
	Native > Derived (with no significant difference between BFL and BSFL)															
0	Dorsolateral OV	Gata3	1331.3310136	1.6939441	0.3456683	3.2354001	0.0000078	1331.3310136	1.0645338	0.3219458	2.0914939	0.0031375	1331.3310136	-0.6294103	0.3461245	-1.5469326	0.2638393
0	Mesenchyme	Prrx2	1044.6623627	2.7554669	0.3454885	6.7527114	5.39E-14	1044.6623627	2.8262311	0.3225191	7.0921895	5.09E-17	5315.7015586	-0.1373749	0.5102128	-1.0999019	0.9376725
0	Optic vesicle	Mitf	199.3014781	0.9789669	0.3889406	1.9710534	0.0330578	199.3014781	0.9684226	0.3640904	1.9567000	0.0203076	199.3014781	-0.0105443	0.3914693	-1.0073355	0.9933614
0	Organ of Corti	Bcl2	999.6111787	0.5550954	0.1956742	1.4692658	0.0147007	999.6111787	1.0047833	0.1825404	2.0066420	0.0000003	999.6111787	0.4496878	0.1969892	1.3657447	0.1222608
0	Otic competence	Foxi1	19.7743797	2.0924293	0.6915876	4.2646557	0.0087098	19.7743797	2.6031628	0.6742720	6.0761725	0.0004584	19.7743797	0.5107336	0.7136593	1.4247745	0.7807834
0	Retinoic acid-related	Crabp2	8684.9608898	0.7259856	0.2370325	1.6540302	0.0078296	8684.9608898	0.9919703	0.2201909	1.9888993	0.0000343	8684.9608898	0.2659847	0.2371500	1.2024565	0.5871380
0	Retinoic acid-related	**Cyp26a1**	1477.3128156	2.8702273	0.5185832	**7.3118037**	**0.0000003**	1477.3128156	2.1635287	0.4876253	**4.4800930**	**0.0000461**	1477.3128156	-0.7066987	0.5190726	-1.6320652	0.4677640
0	Retinoic acid-related	**Cyp26c1**	2458.7024519	5.9293370	0.7460993	**60.9408189**	**6.72E-14**	2458.7024519	4.3659944	0.7184721	**20.6203142**	**1.16E-08**	2458.7024519	-1.5633426	0.7466609	-2.9553778	0.1714277
0	Ventral OV	Lfng	3205.8375734	2.3509780	0.4822222	5.1016997	0.0000087	3205.8375734	2.1724532	0.4525804	4.5078929	0.0000091	3205.8375734	-0.1785247	0.4824876	-1.1317260	0.9086883
0	Wnt-related	Fzd2	4924.6209410	0.9771985	0.2254292	1.9686389	0.0000916	4924.6209410	0.5729371	0.2092634	1.4875489	0.0165412	4924.6209410	-0.4042614	0.2255633	-1.3234112	0.2739928
0	Wnt-related	Wnt2b	728.7379654	3.4568407	0.3284533	10.9802629	7.41E-24	728.7379654	3.3451516	0.3063928	10.1622758	5.89E-26	728.7379654	-0.1116891	0.3329365	-1.0804925	0.9186208
	Native > Derived (with significant BSFL < BFL)															
-	Ventral OV	**Otx1**	782.9122695	5.3229764	0.6790598	**40.0290749**	**1.52E-13**	782.9122695	2.9729558	0.6448019	**7.8514321**	**0.0000216**	782.9122695	-2.3500205	0.6799505	-5.0983151	0.0065886
-	Retinoic acid-related	**Tbx1**	1594.7217169	5.9589362	0.4393998	**62.2040340**	**2.70E-39**	1594.7217169	3.4524009	0.4045875	**10.9465239**	**3.41E-16**	1594.7217169	-2.5065353	0.4408851	-5.6825376	0.0000006
-	Mesenchyme	Pou3f4	664.9852440	4.3937900	0.5528407	21.0214465	6.70E-14	664.9852440	1.4387421	0.5167302	2.7108440	0.0146153	664.9852440	-2.9550479	0.5533831	-7.7545762	0.0000033
	Native < Derived (with no significant difference between BFL and BSFL)															
0	Dorsal OV	Jun	13550.0147802	-3.5659728	0.3284944	-11.8430829	2.48E-25	13550.0147802	-3.6591241	0.3060073	-12.6329889	5.47E-31	13550.0147802	-0.0931513	0.3281435	-1.0666977	0.9327536
0	FGF signaling (inhibitor)	Spry1	2921.0777821	-1.8317860	0.2632824	-3.5597750	7.47E-11	2921.0777821	-1.1398677	0.2449450	-2.2036081	0.0000178	2921.0777821	0.6919184	0.2630238	1.6154302	0.0594942
0	FGF signaling (inhibitor)	Spry2	2367.7709717	-0.7347595	0.1791231	-1.6641201	0.0002327	2367.7709717	-1.1429548	0.1661821	-2.2083285	7.96E-11	2367.7709717	-0.4081953	0.1787482	-1.3270247	0.1221495
0	Retinoic acid-related	RARa	2339.5008519	-0.7443416	0.1192486	-1.6752096	6.71E-09	2339.5008519	-0.8415696	0.1107582	-1.7919987	5.12E-13	2339.5008519	-0.0972280	0.1188847	-1.0697161	0.7353806
0	Retinoic acid-related	**RARb**	489.5155782	-1.4123278	0.4729522	**-2.6616627**	**0.0097664**	489.5155782	-2.6423289	0.4433955	**-6.2433871**	**2.29E-08**	489.5155782	-1.2300012	0.4709130	-2.3456718	0.0619938
0	Sensory	Atoh1	48.6688100	-4.0974215	0.7440062	-17.1177538	0.0000004	48.6688100	-2.3821284	0.7222018	-5.2130525	0.0032175	48.6688100	1.7152931	0.7313425	3.2836335	0.1086131
0	Ventral OV	Ncam1	1781.3209575	-1.3744637	0.2982146	-2.5927151	0.0000290	1781.3209575	-2.0640852	0.2774693	-4.1816875	1.62E-12	1781.3209575	-0.6896216	0.2974870	-1.6128604	0.1145616
0	Wnt-related	Dkk4	35.8115687	-3.5941060	0.7968116	-12.0762948	0.0000441	35.8115687	-4.5646510	0.7772398	-23.6644751	3.73E-08	35.8115687	-0.9705450	0.7738008	-1.9595808	0.5194449
0	Wnt-related	Fzd6	2314.7623059	-0.9429210	0.3193147	-1.9224166	0.0107321	2314.7623059	-0.8084687	0.2974343	-1.7513515	0.0174190	2314.7623059	0.1344523	0.3191965	1.0976760	0.8929835
0	Wnt-related	Lgr5	665.6303045	-0.9094436	0.3446700	-1.8783209	0.0245233	665.6303045	-0.9453307	0.3215474	-1.9256303	0.0094942	665.6303045	-0.0358871	0.3441945	-1.0251870	0.9784335
0	Wnt-related	Wnt4	829.1086177	-1.2639600	0.6255810	-2.4015403	0.0984272	829.1086177	-2.4283148	0.5937431	-5.3826433	0.0001911	829.1086177	-1.1643548	0.6250347	-2.2413296	0.2482213

	BFL and Native < BSFL (with no significant difference between Native and BFL)																
-	Retinoic acid-related	**Aldh1a3**	13382.1662654	-4.9330609	0.6118110	**-30.5491619**	**2.74E-14**	13382.1662654	0.3410507	0.5803349	1.2666788	0.6718958	13382.1662654	5.2741116	0.6119283	**38.6959742**	**1.16E-15**
	BFL and Native > BSFL (with no significant difference between Native and BFL)																
-	Mesoderm	Onecut	162.7048718	2.7569259	0.5319173	6.7595441	0.0000020	162.7048718	-0.1026558	0.4912084	-1.0737483	0.8877048	162.7048718	-2.8595817	0.5321836	-7.2580487	0.0000027
	BSFL and Native > BFL (with no significant difference between Native and BSFL)																
+	BMP-related	Id1	5067.0840500	-0.3529121	0.1887385	-1.2771359	0.1306106	5067.0840500	0.7224815	0.1754080	1.6500177	0.0001701	5067.0840500	1.0753936	0.1889832	2.1072970	0.0000005
+	BMP-related	Id3	7413.7001836	-0.2020064	0.2139430	-1.1502970	0.4931578	7413.7001836	0.7854160	0.1987525	1.7235893	0.0003259	7413.7001836	0.9874225	0.2140935	1.9826396	0.0000934
+	Dorsal OV	Dach1	4796.9170533	0.1205914	0.2093725	1.0871804	0.6944759	4796.9170533	1.0054944	0.1945936	2.0076314	0.0000016	4796.9170533	0.8849030	0.2096506	1.8466405	0.0004562
+	Dorsal OV	Dach2	986.1077025	-0.1574057	0.3609856	-1.1152798	0.7716949	986.1077025	1.1154733	0.3376271	2.1666608	0.0031641	986.1077025	1.2728790	0.3618058	2.4164330	0.0054482
+	Dorsal OV	EphA4	5024.9650892	0.0051095	0.1638740	1.0035479	0.9863275	5024.9650892	0.6568141	0.1522143	1.5765972	0.0000766	5024.9650892	0.6517046	0.1641183	1.5710233	0.0011740
+	Dorsal OV	**Hmx2**	828.5392750	0.4035107	0.3730714	1.3227228	0.4226063	828.5392750	5.7374606	0.3747027	**53.3516349**	**1.68E-50**	828.5392750	5.3339498	0.3976253	**40.3347061**	**1.08E-37**
+	Dorsal OV	**Hmx3**	704.1047177	-0.0205340	0.2685588	-1.0143349	0.9632733	704.1047177	6.0539274	0.3094152	**66.4375691**	**3.02E-82**	704.1047177	6.0744614	0.3243236	**67.3899425**	**6.78E-74**
+	Dorsal OV	Sox9	7563.1018631	0.0173493	0.2286178	1.0120982	0.9635116	7563.1018631	1.1947164	0.2124749	2.2889982	0.0000001	7563.1018631	1.1773671	0.2288135	2.2616365	0.0000085
+	OP	Pax2	2911.8296757	-0.5493667	0.4325843	-1.4634432	0.3345986	2911.8296757	1.8973867	0.4053782	3.7253778	0.0000158	2911.8296757	2.4467535	0.4330571	5.4518788	0.0000007
+	OP and OV	Foxg1	976.8555367	0.6069531	0.4587059	1.5230392	0.3121020	976.8555367	1.7842559	0.4306795	3.4444075	0.0001545	976.8555367	1.1773028	0.4595645	2.2615357	0.0694086
+	PPE	Eya1	9529.9034448	-0.0975044	0.3295217	-1.0699211	0.8484176	9529.9034448	1.6428712	0.3070865	3.1228671	0.0000006	9529.9034448	1.7403756	0.3296729	3.3412213	0.0000044
+	PPE	Six1	9432.1185848	0.0911048	0.2701474	1.0651856	0.8259839	9432.1185848	2.0609063	0.2513870	4.1724833	5.56E+18	9432.1185848	1.9698014	0.2704082	3.9171420	2.84E-11
+	Wnt-related	Fzd7	11143.3226105	-0.3585225	0.2291769	-1.2821122	0.2186511	11143.3226105	0.9018789	0.2129240	1.8684979	0.0001063	11143.3226105	1.2604015	0.2292863	2.3956240	0.0000015
	BSFL and Native < BFL (with no significant difference between Native and BSFL)																
+	Anterior placodes	Six3	3.6901657	-0.3274877	0.8211216	-1.2548263	0.7917201	3.6901657	-1.4065103	0.8018018	-2.6509515	0.1454732	3.6901657	-1.0790226	0.8137738	-2.1126043	0.4843370
+	FGF-related	Fgf2	132.1992956	-0.1023181	0.4658282	-1.0734970	0.8880641	132.1992956	-1.7046412	0.4339299	-3.2594787	0.0003561	132.1992956	-1.6023231	0.4626087	-3.0363185	0.0064530
+	NNE, non-otic	Foxi2	29.3895548	0.2208568	0.7595466	1.1654255	0.8512941	29.3895548	-1.8623408	0.7289971	-3.6359714	0.0265482	29.3895548	-2.0831976	0.7558414	-4.2374538	0.0445974
+	SHH-related	Hhip	325.9302686	-0.2738227	0.2384550	-1.2090071	0.3901179	325.9302686	-1.6063179	0.2195261	-3.0447376	3.88E-12	325.9302686	-1.3324952	0.2354137	-2.5183786	0.0000006
+	SHH-related	Ptch1	8426.2280257	-0.4359889	0.2559203	-1.3528378	0.1740941	8426.2280257	-1.6650813	0.2377260	-3.1713152	3.38E-11	8426.2280257	-1.2290923	0.2558045	-2.3441946	0.0000405

Bibliography

1. Shearer AE, MS Hildebrand and R Smith (1999). Hereditary hearing loss and deafness overview. In GeneReviews® [Internet], Adam, M, H Ardinger, R Pagon, S Wallace, L Bean, H Mefford, K Stephens, A Amemiya and N Ledbetter, eds. (Seattle: University of Washington).

2. World Health Organization (2017). Deafness and hearing loss. http://www.who.int/mediacentre/factsheets/fs300/en/.

3. Agrawal Y, JP Carey, CC Della Santina, MC Schubert and LB Minor (2009). Disorders of balance and vestibular function in US adults: data from the National Health and Nutrition Examination Survey, 2001-2004. Arch Intern Med 169: 938–944.

4. Blackwell D, J Lucas and T Clarke (2014). Summary health statistics for U.S. adults: national health interview survey, 2012. Vital Health Stat 10: 1–161.

5. Schaefer S and R Duncan (2018). Structure and function of the auditory periphery. In Neurobiology of Hearing, (Springer-Verlag), Book chapter in preparation.

6. Chen P, JE Johnson, HY Zoghbi and N Segil (2002). The role of Math1 in inner ear development: Uncoupling the establishment of the sensory primordium from hair cell fate determination. Development 129: 2495–2505.

7. Chen P and N Segil (1999). p27(Kip1) links cell proliferation to morphogenesis in the developing organ of Corti. Development 126: 1581–1590.

8. Spoendlin H (1985). Anatomy of cochlear innervation. Am J Otolaryngol 6: 453–467.

9. Berglund AM and DK Ryugo (1987). Hair cell innervation by spiral ganglion neurons in the mouse. J Comp Neurol 255: 560–570.

10. Ryan A and P Dallos (1975). Effect of absence of cochlear outer hair cells on behavioural auditory threshold. Nature 253: 44–46.

11. Rabbitt RD, ER Damiano and JW Grant (2004). Biomechanics of the semicircular canals and otolith organs. In The Vestibular System, (New York, NY: Springer), pp. 153–201.

12. Wersäll J and D Bagger-Sjöbäck (1974). Morphology of the vestibular sense organ. In Vestibular System Part 1: Basic Mechanisms, Kornhuber, H, ed. (Berlin, Heidelberg: Springer), pp. 123–170.

13. Holt JC, A Lysakowski and JM Goldberg (2010). The efferent vestibular system. In Auditory and Vestibular Efferents, Ryugo, D, R Fay and A Popper, eds. (New York, NY: Springer), pp. 135–186.

14. Flock A and HC Cheung (1977). Actin filaments in sensory hairs of inner ear receptor cells. J Cell Biol 75: 339–343.

15. Sahly I, A El-Amraoui, M Abitbol, C Petit and J-L Dufier (1997). Expression of myosin VIIA during mouse embryogenesis. Anat Embryol (Berl) 196: 159–170.

16. Hume CR, DL Bratt and EC Oesterle (2007). Expression of LHX3 and SOX2 during mouse inner ear development. Gene Expr Patterns 7: 798–807.

17. Gibson F, J Walsh, P Mburu, A Varela, KA Brown, M Antonio, KW Beisel, KP Steel and SDM Brown (1995). A type VII myosin encoded by the mouse deafness gene shaker-1. Nature 374: 62–64.

18. Weil D, S Blanchard, J Kaplan, P Guilford, F Gibson, J Walsh, P Mburu, A Varela, J Levilliers, MD Weston, PM Kelley, WJ Kimberling, M Wagenaar, F Levi-Acobas, D Larget-Piet, A Munnich, KP Steel, SDM Brown and C Petit (1995). Defective myosin VIIA gene responsible for Usher syndrome type 1B. Nature 374: 60–61.

19. Burns JC and JT Corwin (2014). Responses to cell loss become restricted as the supporting cells in mammalian vestibular organs grow thick junctional actin bands that develop high stability. J Neurosci 34: 1998–2011.

20. Burns J, JJ Christophel, MS Collado, C Magnus, M Carfrae and JT Corwin (2008). Reinforcement of cell junctions correlates with the absence of hair cell regeneration in mammals and its occurrence in birds. J Comp Neurol 511: 396–414.

21. Khimich D, R Nouvian, R Pujol, S tom Dieck, A Egner, ED Gundelfinger and T Moser (2005). Hair cell synaptic ribbons are essential for synchronous auditory signalling. Nature 434: 889–894.

22. Matthews G and P Fuchs (2010). The diverse roles of ribbon synapses in sensory neurotransmission. Nat Rev Neurosci 11: 812–822.

23. Moser T, A Brandt and A Lysakowski (2006). Hair cell ribbon synapses. Cell Tissue Res 326: 347–359.

24. Retzius G (1884). Das Gehörorgan der Wirbeltiere, Vol. II. (Stockholm: Samson and Wallin).

25. Burda H, L Ballast and V Bruns (1988). Cochlea in old world mice and rats (Muridae). J Morphol 198: 269–285.

26. Smeds K, G Keidser, J Zakis, H Dillon, A Leijon, F Grant, E Convery and C Brew (2006). Preferred overall loudness. II: Listening through hearing aids in field and laboratory tests. Int J Audiol 45: 12–25.

27. Smeds K and A Leijon (2011). Loudness and hearing loss. In Loudness, Florentine, M, AN Popper and RR Fay, eds. (New York, NY: Springer), pp. 223–259.

28. Johnson EE (2013). Modern prescription theory and application: realistic expectations for speech recognition with hearing aids. Trends Amplif 17: 143–170.

29. Otte J, HF Schuknecht and AG Kerr (1978). Ganglion cell populations in normal and pathological human cochleae. Implications for cochlear implantation. Laryngoscope 88: 1231–1246.

30. Nadol JB Jr, Y-S Young and RJ Glynn (1989). Survival of spiral ganglion cells in profound sensorineural hearing loss: implications for cochlear implantation. Ann Otol Rhinol Laryngol 98: 411–416.

31. Hardie NA and RK Shepherd (1999). Sensorineural hearing loss during development: morphological and physiological response of the cochlea and auditory brainstem. Hear Res 128: 147–165.

32. Limb CJ and AT Roy (2014). Technological, biological, and acoustical constraints to music perception in cochlear implant users. Hear Res 308: 13–26.

33. Friesen LM, RV Shannon, D Baskent and X Wang (2001). Speech recognition in noise as a function of the number of spectral channels: comparison of acoustic hearing and cochlear implants. J Acoust Soc Am 110: 1150–1163.

34. Kokkinakis K, B Azimi, Y Hu and DR Friedland (2012). Single and multiple microphone noise reduction strategies in cochlear implants. Trends Amplif 16: 102–116.

35. Corwin JT and DA Cotanche (1988). Regeneration of sensory hair cells after acoustic trauma. Science 240: 1772–1774.

36. Ryals BM and EW Rubel (1988). Hair cell regeneration after acoustic trauma in adult Coturnix quail. Science 240: 1774–1776.

37. Balak KJ, JT Corwin and JE Jones (1990). Regenerated hair cells can originate from supporting cell progeny: evidence from phototoxicity and laser ablation experiments in the lateral line system. J Neurosci 10: 2502–2512.

38. Lombarte A, HY Yan, AN Popper, JS Chang and C Platt (1993). Damage and regeneration of hair cell ciliary bundles in a fish ear following treatment wtih gentamicin. Hear Res 64: 166–174.

39. Forge A, L Li, JT Corwin and G Nevill (1993). Ultrastructural evidence for hair cell regeneration in the mammalian inner ear. Science 259: 1616–1619.

40. Warchol ME, PR Lambert, BJ Goldstein, A Forge and JT Corwin (1993). Regenerative proliferation in inner ear sensory epithelia from adult guinea pigs and humans. Science 259: 1619–1622.

41. Li H, H Liu and S Heller (2013). Pluripotent stem cells from the adult mouse inner ear. Nat Med 9: 1293–1299.

42. Cox BC, R Chai, A Lenoir, Z Liu, L Zhang, D-H Nguyen, K Chalasani, KA Steigelman, J Fang, EW Rubel, AG Cheng and J Zuo (2014). Spontaneous hair cell regeneration in the neonatal mouse cochlea in vivo. Development 141: 816–829.

43. White PM, A Doetzlhofer, YS Lee, AK Groves and N Segil (2006). Mammalian cochlear supporting cells can divide and trans-differentiate into hair cells. Nature 441: 984–987.

44. Oshima K, CM Grimm, CE Corrales, P Senn, R Martinez Monedero, G Géléoc, A Edge, JR Holt and S Heller (2007). Differential distribution of stem cells in the auditory and vestibular organs of the inner ear. J Assoc Res Otolaryngol 8: 18–31.

45. Malgrange B, S Belachew, M Thiry, L Nguyen, B Rogister, M-L Alvarez, J-M Rigo, TR Van De Water, G Moonen and PP Lefebvre (2002). Proliferative generation of mammalian auditory hair cells in culture. Mech Dev 112: 79–88.

46. Bramhall NF, F Shi, K Arnold, K Hochedlinger and AS Edge (2014). Lgr5-positive supporting cells generate new hair cells in the postnatal cochlea. Stem Cell Rep 2: 311–322.

47. Wang T, R Chai, GS Kim, N Pham, L Jansson, D-H Nguyen, B Kuo, LA May, J Zuo, LL Cunningham and AG Cheng (2015). Lgr5+ cells regenerate hair cells via proliferation and direct transdifferentiation in damaged neonatal mouse utricle. Nat Commun 6: 6613.

48. Shi F, JS Kempfle and A Edge (2012). Wnt-responsive Lgr5-expressing stem cells are hair cell progenitors in the cochlea. J Neurosci 32: 9639–9648.

49. Chai R, B Kuo, T Wang, EJ Liaw, A Xia, TA Jan, Z Liu, MM Taketo, JS Oghalai, R Nusse, J Zuo and AG Cheng (2012). Wnt signaling induces proliferation of sensory precursors in the postnatal mouse cochlea. Proc Natl Acad Sci 109: 8167–8172.

50. Jan TA, R Chai, ZN Sayyid, R van Amerongen, A Xia, T Wang, ST Sinkkonen, YA Zeng, JR Levin, S Heller, R Nusse and A Cheng (2013). Tympanic border cells are Wnt-responsive and can act as progenitors for postnatal mouse cochlear cells. Development 140: 1196–1206.

51. McLean WJ, X Yin, L Lu, DR Lenz, D McLean, R Langer, JM Karp and ASB Edge (2017). Clonal expansion of Lgr5-positive cells from mammalian cochlea and high-purity generation of sensory hair cells. Cell Rep 18: 1917–1929.

52. Géléoc G and JR Holt (2014). Sound strategies for hearing restoration. Science 344:.

53. Lanford PJ, Y Lan, R Jiang, C Lindsell, G Weinmaster, T Gridley and MW Kelley (1999). Notch signalling pathway mediates hair cell development in mammalian cochlea. Nat Genet 21: 289–292.

54. Lanford PJ, R Shailam, CR Norton, T Ridley and MW Kelley (2000). Expression of Math1 and HES5 in the cochleae of wildtype and Jag2 mutant mice. J Assoc Res Otolaryngol 1: 161–171.

55. Maass JC, R Gu, ML Basch, J Waldhaus, EM Lopez, A Xia, JS Oghalai, S Heller and AK Groves (2015). Changes in the regulation of the Notch signaling pathway are temporally correlated with regenerative failure in the mouse cochlea. Front Cell Neurosci 9.

56. Mizutari K, M Fujioka, M Hosoya, N Bramhall, HJ Okano, H Okano and ASB Edge (2013). Notch inhibition induces cochlear hair cell regeneration and recovery of hearing after acoustic trauma. Neuron 77: 58–69.

57. Kim YH and Y Raphael (2007). Cell division and maintenance of epithelial integrity in the deafened auditory epithelium. Cell Cycle 6: 612–619.

58. Li H, G Roblin, H Liu and S Heller (2003). Generation of hair cells by stepwise differentiation of embryonic stem cells. Proc Natl Acad Sci 100: 13495–13500.

59. Oshima K, K Shin, M Diensthuber, AW Peng, AJ Ricci and S Heller (2010). Mechanosensitive hair cell-like cells from embryonic and induced pluripotent stem cells. Cell 141: 704–716.

60. Chen W, N Jongkamonwiwat, L Abbas, SJ Eshtan, SL Johnson, S Kuhn, M Milo, JK Thurlow, PW Andrews, W Marcotti, HD Moore and MN Rivolta (2012). Restoration of auditory evoked responses by human ES-cell-derived otic progenitors. Nature 490: 278–282.

61. Ouji Y, S Ishizaka, F Nakamura-Uchiyama and M Yoshikawa (2012). In vitro differentiation of mouse embryonic stem cells into inner ear hair cell-like cells using stromal cell conditioned medium. Cell Death Dis 3: e314.

62. Ouji Y, S Ishizaka, F Nakamura-Uchiyama, A Wanaka and M Yoshikawa (2013). Induction of inner ear hair cell-like cells from Math1-transfected mouse ES cells. Cell Death Dis 4: e700.

63. Ronaghi M, M Nasr, M Ealy, R Durruthy-Durruthy, J Waldhaus, GH Diaz, L-M Joubert, K Oshima and S Heller (2014). Inner Ear Hair Cell-Like Cells from Human Embryonic Stem Cells. Stem Cells Dev 140310065035002.

64. Ohnishi H, D Skerleva, S Kitajiri, T Sakamoto, N Yamamoto, J Ito and T Nakagawa (2015). Limited hair cell induction from human induced pluripotent stem cells using a simple stepwise method. Neurosci Lett 599: 49–54.

65. Ding J, Z Tang, J Chen, H Shi, J Chen, C Wang, C Zhang, L Li, P Chen and J Wang (2016). Induction of differentiation of human embryonic stem cells into functional hair-cell-like cells in the absence of stromal cells. Int J Biochem Cell Biol 81: 208–222.

66. Kil K, MY Choi and K Ho Park (2016). In vitro differentiation of human Wharton's jelly-derived mesenchymal stem cells into auditory hair cells and neurons. J Int Adv Otol 12: 37–42.

67. Ouji Y, M Sakagami, H Omori, S Higashiyama, N Kawai, T Kitahara, A Wanaka and M Yoshikawa (2017). Efficient induction of inner ear hair cell-like cells from mouse ES cells using combination of Math1 transfection and conditioned medium from ST2 stromal cells. Stem Cell Res 23: 50–56.

68. Koehler KR, AM Mikosz, AI Molosh, D Patel and E Hashino (2013). Generation of inner ear sensory epithelia from pluripotent stem cells in 3D culture. Nature 500: 217–221.

69. Koehler KR and E Hashino (2014). 3D mouse embryonic stem cell culture for generating inner ear organoids. Nat Protoc 9: 1229–1244.

70. DeJonge RE, X-P Liu, CR Deig, S Heller, KR Koehler and E Hashino (2016). Modulation of Wnt signaling enhances inner ear organoid development in 3D culture. PLOS ONE 11: e0162508.

71. Koehler KR, J Nie, E Longworth-Mills, X-P Liu, J Lee, JR Holt and E Hashino (2017). Generation of inner ear organoids containing functional hair cells from human pluripotent stem cells. Nat Biotechnol 35: 583–589.

72. Wataya T, S Ando, K Muguruma, H Ikeda, K Watanabe, M Eiraku, M Kawada, J Takahashi, N Hashimoto and Y Sasai (2008). Minimization of exogenous signals in ES cell culture induces rostral hypothalamic differentiation. Proc Natl Acad Sci 105: 11796–11801.

73. Eiraku M, K Watanabe, M Matsuo-Takasaki, M Kawada, S Yonemura, M Matsumura, T Wataya, A Nishiyama, K Muguruma and Y Sasai (2008). Self-organized formation of polarized cortical tissues from ESCs and its active manipulation by extrinsic signals. Cell Stem Cell 3: 519–532.

74. Schaefer SA, L Liu and RK Duncan. A step in the right direction: early inhibition of TGFB signaling is necessary for derived otic vesicles to achieve ultimate inner ear organoid fate. Manuscript in preparation.

75. Liu X-P, KR Koehler, AM Mikosz, E Hashino and JR Holt (2016). Functional development of mechanosensitive hair cells in stem cell-derived organoids parallels native vestibular hair cells. Nat Commun 7: 11508.

76. Perea-Gomez A and SM Meilhac (2015). Chapter 10 - Formation of the anterior-posterior axis in mammals. In Principles of Developmental Genetics (Second Edition), Moody, SA, ed. (Oxford: Academic Press), pp. 171–188.

77. Robertson EJ (2014). Dose-dependent Nodal/Smad signals pattern the early mouse embryo. Semin Cell Dev Biol 32: 73–79.

78. Zinski J, B Tajer and MC Mullins (2017). TGF-β family signaling in early vertebrate development. Cold Spring Harb Perspect Biol a033274.

79. Varlet I, J Collignon and EJ Robertson (1997). Nodal expression in the primitive endoderm is required for specification of the anterior axis during mouse gastrulation. Development 124: 1033–1044.

80. Brennan J, CC Lu, DP Norris, TA Rodriguez, R Beddington and E Robertson (2001). Nodal signalling in the epiblast patterns the early mouse embryo. Nature 411: 965–969.

81. Perea-Gomez A, M Rhinn and SL Ang (2003). Role of the anterior visceral endoderm in restricting posterior signals in the mouse embryo. Int J Dev Biol 45: 311–320.

82. Perea-Gomez A, FD Vella, W Shawlot, M Oulad-Abdelghani, C Chazaud, C Meno, V Pfister, L Chen, E Robertson and H Hamada (2002). Nodal antagonists in the anterior visceral endoderm prevent the formation of multiple primitive streaks. Dev Cell 3: 745–756.

83. Kimura C, K Yoshinaga, E Tian, M Suzuki, S Aizawa and I Matsuo (2000). Visceral endoderm mediates forebrain development by suppressing posteriorizing signals. Dev Biol 225: 304–321.

84. Thomas P and R Beddington (1996). Anterior primitive endoderm may be responsible for patterning the anterior neural plate in the mouse embryo. Curr Biol 6: 1487–1496.

85. Conlon FL, KM Lyons, N Takaesu, KS Barth, A Kispert, B Herrmann and EJ Robertson (1994). A primary requirement for nodal in the formation and maintenance of the primitive streak in the mouse. Development 120: 1919–1928.

86. Zhou X, H Sasaki, L Lowe, BL Hogan and MR Kuehn (1993). Nodal is a novel TGF-beta-like gene expressed in the mouse node during gastrulation. 361: 543–547.

87. Iannaccone P, X Zhou, M Khokha, D Boucher and M Kuehn (1992). Insertional mutation of a gene involved in growth regulation of the early mouse embryo. Dev Dyn 194: 198–208.

88. Camus A, A Perea-Gomez, A Moreau and J Collignon (2006). Absence of Nodal signaling promotes precocious neural differentiation in the mouse embryo. Dev Biol 295: 743–755.

89. Li L, C Liu, S Biechele, Q Zhu, L Song, F Lanner, N Jing and J Rossant (2013). Location of transient ectodermal progenitor potential in mouse development. Development 140: 4533–4543.

90. Hinck AP (2012). Structural studies of the TGF-βs and their receptors - insights into evolution of the TGF-β superfamily. FEBS Lett 586: 1860–1870.

91. Gadue P, TL Huber, PJ Paddison and GM Keller (2006). Wnt and TGF-β signaling are required for the induction of an in vitro model of primitive streak formation using embryonic stem cells. Proc Natl Acad Sci 103: 16806–16811.

92. D'Amour KA, AD Agulnick, S Eliazer, OG Kelly, E Kroon and EE Baetge (2005). Efficient differentiation of human embryonic stem cells to definitive endoderm. Nat Biotechnol 23: 1534–1541.

93. Yasunaga M, S Tada, S Torikai-Nishikawa, Y Nakano, M Okada, LM Jakt, S Nishikawa, T Chiba, T Era and S-I Nishikawa (2005). Induction and monitoring of definitive and visceral endoderm differentiation of mouse ES cells. Nat Biotechnol 23: 1542–1550.

94. Kubo A, K Shinozaki, J Shannon, V Kouskoff, M Kennedy, S Woo, H Fehling and G Keller (2004). Development of definitive endoderm from embryonic stem cells in culture. Development 131: 1651–1662.

95. Matzuk MM, TR Kumar, A Vassalli, JR Bickenbach, DR Roop, R Jaenisch and A Bradley (1995). Functional analysis of activins during mammalian development. Nature 374: 354–356.

96. Vallier L, T Touboul, Z Chng, M Brimpari, N Hannan, E Millan, LE Smithers, M Trotter, P Rugg-Gunn, A Weber and RA Pedersen (2009). Early cell fate decisions of human embryonic stem cells and mouse epiblast stem cells are controlled by the same signalling pathways. PLoS ONE 4: e6082.

97. Patani R, A Compston, CA Puddifoot, DJA Wyllie, GE Hardingham, ND Allen and S Chandran (2009). Activin/Nodal inhibition alone accelerates highly efficient neural conversion from human embryonic stem cells and imposes a caudal positional identity. PLoS ONE 4: e7327.

98. Smith JR, L Vallier, G Lupo, M Alexander, WA Harris and RA Pedersen (2008). Inhibition of Activin/Nodal signaling promotes specification of human embryonic stem cells into neuroectoderm. Dev Biol 313: 107–117.

99. Watanabe K, D Kamiya, A Nishiyama, T Katayama, S Nozaki, H Kawasaki, Y Watanabe, K Mizuseki and Y Sasai (2005). Directed differentiation of telencephalic precursors from embryonic stem cells. Nat Neurosci 8: 288–296.

100. Loebel D, C Watson, R De Young and P Tam (2003). Lineage choice and differentiation in mouse embryos and embryonic stem cells. Dev Biol 264: 1–14.

101. Ben-Haim N, C Lu, M Guzman-Ayala, L Pescatore, D Mesnard, M Bischofberger, F Naef, EJ Robertson and DB Constam (2006). The nodal precursor acting via activin receptors induces mesoderm by maintaining a source of its convertases and BMP4. Dev Cell 11: 313–323.

102. Chambers SM, CA Fasano, EP Papapetrou, M Tomishima, M Sadelain and L Studer (2009). Highly efficient neural conversion of human ES and iPS cells by dual inhibition of SMAD signaling. Nat Biotechnol 27: 275–280.

103. Wilson PA and A Hemmati-Brivanlou (1995). Induction of epidermis and inhibition of neural fate by Bmp-4. Nature 376: 331–333.

104. Di-Gregorio A, M Sancho, DW Stuckey, LA Crompton, J Godwin, Y Mishina and TA Rodriguez (2007). BMP signalling inhibits premature neural differentiation in the mouse embryo. Development 134: 3359–3369.

105. Hemmati-Brivanlou A and D Melton (1997). Vertebrate embryonic cells will become nerve cells unless told otherwise. Cell 88: 13–17.

106. Levine AJ and AH Brivanlou (2007). Proposal of a model of mammalian neural induction. Dev Biol 308: 247–256.

107. Muñoz-Sanjuán I and AH Brivanlou (2002). Neural induction, the default model and embryonic stem cells. Nat Rev Neurosci 3: 271–280.

108. Bachiller D, J Klingensmith, C Kemp, JA Belo, RM Anderson, SR May, JA McMahon, AP McMahon, RM Harland and J Rossant (2000). The organizer factors Chordin and Noggin are required for mouse forebrain development. Nature 403: 658–661.

109. Klingensmith J, S-L Ang, D Bachiller and J Rossant (1999). Neural induction and patterning in the mouse in the absence of the node and its derivatives. Dev Biol 216: 535–549.

110. Mishina Y, A Suzuki, N Ueno and RR Behringer (1995). Bmpr encodes a type I bone morphogenetic protein receptor that is essential for gastrulation during mouse embryogenesis. Genes Dev 9: 3027–3037.

111. Roelen BA, HY Lin, V Knežević, E Freund and CL Mummery (1994). Expression of TGF-βs and their receptors during implantation and organogenesis of the mouse embryo. Dev Biol 166: 716–728.

112. Davis S, S Miura, C Hill, Y Mishina and J Klingensmith (2004). BMP receptor IA is required in the mammalian embryo for endodermal morphogenesis and ectodermal patterning. Dev Biol 270: 47–63.

113. Harvey NT, JN Hughes, A Lonic, C Yap, C Long, PD Rathjen and J Rathjen (2010). Response to BMP4 signalling during ES cell differentiation defines intermediates of the ectoderm lineage. J Cell Sci 123: 1796–1804.

114. Surmacz B, H Fox, A Gutteridge, S Lubitz and P Whiting (2012). Directing differentiation of human embryonic stem cells toward anterior neural ectoderm using small molecules. Stem Cells 30: 1875–1884.

115. Zhou J, P Su, D Li, S Tsang, E Duan and F Wang (2010). High-efficiency induction of neural conversion in human ESCs and human induced pluripotent stem cells with a single chemical inhibitor of transforming growth factor beta superfamily receptors. Stem Cells 28: 1741–1750.

116. Kim D-S, JS Lee, JW Leem, YJ Huh, JY Kim, H-S Kim, I-H Park, GQ Daley, D-Y Hwang and D-W Kim (2010). Robust enhancement of neural differentiation from human ES and iPS cells regardless of their innate difference in differentiation propensity. Stem Cell Rev Rep 6: 270–281.

117. Zirra A, S Wiethoff and R Patani (2016). Neural conversion and patterning of human pluripotent stem cells: a developmental perspective. Stem Cells Int 2016: 1–14.

118. Groves AK and C LaBonne (2014). Setting appropriate boundaries: Fate, patterning and competence at the neural plate border. Dev Biol 389: 2–12.

119. Kretzschmar M, J Doody and J Massagué (1997). Opposing BMP and EGF signalling pathways converge on the TGF-β family mediator Smad1. Nature 389: 618–622.

120. Pera EM, A Ikeda, E Eivers and EM De Robertis (2003). Integration of IGF, FGF, and anti-BMP signals via Smad1 phosphorylation in neural induction. Genes Dev 17: 3023–3028.

121. Cho A, Y Tang, J Davila, S Deng, L Chen, E Miller, M Wernig and IA Graef (2014). Calcineurin signaling regulates neural induction through antagonizing the BMP pathway. Neuron 82: 109–124.

122. Wang C, C Xia, W Bian, L Liu, W Lin, Y-G Chen, S-L Ang and N Jing (2006). Cell aggregation-induced FGF8 elevation is essential for P19 cell neural differentiation. Mol Biol Cell 17: 3075–3084.

123. Yoo YD, CT Huang, X Zhang, TM Lavaute and S-C Zhang (2011). Fibroblast growth factor regulates human neuroectoderm specification through ERK1/2-PARP-1 pathway. Stem Cells 29: 1975–1982.

124. LaVaute TM, YD Yoo, MT Pankratz, JP Weick, JR Gerstner and S-C Zhang (2009). Regulation of neural specification from human embryonic stem cells by BMP and FGF. Stem Cells 27: 1741–1749.

125. Brafman D and K Willert (2017). Wnt/β-catenin signaling during early vertebrate neural development: Wnt signaling in neural development. Dev Neurobiol 77: 1239–1259.

126. Wilson SI and T Edlund (2001). Neural induction: toward a unifying mechanism. Nat Neurosci 4: 1161–1168.

127. Stern CD (2005). Neural induction: old problem, new findings, yet more questions. Development 132: 2007–2021.

128. Wilson SI, A Rydström, T Trimborn, K Willert, R Nusse, TM Jessell and T Edlund (2001). The status of Wnt signalling regulates neural and epidermal fates in the chick embryo. Nature 411: 325–330.

129. Pieper M, K Ahrens, E Rink, A Peter and G Schlosser (2012). Differential distribution of competence for panplacodal and neural crest induction to non-neural and neural ectoderm. Development 139: 1175–1187.

130. Kwon H-J, N Bhat, EM Sweet, RA Cornell and BB Riley (2010). Identification of early requirements for preplacodal ectoderm and sensory organ development. PLoS Genet 6: e1001133.

131. Leung AW, D Kent Morest and JYH Li (2013). Differential BMP signaling controls formation and differentiation of multipotent preplacodal ectoderm progenitors from human embryonic stem cells. Dev Biol 379: 208–220.

132. Dincer Z, J Piao, L Niu, Y Ganat, S Kriks, B Zimmer, S-H Shi, V Tabar and L Studer (2013). Specification of functional cranial placode derivatives from human pluripotent stem cells. Cell Rep 5: 1387–1402.

133. Ealy M, DC Ellwanger, N Kosaric, AP Stapper and S Heller (2016). Single-cell analysis delineates a trajectory toward the human early otic lineage. Proc Natl Acad Sci 113: 8508–8513.

134. Zhang S-C, M Wernig, ID Duncan, O Brüstle and JA Thomson (2001). In vitro differentiation of transplantable neural precursors from human embryonic stem cells. Nat Biotechnol 19: 1129–1133.

135. Reubinoff BE, P Itsykson, T Turetsky, MF Pera, E Reinhartz, A Itzik and T Ben-Hur (2001). Neural progenitors from human embryonic stem cells. Nat Biotechnol 19: 1134–1140.

136. Lee G, H Kim, Y Elkabetz, G Al Shamy, G Panagiotakos, T Barberi, V Tabar and L Studer (2007). Isolation and directed differentiation of neural crest stem cells derived from human embryonic stem cells. Nat Biotechnol 25: 1468–1475.

137. Menendez L, TA Yatskievych, PB Antin and S Dalton (2011). Wnt signaling and a Smad pathway blockade direct the differentiation of human pluripotent stem cells to multipotent neural crest cells. Proc Natl Acad Sci 108: 19240–19245.

138. Coraux C, C Hilmi, M Rouleau, A Spadafora, J Hinnrasky, J-P Ortonne, C Dani and D Aberdam (2003). Reconstituted skin from murine embryonic stem cells. Curr Biol 13: 849–853.

139. Itoh M, M Kiuru, MS Cairo and AM Christiano (2011). Generation of keratinocytes from normal and recessive dystrophic epidermolysis bullosa-induced pluripotent stem cells. Proc Natl Acad Sci 108: 8797–8802.

140. Metallo CM, L Ji, JJ de Pablo and SP Palecek (2008). Retinoic acid and bone morphogenetic protein signaling synergize to efficiently direct epithelial differentiation of human embryonic stem cells. Stem Cells 26: 372–380.

141. Green H, K Easley and S Iuchi (2003). Marker succession during the development of keratinocytes from cultured human embryonic stem cells. Proc Natl Acad Sci 100: 15625–15630.

142. Alvarez Y, MT Alonso, V Vendrell, LC Zelarayan, P Chamero, T Theil, MR Bösl, S Kato, M Maconochie, D Riethmacher and T Schimmang (2003). Requirements for FGF3 and FGF10 during inner ear formation. Development 130: 6329–6338.

143. Wright TJ and SL Mansour (2003). Fgf3 and Fgf10 are required for mouse otic placode induction. Development 130: 3379–3390.

144. Wilkinson DG, G Peters, C Dickson and AP McMahon (1988). Expression of the FGF-related proto-oncogene int-2 during gastrulation and neurulation in the mouse. EMBO J 7: 691.

145. Zou D, D Silvius, S Rodrigo-Blomqvist, S Enerbäck and P-X Xu (2006). Eya1 regulates the growth of otic epithelium and interacts with Pax2 during the development of all sensory areas in the inner ear. Dev Biol 298: 430–441.

146. Mansouri A, M Hallonet and P Gruss (1996). Pax genes and their roles in cell differentiation and development. Curr Opin Cell Biol 8: 851–857.

147. Favor J, R Sandulache, A Neuhäuser-Klaus, W Pretsch, B Chatterjee, E Senft, W Wurst, V Blanquet, P Grimes, R Spörle and others (1996). The mouse Pax21Neu mutation is identical to a human PAX2 mutation in a family with renal-coloboma syndrome and results in developmental defects of the brain, ear, eye, and kidney. Proc Natl Acad Sci 93: 13870–13875.

148. Torres M, E Gómez-Pardo and P Gruss (1996). Pax2 contributes to inner ear patterning and optic nerve trajectory. Development 122: 3381–3391.

149. Burton Q, LK Cole, M Mulheisen, W Chang and DK Wu (2004). The role of Pax2 in mouse inner ear development. Dev Biol 272: 161–175.

150. Bouchard M, D de Caprona, M Busslinger, P Xu and B Fritzsch (2010). Pax2 and Pax8 cooperate in mouse inner ear morphogenesis and innervation. BMC Dev Biol 10: 89.

151. Riley BB and BT Phillips (2003). Ringing in the new ear: resolution of cell interactions in otic development. Dev Biol 261: 289–312.

152. Chen Y, H Yu, Y Zhang, W Li, N Lu, W Ni, Y He, J Li, S Sun, Z Wang and H Li (2013). Cotransfection of Pax2 and Math1 promote in situ cochlear hair cell regeneration after neomycin insult. Sci Rep 3: 1–9.

153. Mansour SL, JM Goddard and MR Capecchi (1993). Mice homozygous for a targeted disruption of the proto-oncogene int-2 have developmental defects in the tail and inner ear. Development 117: 13–28.

154. Pauley S, TJ Wright, U Pirvola, D Ornitz, K Beisel and B Fritzsch (2003). Expression and function of FGF10 in mammalian inner ear development. Dev Dyn 227: 203–215.

155. Hatch EP, CA Noyes, X Wang, TJ Wright and SL Mansour (2007). Fgf3 is required for dorsal patterning and morphogenesis of the inner ear epithelium. Development 134: 3615–3625.

156. Urness LD, CN Paxton, X Wang, GC Schoenwolf and SL Mansour (2010). FGF signaling regulates otic placode induction and refinement by controlling both ectodermal target genes and hindbrain Wnt8a. Dev Biol 340: 595–604.

157. Zelarayan LC, V Vendrell, Y Alvarez, E Domínguez-Frutos, T Theil, MT Alonso, M Maconochie and T Schimmang (2007). Differential requirements for FGF3, FGF8 and FGF10 during inner ear development. Dev Biol 308: 379–391.

158. Ladher RK, TJ Wright, AM Moon, SL Mansour and GC Schoenwolf (2005). FGF8 initiates inner ear induction in chick and mouse. Genes Dev 19: 603–613.

159. Mahoney Rogers AA, J Zhang and K Shim (2011). Sprouty1 and Sprouty2 limit both the size of the otic placode and hindbrain Wnt8a by antagonizing FGF signaling. Dev Biol 353: 94–104.

160. Ladher RK (2017). Changing shape and shaping change: Inducing the inner ear. Semin Cell Dev Biol 65: 39–46.

161. Ohyama T and AK Groves (2004). Generation of Pax2-Cre mice by modification of a Pax2 bacterial artificial chromosome. Genesis 38: 195–199.

162. Ohyama T, OA Mohamed, MM Taketo, D Dufort and AK Groves (2006). Wnt signals mediate a fate decision between otic placode and epidermis. Development 133: 865–875.

163. Riccomagno MM, L Martinu, M Mulheisen, DK Wu and DJ Epstein (2002). Specification of the mammalian cochlea is dependent on Sonic hedgehog. Genes Dev 16: 2365–2378.

164. Riccomagno MM, S Takada and DJ Epstein (2005). Wnt-dependent regulation of inner ear morphogenesis is balanced by the opposing and supporting roles of Shh. Genes Dev 19: 1612–1623.

165. Jayasena CS, T Ohyama, N Segil and AK Groves (2008). Notch signaling augments the canonical Wnt pathway to specify the size of the otic placode. Development 135: 2251–2261.

166. Bower M, R Salomon, J Allanson, C Antignac, F Benedicenti, E Benetti, G Binenbaum, UB Jensen, P Cochat, S DeCramer, J Dixon, R Drouin, MJ Falk, H Feret, R Gise, A Hunter, K Johnson, R Kumar, MP Lavocat, L Martin, V Morinière, D Mowat, L Murer, HT Nguyen, G Peretz-Amit, E Pierce, E Place, N Rodig, A Salerno, S Sastry, T Sato, JA Sayer, GCP Schaafsma, L Shoemaker, DW Stockton, W-H Tan, R Tenconi, P Vanhille, A Vats, X Wang, B Warman, RG Weleber, SM White, C Wilson-Brackett, DJ Zand, M Eccles, LA Schimmenti and L Heidet (2012). Update of PAX2 mutations in renal coloboma syndrome and establishment of a locus-specific database. Hum Mutat 33: 457–466.

167. Dressler GR, U Deutsch, K Chowdhury, HO Nornes and P Gruss (1990). Pax2, a new murine paired-box-containing gene and its expression in the developing excretory system. Development 109: 787–795.

168. Püschel AW, M Westerfield and GR Dressler (1992). Comparative analysis of Pax-2 protein distributions during neurulation in mice and zebrafish. Mech Dev 38: 197–208.

169. Nornes HO, GR Dressler, EW Knapik, U Deutsch and P Gruss (1990). Spatially and temporally restricted expression of Pax2 during murine neurogenesis. Development 109: 797–809.

170. Ornitz DM, J Xu, JS Colvin, DG McEwen, CA MacArthur, F Coulier, G Gao and M Goldfarb (1996). Receptor specificity of the fibroblast growth factor family. J Biol Chem 271: 15292–15297.

171. Zhang X, OA Ibrahimi, SK Olsen, H Umemori, M Mohammadi and DM Ornitz (2006). Receptor specificity of the fibroblast growth factor family: the complete mammalian FGF family. J Biol Chem 281: 15694–15700.

172. Pirvola U, B Spencer-Dene, L Xing-Qun, P Kettunen, I Thesleff, B Fritzsch, C Dickson and J Ylikoski (2000). FGF/FGFR-2 (IIIb) signaling is essential for inner ear morphogenesis. J Neurosci 20: 6125–6134.

173. Keller SA, JM Jones, A Boyle, LL Barrow, PD Killen, DG Green, NV Kapousta, PF Hitchcock, RT Swank and MH Meisler (1994). Kidney and retinal defects (Krd), a transgene-induced mutation with a deletion of mouse chromosome 19 that includes the Pax2 locus. Genomics 23: 309–320.

174. Sanyanusin P, LA McNoe, MJ Sullivan, RG Weaver and MR Eccles (1995). Mutation of PAX2 in two siblings with renal-coloboma syndrome. Hum Mol Genet 4: 2183–2184.

175. Torres M, E Gómez-Pardo, GR Dressler and P Gruss (1995). Pax-2 controls multiple steps of urogenital development. Development 121: 4057–4065.

176. Bouchard M, P Pfeffer and M Busslinger (2000). Functional equivalence of the transcription factors Pax2 and Pax5 in mouse development. Development 127: 3703–3713.

177. Christ S, UW Biebel, S Hoidis, S Friedrichsen, K Bauer and JWT Smolders (2004). Hearing loss in athyroid Pax8 knockout mice and effects of thyroxine substitution. Audiol Neurotol 9: 88–106.

178. Soofi A, I Levitan and GR Dressler (2012). Two novel EGFP insertion alleles reveal unique aspects of Pax2 function in embryonic and adult kidneys. Dev Biol 365: 241–250.

179. Ornitz DM and N Itoh (2001). Fibroblast growth factors. Genome Biol 2: 1–12.

180. Represa J, Y León, C Miner and F Giraldez (1991). The int-2 proto-oncogene is responsible for induction of the inner ear. Nature 353: 561–563.

181. Kiernan AE, KP Steel and DM Fekete (2002). Development of the mouse inner ear. In Mouse Development: Patterning, Morphogenesis, and Organogenesis, (San Diego: Academic Press), pp. 539–566.

182. Liu M, FA Pereira, SD Price, M Chu, C Shope, D Himes, RA Eatock, WE Brownell, A Lysakowski and M-J Tsai (2000). Essential role of BETA2/NeuroD1 in development of the vestibular and auditory systems. Genes Dev 14: 2839–2854.

183. Bermingham NA, B Hassan, S Price, M Vollrath, N Ben-Arie, R Eatock, H Bellen, A Lysakowski and H Zoghbi (1999). Math1: an essential gene for the generation of inner ear hair cells. Science 284: 1837–1841.

184. Wu DK and MW Kelley (2012). Molecular mechanisms of inner ear development. Cold Spring Harb Perspect Biol 4: a008409.

185. Ulloa F and E Martí (2009). Wnt won the war: Antagonistic role of Wnt over Shh controls dorso-ventral patterning of the vertebrate neural tube. Dev Dyn 239: 69–76.

186. Liu W, G Li, JS Chien, S Raft, H Zhang, C Chiang and DA Frenz (2002). Sonic hedgehog regulates otic capsule chondrogenesis and inner ear development in the mouse embryo. Dev Biol 248: 240–250.

187. Brown AS and DJ Epstein (2011). Otic ablation of smoothened reveals direct and indirect requirements for Hedgehog signaling in inner ear development. Development 138: 3967–3976.

188. Ma Q, Z Chen, I del Barco Barrantes, JL de la Pompa and DJ Anderson (1998). neurogenin1 is essential for the determination of neuronal precursors for proximal cranial sensory ganglia. Neuron 20: 469–482.

189. Washausen S and W Knabe (2017). Pax2/Pax8-defined subdomains and the occurrence of apoptosis in the posterior placodal area of mice. Brain Struct Funct 222: 2671–2695.

190. Jacques BE, C Puligilla, RM Weichert, A Ferrer-Vaquer, A-K Hadjantonakis, MW Kelley and A Dabdoub (2012). A dual function for canonical Wnt/β-catenin signaling in the developing mammalian cochlea. Development 139: 4395–4404.

191. Shi F, L Hu, BE Jacques, JF Mulvaney, A Dabdoub and ASB Edge (2014). β-Catenin is required for hair-cell differentiation in the cochlea. J Neurosci 34: 6470–6479.

192. Kiernan AE, AL Pelling, KK Leung, AS Tang, DM Bell, C Tease, R Lovell-Badge, KP Steel and KS Cheah (2005). Sox2 is required for sensory organ development in the mammalian inner ear. Nature 434: 1031–1035.

193. Woods C, M Montcouquiol and MW Kelley (2004). Math1 regulates development of the sensory epithelium in the mammalian cochlea. Nat Neurosci 7: 1310–1318.

194. Puligilla C, A Dabdoub, SD Brenowitz and MW Kelley (2010). Sox2 induces neuronal formation in the developing mammalian cochlea. J Neurosci 30: 714–722.

195. Wood HB and V Episkopou (1999). Comparative expression of the mouse Sox1, Sox2 and Sox3 genes from pre-gastrulation to early somite stages. Mech Dev 86: 197–201.

196. Zou D, C Erickson, E-H Kim, D Jin, B Fritzsch and P-X Xu (2008). Eya1 gene dosage critically affects the development of sensory epithelia in the mammalian inner ear. Hum Mol Genet 17: 3340–3356.

197. Mak ACY, IYY Szeto, B Fritzsch and KSE Cheah (2009). Differential and overlapping expression pattern of SOX2 and SOX9 in inner ear development. Gene Expr Patterns 9: 444–453.

198. Brooker R, K Hozumi and J Lewis (2006). Notch ligands with contrasting functions: Jagged1 and Delta1 in the mouse inner ear. Development 133: 1277–1286.

199. Dabdoub A, C Puligilla, JM Jones, B Fritzsch, KS Cheah, LH Pevny and MW Kelley (2008). Sox2 signaling in prosensory domain specification and subsequent hair cell differentiation in the developing cochlea. Proc Natl Acad Sci 105: 18396–18401.

200. Brigande JV and S Heller (2009). Quo vadis, hair cell regeneration? Nat Neurosci 12: 679–685.

201. Rubel EW, SA Furrer and JS Stone (2013). A brief history of hair cell regeneration research and speculations on the future. Hear Res 297: 42–51.

202. Zheng JL and W-Q Gao (2000). Overexpression of Math1 induces robust production of extra hair cells in postnatal rat inner ears. Nat Neurosci 3: 580–586.

203. Puligilla C and MW Kelley (2017). Dual role for Sox2 in specification of sensory competence and regulation of Atoh1 function. Dev Neurobiol 77: 3–13.

204. Kempfle JS, JL Turban and ASB Edge (2016). Sox2 in the differentiation of cochlear progenitor cells. Sci Rep 6: 23293.

205. Shi F, Y Cheng, XL Wang and ASB Edge (2010). β-catenin up-regulates Atoh1 expression in neural progenitor cells by interaction with an Atoh1 3' enhancer. J Biol Chem 285: 392–400.

206. Ahmed M, EYM Wong, J Sun, J Xu, F Wang and P-X Xu (2012). Eya1-Six1 interaction is sufficient to induce hair cell fate in the cochlea by activating Atoh1 expression in cooperation with Sox2. Dev Cell 22: 377–390.

207. Kiernan AE (2013). Notch signaling during cell fate determination in the inner ear. Semin Cell Dev Biol 24: 470–479.

208. Neves J, C Parada, M Chamizo and F Giraldez (2011). Jagged 1 regulates the restriction of Sox2 expression in the developing chicken inner ear: a mechanism for sensory organ specification. Development 138: 735–744.

209. Basch ML, T Ohyama, N Segil and AK Groves (2011). Canonical Notch signaling is not necessary for prosensory induction in the mouse cochlea: insights from a conditional mutant of RBPjκ. J Neurosci 31: 8046–8058.

210. Yamamoto N, W Chang and MW Kelley (2011). Rbpj regulates development of prosensory cells in the mammalian inner ear. Dev Biol 353: 367–379.

211. Tateya T, I Imayoshi, I Tateya, K Hamaguchi, H Torii, J Ito and R Kageyama (2013). Hedgehog signaling regulates prosensory cell properties during the basal-to-apical wave of hair cell differentiation in the mammalian cochlea. Development 140: 3848–3857.

212. Bok J, C Zenczak, CH Hwang and DK Wu (2013). Auditory ganglion source of Sonic hedgehog regulates timing of cell cycle exit and differentiation of mammalian cochlear hair cells. Proc Natl Acad Sci 110: 13869–13874.

213. Driver EC, SP Pryor, P Hill, J Turner, U Ruther, LG Biesecker, AJ Griffith and MW Kelley (2008). Hedgehog Signaling Regulates Sensory Cell Formation and Auditory Function in Mice and Humans. J Neurosci 28: 7350–7358.

214. Liu Z, T Owen, L Zhang and J Zuo (2010). Dynamic expression pattern of Sonic hedgehog in developing cochlear spiral ganglion neurons. Dev Dyn 239: 1674–1683.

215. Son EJ, J-H Ma, H Ankamreddy, J-O Shin, JY Choi, DK Wu and J Bok (2015). Conserved role of Sonic Hedgehog in tonotopic organization of the avian basilar papilla and mammalian cochlea. Proc Natl Acad Sci 3746–3751.

216. Ohyama T, ML Basch, Y Mishina, KM Lyons, N Segil and AK Groves (2010). BMP signaling is necessary for patterning the sensory and nonsensory regions of the developing mammalian cochlea. J Neurosci 30: 15044–15051.

217. Munnamalai V and DM Fekete (2016). Notch-Wnt-Bmp crosstalk regulates radial patterning in the mouse cochlea in a spatiotemporal manner. Development 143: 4003–4015.

218. Żak M, SFL Klis and W Grolman (2015). The Wnt and Notch signalling pathways in the developing cochlea: Formation of hair cells and induction of regenerative potential. Int J Dev Neurosci 47: 247–258.

219. Kiernan AE, N Ahituv, H Fuchs, R Balling, KB Avraham, KP Steel and MH de Angelis (2001). The Notch ligand Jagged1 is required for inner ear sensory development. Proc Natl Acad Sci 98: 3873–3878.

220. Hayashi T, CA Ray and O Bermingham-McDonogh (2008). Fgf20 Is required for sensory epithelial specification in the developing cochlea. J Neurosci 28: 5991–5999.

221. Pirvola U, J Ylikoski, R Trokovic, JM Hébert, SK McConnell and J Partanen (2002). FGFR1 is required for the development of the auditory sensory epithelium. Neuron 35: 671–680.

222. Oesterle EC, S Campbell, RR Taylor, A Forge and CR Hume (2008). Sox2 and Jagged1 expression in normal and drug-damaged adult mouse inner ear. J Assoc Res Otolaryngol 9: 65–89.

223. Dechesne CJ, D Rabejac and G Desmadryl (1994). Development of calretinin immunoreactivity in the mouse inner ear. J Comp Neurol 346: 517–529.

224. Burns JC, MC Kelly, M Hoa, RJ Morell and MW Kelley (2015). Single-cell RNA-Seq resolves cellular complexity in sensory organs from the neonatal inner ear. Nat Commun 6: 8557.

225. Hartman BH, R Durruthy-Durruthy, RD Laske, S Losorelli and S Heller (2015). Identification and characterization of mouse otic sensory lineage genes. Front Cell Neurosci 9:.

226. Durruthy-Durruthy R, A Gottlieb, BH Hartman, J Waldhaus, RD Laske, R Altman and S Heller (2014). Reconstruction of the mouse otocyst and early neuroblast lineage at single-cell resolution. Cell 157: 964–978.

227. Andrabi M, S Kuraku, N Takata, Y Sasai and NR Love (2015). Comparative, transcriptome analysis of self-organizing optic tissues. Sci Data 2: 150030.

228. Quadrato G, T Nguyen, EZ Macosko, JL Sherwood, S Min Yang, DR Berger, N Maria, J Scholvin, M Goldman, JP Kinney, ES Boyden, JW Lichtman, ZM Williams, SA McCarroll and P Arlotta (2017). Cell diversity and network dynamics in photosensitive human brain organoids. Nature 545: 48–53.

229. Takasato M, PX Er, HS Chiu, B Maier, GJ Baillie, C Ferguson, RG Parton, EJ Wolvetang, MS Roost, SM Chuva de Sousa Lopes and MH Little (2015). Kidney organoids from human iPS cells contain multiple lineages and model human nephrogenesis. Nature 526: 564–568.

230. Ren W, E Aihara, W Lei, N Gheewala, H Uchiyama, RF Margolskee, K Iwatsuki and P Jiang (2017). Transcriptome analyses of taste organoids reveal multiple pathways involved in taste cell generation. Sci Rep 7: 4004.

231. Schaefer SA, AY Higashi, B Loomis, T Schrepfer, G Wan, G Corfas, GR Dressler and RK Duncan (In press). From otic induction to hair cell production: Pax2EGFP cell line illuminates key stages of development in mouse inner ear organoid model. Stem Cells Dev.

232. Burns JC and JS Stone (2017). Development and regeneration of vestibular hair cells in mammals. Semin Cell Dev Biol 65: 96–105.

233. Groves AK and DM Fekete (2012). Shaping sound in space: the regulation of inner ear patterning. Development 139: 245–257.

234. Eiraku M and Y Sasai (2011). Mouse embryonic stem cell culture for generation of three-dimensional retinal and cortical tissues. Nat Protoc 7: 69–79.

235. Eiraku M, N Takata, H Ishibashi, M Kawada, E Sakakura, S Okuda, K Sekiguchi, T Adachi and Y Sasai (2011). Self-organizing optic-cup morphogenesis in three-dimensional culture. Nature 472: 51–56.

236. Tropepe V, S Hitoshi, C Sirard, TW Mak, J Rossant and D van der Kooy (2001). Direct neural fate specification from embryonic stem cells: a primitive mammalian neural stem cell stage acquired through a default mechanism. Neuron 30: 65–78.

237. Kwon H-J and BB Riley (2009). Mesendodermal signals required for otic induction: Bmp-antagonists cooperate with Fgf and can facilitate formation of ectopic otic tissue. Dev Dyn 238: 1582–1594.

238. Groves AK and M Bronner-Fraser (2000). Competence, specification and commitment in otic placode induction. Development 127: 3489–3499.

239. Martin K and AK Groves (2006). Competence of cranial ectoderm to respond to Fgf signaling suggests a two-step model of otic placode induction. Development 133: 877–887.

240. Pfeffer PL, B Payer, G Reim, M Pasca di Magliano and M Busslinger (2002). The activation and maintenance of Pax2 expression at the mid-hindbrain boundary is controlled by separate enhancers. Development 129: 307–318.

241. Wang J, Y Wu, F Zhao, Y Wu, W Dong, J Zhao, Z Zhu and D Liu (2015). Fgf-signaling-dependent Sox9a and Atoh1a regulate otic neural development in zebrafish. J Neurosci 35: 234–244.

242. Yang L, P O'Neill, K Martin, JC Maass, V Vassilev, R Ladher and AK Groves (2013). Analysis of FGF-Dependent and FGF-Independent Pathways in Otic Placode Induction. PLoS ONE 8: e55011.

243. Schindelin J, I Arganda-Carreras, E Frise, V Kaynig, M Longair, T Pietzsch, S Preibisch, C Rueden, S Saalfeld, B Schmid, J-Y Tinevez, DJ White, V Hartenstein, K Eliceiri, P Tomancak and A Cardona (2012). Fiji: an open-source platform for biological-image analysis. Nat Methods 9: 676–682.

244. Crumling MA, M Tong, KL Aschenbach, LQ Liu, CM Pipitone and RK Duncan (2009). P2X antagonists inhibit styryl dye entry into hair cells. Neuroscience 161: 1144–1153.

245. Radde-Gallwitz K, L Pan, L Gan, X Lin, N Segil and P Chen (2004). Expression of Islet1 marks the sensory and neuronal lineages in the mammalian inner ear. J Comp Neurol 477: 412–421.

246. Steevens AR, DL Sookiasian, JC Glatzer and AE Kiernan (2017). SOX2 is required for inner ear neurogenesis. Sci Rep 7: 4086.

247. Wong AB, MA Rutherford, M Gabrielaitis, T Pangršič, F Göttfert, T Frank, S Michanski, S Hell, F Wolf, C Wichmann and T Moser (2014). Developmental refinement of hair cell synapses tightens the coupling of Ca2+ influx to exocytosis. EMBO J 33: 247–264.

248. Lawoko-Kerali G, MN Rivolta and M Holley (2002). Expression of the transcription factors GATA3 and Pax2 during development of the mammalian inner ear. J Comp Neurol 442: 378–391.

249. Chaudhry MA, TZ Vitalis, BD Bowen and JM Piret (2008). Basal medium composition and serum or serum replacement concentration influences on the maintenance of murine embryonic stem cells. Cytotechnology 58: 173–179.

250. Muguruma K, A Nishiyama, Y Ono, H Miyawaki, E Mizuhara, S Hori, A Kakizuka, K Obata, Y Yanagawa, T Hirano and Y Sasai (2010). Ontogeny-recapitulating generation and tissue integration of ES cell-derived Purkinje cells. Nat Neurosci 13: 1171–1180.

251. Bok J, M Bronner-Fraser and DK Wu (2005). Role of the hindbrain in dorsoventral but not anteroposterior axial specification of the inner ear. Development 132: 2115–2124.

252. Oishi N, A Kendall and J Schacht (2014). Metformin protects against gentamicin-induced hair cell death in vitro but not ototoxicity in vivo. Neurosci Lett 583: 65–69.

253. Zheng W, L Huang, Z Wei, D Silvius, B Tang and P Xu (2003). The role of Six1 in mammalian auditory system development. Development 130: 3989–4000.

254. Evans MJ and MH Kaufman (1981). Establishment in culture of pluripotential cells from mouse embryos. Nature 292: 154–156.

255. Martin GR (1981). Isolation of a pluripotent cell line from early mouse embryos cultured in medium conditioned by teratocarcinoma stem cells. Proc Natl Acad Sci U S A 78: 7634–7638.

256. Ursu A, DJ Illich, Y Takemoto, AT Porfetye, M Zhang, A Brockmeyer, P Janning, N Watanabe, H Osada, IR Vetter, S Ziegler, HR Schöler and H Waldmann (2016). Epiblastin A induces reprogramming of epiblast stem cells into embryonic stem cells by inhibition of casein kinase 1. Cell Chem Biol 23: 494–507.

257. Illich DJ, M Zhang, A Ursu, R Osorno, K-P Kim, J Yoon, MJ Araúzo-Bravo, G Wu, D Esch, D Sabour, D Colby, KS Grassme, J Chen, B Greber, S Höing, W Herzog, S Ziegler, I Chambers, S Gao, H Waldmann and HR Schöler (2016). Distinct signaling requirements for the establishment of ESC pluripotency in late-stage EpiSCs. Cell Rep 15: 787–800.

258. Zhang H, S Gayen, J Xiong, B Zhou, AK Shanmugam, Y Sun, H Karatas, L Liu, RC Rao, S Wang, AI Nesvizhskii, S Kalantry and Y Dou (2016). MLL1 inhibition reprograms epiblast stem cells to naive pluripotency. Cell Stem Cell 18: 481–494.

259. Tesar PJ, JG Chenoweth, FA Brook, TJ Davies, EP Evans, DL Mack, RL Gardner and RDG McKay (2007). New cell lines from mouse epiblast share defining features with human embryonic stem cells. Nature 448: 196–199.

260. Brons IGM, LE Smithers, MWB Trotter, P Rugg-Gunn, B Sun, SM Chuva de Sousa Lopes, SK Howlett, A Clarkson, L Ahrlund-Richter, RA Pedersen and L Vallier (2007). Derivation of pluripotent epiblast stem cells from mammalian embryos. Nature 448: 191–195.

261. Hiler D, X Chen, J Hazen, S Kupriyanov, PA Carroll, C Qu, B Xu, D Johnson, L Griffiths, S Frase, AR Rodriguez, G Martin, J Zhang, J Jeon, Y Fan, D Finkelstein, RN Eisenman, K Baldwin and MA Dyer (2015). Quantification of retinogenesis in 3D cultures reveals epigenetic memory and higher efficiency in iPSCs derived from rod photoreceptors. Cell Stem Cell 17: 101–115.

262. Doetschman TC, H Eistetter, M Katz, W Schmidt and R Kemler (1985). The in vitro development of blastocyst-derived embryonic stem cell lines: formation of visceral yolk sac, blood islands and myocardium. Development 87: 27–45.

263. Inman GJ, FJ Nicolás, JF Callahan, JD Harling, LM Gaster, AD Reith, NJ Laping and CS Hill (2002). SB-431542 is a potent and specific inhibitor of transforming growth factor-β superfamily type I activin receptor-like kinase (ALK) receptors ALK4, ALK5, and ALK7. Mol Pharmacol 62: 65–74.

264. Afgan E, D Baker, M van den Beek, D Blankenberg, D Bouvier, M Čech, J Chilton, D Clements, N Coraor, C Eberhard, B Grüning, A Guerler, J Hillman-Jackson, G Von Kuster, E Rasche, N Soranzo, N Turaga, J Taylor, A Nekrutenko and J Goecks (2016). The Galaxy platform for accessible, reproducible and collaborative biomedical analyses: 2016 update. Nucleic Acids Res 44: W3–W10.

265. Andrews S (2010). A quality control tool for high throughput sequence data. Available online at http://www.bioinformatics.babraham.ac.uk/projects/fastqc/.

266. Kim D, B Langmead and SL Salzberg (2015). HISAT: a fast spliced aligner with low memory requirements. Nat Methods 12: 357–360.

267. Zhao S and B Zhang (2015). A comprehensive evaluation of ensembl, RefSeq, and UCSC annotations in the context of RNA-seq read mapping and gene quantification. BMC Genomics 16: 97.

268. Anders S, PT Pyl and W Huber (2015). HTSeq--a Python framework to work with high-throughput sequencing data. Bioinformatics 31: 166–169.

269. Love MI, W Huber and S Anders (2014). Moderated estimation of fold change and dispersion for RNA-seq data with DESeq2. Genome Biol 15:.

270. Ying Q-L, J Wray, J Nichols, L Batlle-Morera, B Doble, J Woodgett, P Cohen and A Smith (2008). The ground state of embryonic stem cell self-renewal. Nature 453: 519–523.

271. Chea HK, CV Wright and BJ Swalla (2005). Nodal signaling and the evolution of deuterostome gastrulation. Dev Dyn 234: 269–278.

272. Vallier L, S Mendjan, S Brown, Z Chng, A Teo, LE Smithers, MWB Trotter, C Cho, A Martinez, P Rugg-Gunn, G Brons and RA Pedersen (2009). Activin/Nodal signalling maintains pluripotency by controlling Nanog expression. Development 136: 1339–1349.

273. Ichida JK, J Blanchard, K Lam, EY Son, JE Chung, D Egli, KM Loh, AC Carter, FP Di Giorgio, K Koszka, D Huangfu, H Akutsu, DR Liu, LL Rubin and K Eggan (2009). A small-molecule inhibitor of Tgf-β signaling replaces sox2 in reprogramming by inducing nanog. Cell Stem Cell 5: 491–503.

274. Takahashi K and S Yamanaka (2006). Induction of pluripotent stem cells from mouse embryonic and adult fibroblast cultures by defined factors. Cell 126: 663–676.

275. Chen AE, M Borowiak, RI Sherwood, A Kweudjeu and DA Melton (2013). Functional evaluation of ES cell-derived endodermal populations reveals differences between Nodal and Activin A-guided differentiation. Development 140: 675–686.

276. Kaufman-Francis K, HN Goh, Y Kojima, JB Studdert, V Jones, MD Power, E Wilkie, E Teber, DAF Loebel and PPL Tam (2014). Differential response of epiblast stem cells to Nodal and Activin signalling: a paradigm of early endoderm development in the embryo. Philos Trans R Soc B Biol Sci 369: 20130550.

277. Shi Y and J Massagué (2003). Mechanisms of TGF-β signaling from cell membrane to the nucleus. Cell 113: 685–700.

278. Kumar A, V Novoselov, AJ Celeste, NM Wolfman, P ten Dijke and MR Kuehn (2001). Nodal Signaling Uses Activin and Transforming Growth Factor-β Receptor-regulated Smads. J Biol Chem 276: 656–661.

279. Gellibert F, J Woolven, M Fouchet, N Mathews, H Goodland, V Lovegrove, A Laroze, V Nguyen, S Sautet, R Wang, C Janson, W Smith, G Krysa, V Boullay, A De Gouville, S Huet and D Hartlet (2004). Identification of 1,5-naphthyridine derivatives as a novel series of potent and selective TGF-beta type I receptor inhibitors. J Med Chem 47: 4494–4506.

280. Jinnin M, H Ihn and K Tamaki (2005). Characterization of SIS3, a novel specific inhibitor of Smad3, and its effect on transforming growth factor-β1-induced extracellular matrix expression. Mol Pharmacol 69: 597–607.

281. Hemberger M, W Dean and W Reik (2009). Epigenetic dynamics of stem cells and cell lineage commitment: digging Waddington's canal. Nat Rev Mol Cell Biol 10: 526–537.

282. Clark SJ, HJ Lee, SA Smallwood, G Kelsey and W Reik (2016). Single-cell epigenomics: powerful new methods for understanding gene regulation and cell identity. Genome Biol 17: 72.

283. Bok J, S Raft, K-A Kong, SK Koo, UC Dräger and DK Wu (2011). Transient retinoic acid signaling confers anterior-posterior polarity to the inner ear. Proc Natl Acad Sci 108: 161–166.

284. Janesick A, J Shiotsugu, M Taketani and B Blumberg (2012). RIPPLY3 is a retinoic acid-inducible repressor required for setting the borders of the pre-placodal ectoderm. Development 139: 1213–1224.

285. Yutzey KE (2010). DiGeorge syndrome, Tbx1, and retinoic acid signaling come full circle. Circ Res 106: 630–632.

286. Roberts C, SM Ivins, CT James and PJ Scambler (2005). Retinoic acid down-regulates Tbx1 expression in vivo and in vitro. Dev Dyn 232: 928–938.

287. Raft S (2004). Suppression of neural fate and control of inner ear morphogenesis by Tbx1. Development 131: 1801–1812.

288. Morsli H, F Tuorto, D Choo, MP Postiglione, A Simeone and DK Wu (1999). Otx1 and Otx2 activities are required for the normal development of the mouse inner ear. Development 126: 2335–2343.

289. Arnold JS, EM Braunstein, T Ohyama, AK Groves, JC Adams, MC Brown and BE Morrow (2006). Tissue-specific roles of Tbx1 in the development of the outer, middle and inner ear, defective in 22q11DS patients. Hum Mol Genet 15: 1629–1639.

290. Wang W, JF Grimmer, TR Van De Water and T Lufkin (2004). Hmx2 and Hmx3 homeobox genes direct development of the murine inner ear and hypothalamus and can be functionally replaced by Drosophila Hmx. Dev Cell 7: 439–453.

291. Maeshima A, K Maeshima, Y Nojima and I Kojima (2002). Involvement of Pax-2 in the action of activin A on tubular cell regeneration. J Am Soc Nephrol 13: 2850–2859.

292. Watson CL, MM Mahe, J Múnera, JC Howell, N Sundaram, HM Poling, JI Schweitzer, JE Vallance, CN Mayhew, Y Sun, G Grabowski, SR Finkbeiner, JR Spence, NF Shroyer, JM Wells and MA Helmrath (2014). An in vivo model of human small intestine using pluripotent stem cells. Nat Med 20: 1310–1314.

293. Dye BR, PH Dedhia, AJ Miller, MS Nagy, ES White, LD Shea and JR Spence (2016). A bioengineered niche promotes in vivo engraftment and maturation of pluripotent stem cell derived human lung organoids. Elife 5: e19732.